CENTRAL NERVOUS SYSTEM DELIVERY AND PHARMACOKINETICS OF NOVEL THERAPEUTICS: IMPLICATIONS FOR COMBINATIONS OF SMALL MOLECULES AND ANTIBODY-DRUG CONJUGATES

A DISSERTATION
SUBMITTED TO THE FACULTY OF THE
UNIVERSITY OF MINNESOTA
BY

JESSICA IRENE GRACE GRIFFITH

IN PARTIAL FULFILLMENT OF THE REQUIREMENTS
FOR THE DEGREE OF
DOCTOR OF PHILOSOPHY

WILLIAM FREDERICK ELMQUIST

JUNE 2022

Jessica Irene Grace Griffith
University of Minnesota
2022

ACKNOWLEDGEMENTS

Arriving at this point in my graduate studies has been something I long envisioned. While the journey has not always been straightforward, the support I received during this time has been steadfast.

First, I would like to thank the University of Minnesota Department of Pharmaceutics for the opportunity to complete this work. Our department's training has helped me grow as a scientist and learn so much outside of the focus of this work. I am grateful for all of our faculty, who are so kind and genuinely delight in their students' success, and for the Department's support to attend the Gordon Research Conference and the Blood-Brain Barrier Consortium.

Many professors outside of the Department of Pharmaceutics taught me so much in my coursework throughout my time at the University of Minnesota. My special thanks goes to Dr. Peter Carr, Dr. Sarah Algeri, and Dr. Helena Zarin for their patience and encouragement in courses that were especially difficult for me. I have always told myself that I am not a "math person", but they certainly helped me learn to think like one.

Third, many thanks to my doctoral dissertation committee members, Dr. Jann Sarkaria, Dr. George Wilcox, Dr. Richard Brundage, and Dr. Ronald Siegel, whose insightful questions and sincere interest have helped move this work forward.

All of this work has hinged on the utilization of a technique I had never used prior to graduate school. Therefore, I am also extremely grateful for the technical expertise and patience of Dr. James Fisher, Dr. Yingchun Zhao, and Dr. Peter Villalta, without whom I would have been utterly lost in the development of the LC-MS/MS methods utilized herein.

This research would not have been possible without our collaborators. I would like to thank Dr. Carolyn Fairbanks, George Wilcox and their labs, who presented us with the opportunity to work on a topic that is so important to my home state of West Virginia. This was an unexpected foray into another field that helped me learn more than I could have possibly foreseen. Thanks is also due to Dr. Jann Sarkaria and his lab members,

especially Ms. Kendra Porath, who have always been on the cutting edge of the treatment of brain tumors, and who make great efforts to nurture the collaboration between our labs. I also would like to thank my labmates, both past and present, for being delightful to work with, and for listening to my revelations and struggles as I have gone through this learning process. Thanks especially to Drs. Afroz Mohammad, Juhee Oh, Minjee Kim, and Surabhi Talele, whose friendship, feedback, and support has been invaluable throughout my time in the Elmquist lab.

I would like to thank Dr. Paul Lockman, without whom I would have never entered this field. I truly love this research, and I am grateful that I came to the University of Minnesota with a firm foundation in the blood-brain barrier and central nervous system tumors.

Thanks goes next to my friends and family all over the country for their unwavering love. I do not know what I would have done without my wonderful mother, Dr. Elizabeth Anne Johnson. I am so grateful for her wisdom and advice, the many boxes of chocolates that arrived by mail, and the countless hours of encouragement and empathy over the phone. Thank you also to my father, Dr. Robert Griffith, for commiserating on the woes of grading many, many papers and for delighting in my successes. Thank you to my sister, Kate, for being my first visitor in the Twin Cities, and for listening and offering advice or silliness, as needed. Thanks to Gabi, for answering the phone when I most need it, and thanks to Allie and James for being the most steadfast and generous friends I could have imagined finding during this time.

Thanks especially to my husband, Ray, for his loving support, encouragement, companionship, and understanding. Graduate school is not easy, but graduate school in the midst of multiple surgeries, a pandemic, getting married, and purchasing a home is simply an epic. Ray, you keep the psych so, so high. I am forever grateful that this time brought us together.

Last, I would like to directly thank Dr. Elmquist. Thank you for believing in me, encouraging me, and teaching me so much. I cherish the fact that you took a chance on me. Thank you for giving me the space and environment that helped me grow into the person that I am still becoming, and for always being honest when I needed a little push.

We are all so lucky that you are such a kind and empathetic advisor, who understands and emphasizes that life outside of the lab is as important as everything that happens within.

DEDICATION

This work is dedicated to my mother

"What the heart thinks great is great.

The Soul's emphasis is always right."

- Ralph Waldo Emerson

ABSTRACT

The central nervous system (CNS) barriers, in particular the blood-brain barrier (BBB), play a critical role in the delivery, safety, and efficacy of drugs. The BBB prevents the distribution of a wide variety of molecules into brain, either due to the limited paracellular transport of large and hydrophilic molecules, or the active efflux of many small, lipophilic compounds with appreciable membrane permeability. Limited brain penetration of drugs can be an asset to the development of molecules for which dose-limiting toxicities are mediated within the CNS. This is of particular interest in the case of opioids, as their CNS side effects can be fatal. On the other hand, the limited delivery of drugs to the brain has been one of the greatest barriers to the development of novel therapies to treat diseases of the CNS, including brain tumors like glioblastoma (GBM). The objective of this dissertation was to assess how the BBB impacts the distribution of drugs in both of the aforementioned cases. In this dissertation, we utilized preclinical pharmacokinetic studies in wild-type and transgenic mice to characterize the CNS disposition of both opioids and antibody-drug conjugates (ADCs) following multiple routes of administration. This work shows that efflux by P-glycoprotein limits the CNS distribution of two opioid agonists with synergistic activity, loperamide and oxymorphindole, and indicates that their synergy is mediated in the peripheral nervous system. The subsequent work on the ADC, ABBV-221, shows that systemic administration of ADCs is unlikely to result in efficacious drug delivery to GBM tumors, but that administration by convection-enhanced delivery significantly enhances the exposure in brain. Together, these studies provide opposing perspectives on how CNS penetration can affect the safety and efficacy of novel therapeutics.

TABLE OF CONTENTS

ACKNOWLEDGEMENTS……**i**

DEDICATION……....**iv**

ABSTRACT……**v**

TABLE OF CONTENTS……..**vi**

LIST OF TABLES……**.x**

LIST OF FIGURES……..**xii**

LIST OF ABBREVIATIONS……**xiv**

CHAPTER 1……..**1**

1.1 CENTRAL NERVOUS SYSTEM BARRIERS……..**2**

1.2 THE BLOOD-BRAIN BARRIER……**2**

1.3 ROLE OF THE CNS BARRIERS IN DRUG DISTRIBUTION……....**7**

1.4 SCOPE OF DISSERTAION…….……**9**

1.5 STATEMENT OF THE PROBLEM..……**11**

1.6 RESEARCH OBJECTIVES……**12**

1.7 RESEARCH APPROACH……..**13**

1.8 SPECIFIC AIMS……..**14**

CHAPTER 2……**17**

2.1 BRIEF HISTORY OF OPIOIDS……...**18**

2.2 OPIOID RECEPTORS AND THEIR PHYSIOLOGY……**20**

2.3 CNS DISTRIBUTION OF OPIOIDS…..……...**22**

CHAPTER 3……**24**

3.1 INTRODUCTION……**25**

3.2 MATERIALS AND METHODS……..……28
3.2.1 CHEMICALS AND REAGENTS……...28
3.2.2 ANIMALS……..28
3.2.3 DRUG PREPARATION AND ADMINISTRATION FOR ORAL ED_{50} CALCULATION……...29
3.2.4 BEHAVIORAL MEASURES ……29
3.2.5 DATA ANAYLSIS FOR BEHAVIORAL MEASURES……..30
3.2.6 SYSTEMIC PHARMACOKINETIC AND CNS DISTRIBUTION STUDIES……31
3.2.7 LC-MS/MS ANALYSIS ……..32
3.2.8 PHARMACOKINETIC PARAMETER ESTIMATION……33
3.2.9 STATISTICAL ANALYSIS……36
3.3 RESULTS……..……...37
3.3.1 ORAL ED_{50} OF LOPERAMIDE WITH AND WITHOUT OMI……37
3.3.2 LOPERAMIDE IV DISPOSITION IN ICR MICE……..……..39
3.3.3 OMI IV DISPOSITION IN ICR MICE……...……43
3.3.4 LOPERAMIDE PO DISPOSITION IN ICR MICE……...46
3.3.5 OMI PO DISPOSITION IN ICR MICE……..49
3.4 DISCUSSION……..51

CHAPTER 4……53
4.1 INTRODUCTION……..……..……..54
4.2 MATERIALS AND METHODS……..55
4.2.1 CHEMICALS AND REAGENTS……...55
4.2.2 ANIMALS……..……55
4.2.3 CNS DISTRIBUTION STUDIES……56
4.2.4 LC-MS/MS ANALYSIS……...57
4.2.5 PHARMACOKINETIC PARAMETER ESTIMATION……....58
4.2.6 RAPID EQUILIBRIUM DIALYSIS…..……...60
4.2.7 STATISTICAL ANALYSIS……61
4.3 RESULTS ……..……..62
4.3.1 LOPERAMIDE DISPOSITION IN TRANSGENIC FVB MICE…….63
4.3.2 OMI DISPOSITION IN TRANSGENIC FVB MICE……71

4.3.3 FREE FRACTION OF LOPERAMIDE AND OMI IN MOUSE BRAIN HOMOGENATE AND PLASMA……78
4.4 DISCUSSION……80
CHAPTER 5……83
5.1 INTRODUCTION……84
5.2 HETEROGENEOUS BLOOD-TUMOR BARRIER PERMEABILITY……85
5.3 INVASIVE TECHNOLOGIES……91
5.4 NON-INVASIVE TECHNOLOGIES……95
5.5 NANOPARTICLES AND TARGETED DELIVERY……100
5.6 CONCLUSION AND FUTURE PERSPECTIVES……110

CHAPTER 6……112
6.1 INTRODUCTION……113
6.2 MATERIALS AND METHODS……117
6.2.1 CHEMICALS, REAGENTS, AND TISSUES……117
6.2.2 ANIMALS……117
6.2.3 MMAE INTRAVENOUS PHARMACOKINETIC STUDIES……118
6.2.4 ABBV-221 INTRAPARITONEAL PHARMACOKINETIC STUDY……119
6.2.5 ABBV-221 AND FREE MMAE CED PHARMACOKINETIC STUDIES……119
6.2.6 MMAE FORCED DECONJUGATION……120
6.2.7 MMAE LC-MS/MS ANAYLSIS……123
6.2.8 PHARMACOKINETIC PARAMETER ESTIMATION……124
6.2.9 STATISTICAL ANALYSIS……125
6.3 RESULTS……126
6.3.1 MMAE INRAVENOUS PHARMACOKINETIC STUDIES……126
6.3.2 ABBV-221 INTRAPARITONEAL PHARMACOKINETIC STUDY……129
6.3.3 MMAE CED PHARMACOKINETIC STUDY……132
6.3.4 ABBV-221 CED PHARMACOKINETIC STUDY……135
6.4 DISCUSSION……140

CHAPTER 7……145

BIBLIOGRAPHY……...**150**

LIST OF TABLES

Table 1.1 Partial List of Brain Endothelial Cell Membrane Transporters……4

Table 1.2 Brain Endothelial Cell Transporters of Xenobiotics/Drugs……..5

Table 3.1 Summary Pharmacokinetic Parameters for Loperamide and OMI in ICR Mice Following IV Administration, Alone and in Combination……..……..……..……..……42

Table 3.2 Summary Pharmacokinetic Parameters for Loperamide and OMI in ICR Mice Following Oral Administration, Alone and in Combination……..……..……..……..……48

Table 4.1 Summary Pharmacokinetic Parameters of Loperamide in Wild-type and Transgenic FVB Mice Following IV Administration with and without OMI……..……..……..……..……..69

Table 4.2 Distributional Advantage for Brain and Spinal Cord in Transgenic FVB Mice……..……..……..……70

Table 4.3 Summary Pharmacokinetic Parameters of OMI Wild-type and Transgenic FVB Mice Following IV Administration with and without Loperamide……..……..……..……..……77

Table 4.4 Unbound Fractions of Loperamide and OMI in Brain and Plasma……..……..……..……..……..79

Table 6.1 Summary Pharmacokinetic Parameters of MMAE……..……128

Table 6.2 Free and Total MMAE Tissue Exposures Following IP Administration of ABBV-221……..……..……..……131

Table 6.3 MMAE Tissue Exposures Following CED of MMAE……..……134

Table 6.4 Free and Total MMAE Tissue Exposures Following CED Administration of ABBV-221……..……..……..……138

Table 6.5 Matrix of P-values Following AUC_{last} Comparisons for ABBV-221 CED Pharmacokinetic Study……..……**139**

LIST OF FIGURES

Figure 1.1 The Blood-brain Barrier (BBB).....**6**

Figure 3.1 Elucidating Synergistic Mechanisms for a Combination of Opioid Agonists……**27**

Figure 3.2 Potency of Oral Loperamide with and without Co-administration of OMI in ICR Mice……..**38**

Figure 3.3 Loperamide IV Pharmacokinetics and CNS Distribution in ICR Mice……**41**

Figure 3.4 OMI IV Pharmacokinetics and CNS Distribution in ICR Mice……**45**

Figure 3.5 Loperamide Oral Pharmacokinetics and CNS Distribution in ICR Mice……..**47**

Figure 3.6 OMI Oral Pharmacokinetics and CNS Distribution in ICR Mice……**50**

Figure 4.1 Loperamide IV Pharmacokinetics and CNS Distribution in FVB Mice……**65**

Figure 4.2 Loperamide IV Pharmacokinetics and CNS Distribution in FVB Mice with Co-administration of OMI……..**66**

Figure 4.3 Loperamide CNS Partitioning in FVB Transporter Knockout Mice……..**67**

Figure 4.4 OMI IV Pharmacokinetics and CNS Distribution in FVB Mice……..**73**

Figure 4.5 OMI IV Pharmacokinetics and CNS Distribution in FVB Mice with Co-administration of Loperamide……..**74**

Figure 4.6 OMI CNS Partitioning in FVB Transporter Knockout Mice……**75**

Figure 5.1 The Blood-tumor Barrier (BTB) ……..**87**

Figure 5.2 Invasive Strategies for Drug Delivery to Brain Tumors……..**92**

Figure 5.3 Blood-brain Barrier Disrupting Strategies for Drug Delivery to Brain Tumors……..……..……..……..……..……..**97**

Figure 5.4 Receptor-mediated Transcytosis for Drug Delivery to Brain Tumors……..……..……..……..……..……**105**

Figure 6.1 Predicted vs Observed Concentrations of MMAE……..……**122**

Figure 6.2 MMAE IV Pharmacokinetic Studies……..……..……..**127**

Figure 6.3 ABBV-221 IP Pharmacokinetic Study……..……..……..**130**

Figure 6.4 MMAE CED Pharmacokinetic Study……..……..……**133**

Figure 6.5 ABBV-221 CED Pharmacokinetic Study……..……..…**137**

LIST OF ABBREVIATIONS

ADC…….Antibody-drug conjugate

AUC…….Area Under the Curve

BBB…….Blood-brain barrier

BCRP…….Breast cancer resistance protein

BCSFB…….Blood-cerebrospinal fluid barrier

BTB…….Blood-tumor barrier

CED…….Convection enhanced delivery

CNS…….Central nervous system

DOR…….δ-opioid receptor

EC…….Endothelial cell

EGFR…….Epiedermal growth factor receptor

FUS…….Focused ultrasound

FVB…….Friend leukemia virus B

ICR…….Institute for Cancer Research

IGFR……..Insulin-like growth factor receptor

IT…….Intrathecal

LRP1…….Lipoprotein-like receptor protein 1

MMAE…….Monomethylauristatin E

MMAF…….Monomethylauristatin F

MOR……..μ-opioid receptor

MRI…….Magnetic resonance imaging

NVU…….Neurovascular unit

OMI…….Oxymorphindole

P-gp…….P-glycoprotein

RMT…….Receptor-mediated transcytosis

TfR…….Transferrin receptor

CHAPTER 1

THESIS OVERVIEW

1.1 CENTRAL NERVOUS SYSTEM BARRIERS

The barriers of the central nervous system (CNS) are a set of highly specialized and selective tissues. These CNS barriers broadly include the blood-brain barrier (BBB), the blood-cerebrospinal fluid barrier (BCSFB), and the arachnoid epithelium, and serve to maintain a strict homeostasis that protects the CNS and allows for optimal neuronal function (Abbott *et al.*, 2010). The CNS barriers are robust barriers that actively exclude many potentially harmful substances from the CNS, but they also have been one of the greatest hurdles to the development of novel therapeutics to treat CNS diseases. In this way, the CNS barriers, in particular the BBB, play a pivotal role in the success or failure of novel drugs with the potential for CNS activity (Pardridge, 2005).

1.2 BLOOD-BRAIN BARRIER

The BBB is by far the major blood-tissue interface in the brain, and creates a vast surface area with the potential for rapid transport of nutrients into the brain and the removal of waste. The current model of the brain microvasculature consists of several different cell types working collectively to form a functional neurovascular unit (NVU) (Abbott *et al.*, 2010; Sweeney *et al.*, 2019). The NVU is comprised of endothelial cells, astrocytes, pericytes, and a complex basal lamina. The specialized endothelial cells lining the vasculature are zipped tightly together by tight junction (TJ) proteins. These polarized endothelial cells are characterized by restricted pinocytic activity, a lack of fenestrations, and the expression of a particular set of receptors and transport proteins on their luminal and abluminal membranes (**Table 1.1,1.2**)(Terasaki and Ohtsuki, 2005; Abbott *et al.*, 2010). The endothelial cells and their tight junctional contacts are surrounded by pericytes that form gap junctions with multiple adjacent endothelial cells and by astrocytic endfeet that cover >99% of the endothelial-pericyte cell surface

(**Figure 1**). The astrocytes in turn extend processes that monitor synaptic activity and react by signaling endothelial cells and pericytes to respond to increased metabolic demands by increasing nutrient delivery. Microglia, the resident immune cells, are extravascular when dormant, but react swiftly to remove cellular debris (phagocytosis) or respond to inflammatory signals associated with disease or injury. All of the cells associated with the NVU play an integral role in maintaining barrier integrity.

Table 1.1 Partial List of Brain Endothelial Cell Membrane Transporters

Transport System	Typical Substrate	SLC Family	Common Name
Carbohydrates			
Hexose	Glucose	SLC2A1	GLUT1
Sodium myo-inositol	Myo-inositol	SLC5A3	SMIT
Monocarboxylates			
Monocarboxylic acid	Lactic acid ketones	SLC16A1	MCT1
Amino Acids			
Large neutral amino acid	Phenylalanine	SLC7A5	LAT1
Small neutral amino acid	Alanine	SLC38A2	SNAT2,-3, -5
Cationic amino acid	Lysine	SLC7A1	CAT1, CAT3
Beta amino acid	Taurine	SLC6A6	TauT
Ala-Ser-Cys	Ala, ser, cys	SLC1A4	ASCT1,-2
Excitatory amino acid	Glutamic acid	SLC1A2	EAAT-1,-2,-3
Glycine	Glycine	SLC6A9, A5	GT-1
Others			
Fatty acids	Essential FA LPC-PC (DHA)	SLC44A1/2 Mfsd2A	FATP-1, -4 Mfsd2A
Nucleoside	Adenosine	SLC29A1 SLC28A1	ENT-1, -2 CNT1-3
Hormones	Thyroid T3 Thyroid T4	SLC16A2 OATP1C1	MCT8 OATP1C1
Biotin, pantothenic acid	Biotin	SLC5A6	SMVT
Folic acid	Folic acid	SLC46A1	PCFT
Copper	Cu^{+}	SLC31A1	CTR1

Table 1.2 Brain Endothelial Cell Transporters of Xenobiotics/Drugs.

Members of the ABC superfamily of transporters demonstrated in brain endothelial cells and non-ABC transporters of organic chemical potentially present are listed.

Transport System	Common Name	Typical Substrate
ATP Binding Cassette Transporter (ABC)		
ABCB1	P-gp	Broad spectrum, xenobiotics
ABCG2	BCRP	mitoxantrone anthracycline xenobiotics
ABCC1	MRP1	GSSG, leukotrienes
ABCC5	MRP5	Thiopurines,Cyclic nucleotides
ABCC4	MRP4	Organic anions
Non ABC Transporters		
SLC22A7 SLC22A8 SLC20A2 SLCO1A4 SLCO2B1	OAT2-3 OATP1A4 OATP2B1 OCTN2 OCT1-3	Organic ions

Figure 1.1 The Blood-Brain Barrier (BBB)

The BBB is composed of specialized endothelial cells and support cells including pericytes and astrocytes. The cross-sectional view illustrates that the majority of the abluminal surface of the endothelial cell is covered by pericytes and astrocytic foot processes. Paracellular transport across the BBB is restricted by tight junction proteins, and even small, lipophilic molecules that might diffuse across the BBB may be subject to active efflux by a variety of proteins. Facilitated active transport, receptor mediated transport, and ion transporters allow for the brain to be supplied with nutrients while maintaining strict homeostasis.

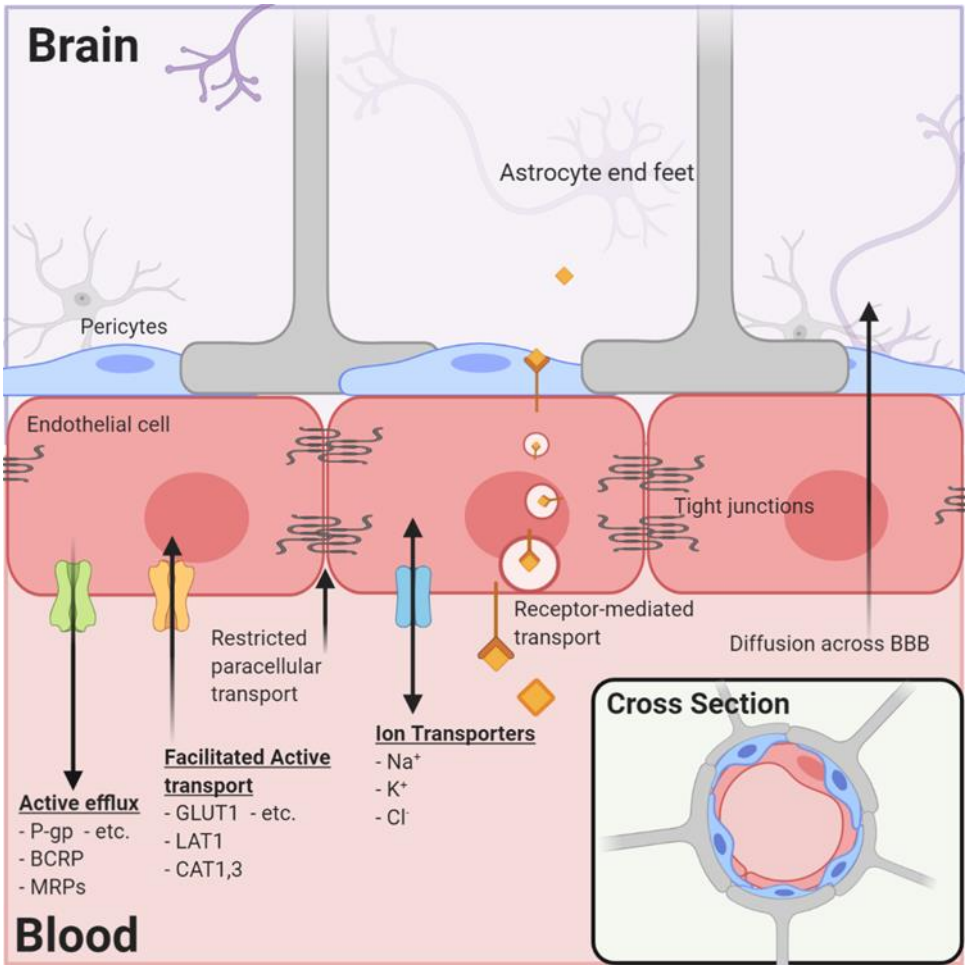

1.3 ROLE OF THE CNS BARRIERS IN DRUG DISTRIBUTION

As previously stated, the CNS barriers play a pivotal role in the distribution and disposition of drugs in the CNS. The BBB in particular is the main barrier of concern for this work. Due to the tightly-associated cellular barrier of the BBB, large biologics and hydrophilic molecules cannot readily enter the brain via paracellular transport mechanisms (Abbott *et al.*, 2010). Therefore, drugs must enter the brain by diffusion across endothelial cells or by facilitated active or passive transport via ion channels or the transport proteins listed in **Tables 1.1 and 1.2**. Due to the limitations in paracellular transport, it has been thought that only small, lipophilic drugs have the best chance of crossing the BBB and reaching the brain parenchyma at appreciable concentrations. However, it is known that lipophilicity of small molecules does not necessarily correlate with brain penetration, and total brain penetration does not necessarily correlate to effect (Boström *et al.*, 2008). This is due to two main reasons. First, many lipophilic xenobiotics are substrates for efflux from endothelial cells by membrane-bound ATP-binding cassette transporters like P-glycoprotein (P-gp, ABCB1, MDR1) and breast cancer resistance protein (BCRP, ABCG2)(**Table 1.2**)(Waghray and Zhang, 2018)**.** These transporters, among others, can effectively pump a wide variety of molecules against a concentration gradient, often preventing the penetration of effective concentrations of drugs into the brain parenchyma. Efforts are being made to design drugs to evade efflux liability (Salphati *et al.*, 2012; M Kim *et al.*, 2019), but these efforts have yet to result in FDA-approved drugs for the greatest areas of clinical need, such as brain tumors, Parkinson's disease, and Alzheimer's disease.

The second factor preventing the CNS penetration and efficacy of small lipophilic compounds is their propensity to be highly bound. According to the Free Drug Hypothesis, only unbound drug is able to diffuse across cell membranes or exert a

pharmacodynamic effect. Molecules that are highly-bound in plasma are likely to have lower brain penetration (Hammarlund-Udenaes *et al.*, 2008). Furthermore, drugs that are highly bound must generally achieve much higher total concentrations in the brain in order to exert appreciable pharmacodynamic effects. Due to limitations imposed by off-target peripheral toxicities, these concentrations are often impossible to achieve via systemic administration. However, in the case where brain permeability is not desired, the difficulty of penetrating the BBB can be an asset to drug development.

1.4 SCOPE OF DISSERTATION

The interplay among efflux, binding, and a drug's potency for its target make predicting CNS permeability, efficacy, and safety a nuanced endeavor. With the development of large molecules intended for CNS diseases, this landscape has only become more complex. On the one hand, the CNS barriers can be an asset to drug development, in that the safety of drugs may be significantly enhanced due to their exclusion from the CNS. On the other hand, CNS barriers have prevented recent advances in molecular engineering and precision medicine that have resulted in improvements in treatment of peripheral disease from translating to diseases of the CNS. This dissertation deals with both aspects of this paradigm.

The first portion of the work is focused on the CNS distribution and pharmacokinetics of a novel combination of opioid agonists with synergistic activity. In this work, the BBB plays a role in enhancing the safety of this combination of small molecules, limiting their ability to induce the undesirable and dangerous side effects that have plagued the use of opioid analgesics. These chapters characterize the systemic and CNS pharmacokinetics of both molecules, loperamide and oxymorphindole, alone and in combination. In its entirety, this work describes the systemic pharmacokinetics, CNS penetration, efflux liability, and potential for pharmacokinetic interactions between the two drugs with reference to the target receptor physiology and nature of the synergistic effects.

The second portion of the work describes the potential for the use of antibody-drug conjugates (ADCs) administered via convection-enhanced delivery (CED) in the treatment of brain tumors. While the BBB has heretofore prevented the efficacious delivery of ADCs to brain tumors following systemic administration (Marin *et al.*, 2021), CED presents a potential mechanism to salvage these therapeutics, which have provided exemplary clinical benefit in other cancers, for the treatment of brain tumors.

This chapter describes the CNS distribution and pharmacokinetics of ADC payload molecules following multiple routes of administration of both free payload and ADC, providing insight into potential benefits and pitfalls of the administration of ADCs via CED.

1.5 STATEMENT OF THE PROBLEM

The distribution of novel therapeutics into brain is a fundamental concern for a variety of drugs which may or may not be intended for the treatment of CNS diseases. In the first case, where CNS distribution may induce undesirable off-target effects, assessing CNS exposure is an important component of determining the safety of novel therapeutics. However, in the second case, where the CNS is the target tissue, it is imperative to determine whether exposure at the site of action is sufficient to be efficacious with reference to undesirable peripheral toxicities. These concerns are evident with both conventional small molecules and novel biologics, and are relevant across therapeutic areas. Major factors impacting the exposure, efficacy, and safety of drugs in the CNS include their size, lipophilicity, protein binding, and efflux liability. Alternative modes of administration, like convection-enhanced delivery, can bypass some of the difficulties associated with brain permeability, but do not avoid all factors that determine brain exposure. The characterization of CNS distribution and pharmacokinetics of novel therapeutics in these various contexts is integral to understand all aspects of their potential effects.

1.6 RESEARCH OBJECTIVES

The overall research objective of this dissertation is to assess the CNS distribution and pharmacokinetics of novel therapeutics that may or may not be intended to target the CNS. This overall research objective is divided into two major goals: 1) to determine the CNS exposure of a combination of opioids where the objective is to evaluate the CNS delivery of a molecule not intended for CNS action, and, 2) to determine the CNS exposure of an antibody-drug conjugate payload intended to treat tumors in the CNS following different routes of administration. The long-term goal of this dissertation is to inform the safe clinical deployment of these novel therapeutics. The research objectives of this dissertation are the following:

CHAPTER 3: Characterize the systemic pharmacokinetics and efficacy of a novel combination of opioids and assess the potential for pharmacokinetic interactions

CHAPTER 4: Assess the role of efflux transporters in the CNS permeability of a novel combination of opioids and assess the potential for interactions at the BBB

CHAPTER 6: Characterize the pharmacokinetics and CNS distribution of ADC payload molecules following systemic and CNS administration of ADCs and free payload

1.7 RESEARCH APPROACH

Central Hypothesis

The central hypothesis of this dissertation is that the CNS barriers represent an important determinant of drug delivery to the CNS, thereby modulating both CNS efficacy and/or off-target CNS effects.

Research Collaboration

Collaboration is central to this work. First, our collaborators in the Wilcox and Fairbanks labs at the University of Minnesota have developed and validated animal models to ascertain the analgesic and antihyperalgesic efficacy of novel therapeutics. Their work provides a compelling basis for assessing novel combinations of opioids for future clinical viability, and their expertise in pain signaling both peripheral to and inside the CNS is invaluable in this work. Second, our research collaborators at the Mayo Clinic have successfully established a method to administer therapeutics to mice via CED, and have tested this method in their extensive library of patient-derived xenograft models of GBM. This method has been integral to the data herein for assessing the CNS and systemic distribution and pharmacokinetics of ADCs and payload molecules following this route of administration.

1.8 SPECIFIC AIMS

Specific Aim 1. (CHAPTER 3)

Determine the potential for significant pharmacokinetic interactions between loperamide and oxymorphindole that could affect the safety or efficacy of the combination.

- **Rationale:** Previous work has shown that specific combination of opioids have synergistic efficacy at many-fold lower doses than those currently employed in the clinic. However, the mechanism of this synergy has not yet been entirely elucidated, and the pharmacokinetics of these combinations, which might factor in their safety, have not been examined.
- **Working hypothesis:** The working hypothesis for this aim is that there are no significant pharmacokinetic interactions between oxymorphindole and loperamide that might alter their efficacy or safety in combination.
- **Approach:** This hypothesis will be tested through the determination of drug distribution and pharmacokinetic parameters following oral and IV administration of loperamide, oxymorphindole, or the combination to Institute for Cancer Research (ICR) mice.

Specific Aim 2. (CHAPTER 4)

Determine the efflux substrate status of oxymorphindole and assess the potential for interactions between loperamide and oxymoprhindole at the barriers of the CNS.

- **Rationale:** Loperamide is an avid P-gp substrate, a characteristic that allows it to be used as an antidiarrheal medication without the significant CNS effects that are commonly associated with opioid agonists. However, the substrate status of oxymorphindole has never been determined, and could contribute to interactions with loperamide at the CNS barriers that may result in undesired effects. This transporter liability should be determined, and potential interactions well understood, prior to further development.
- **Working hypothesis:** Due to the similarity of oxymorphindole (OMI) structure with other P-gp substrates, the working hypothesis for this aim is that OMI is a P-gp substrate.
- **Approach:** This hypothesis will be tested by assessing drug distribution into the CNS of transgenic friend leukemia virus (FVB) mice lacking either P-gp, BCRP, or both following IV administration of loperamide, oxymorphidole, or the combination.

Specific Aim 3. (CHAPTER 6)

Characterize the CNS and systemic exposure of payload molecules following the administration of ADCs via CED.

- **Rationale:** Previous studies have shown that the efficacy of ADCs in the treatment of brain tumors is limited by poor delivery and off-target toxicities. Administration of these drugs via CED could improve this therapeutic index, but the exposure of active payload at both the target site and sites of toxicity has not been assessed.
- **Working hypothesis:** The working hypothesis of this aim is that administration via CED will result in increased CNS exposure while limiting systemic exposure.
- **Approach:** This hypothesis will be tested by assessing brain and systemic exposure of ADC payloads following the administration of ADCs via CED. These exposures will be compared to those following the administration of free payload via CED as well as the systemic administration of ADCs.

CHAPTER 2

BRIEF REVIEW: OPIOID AGONISTS AND THE CENTRAL NERVOUS SYSTEM

2.1 A BRIEF HISTORY OF OPIOIDS

Opioids were some of the first drugs to have been isolated and synthesized (Presley and Lindsley, 2018a). Originally derived from the opium poppy, the benefits and risks of opioids have been apparent for nearly as long as they have been in use, even if their mechanisms were poorly understood for the majority of the nearly 8,000 years of their recorded importance. While the oldest known association between opium poppies and humans dates to the Neolithic period, these associations point to the use of poppy seeds rather than the capsules (the flowering bulb from which opium is collected) in which the highest concentrations of opioid alkaloids occur (Kumar, 2022). Therefore, some of the oldest specific evidence of the use of alkaloid-containing derivatives of the opium poppy have been found in artifacts from ancient Mediterranean civilizations like the Mycenaeans on mainland Greece and Minoans on Crete (Kumar, 2022). A popular theory is that the first reference to opium poppies could be found in Sumerian tablets, but this transcription has now been refuted (Krikorian, 1975) . The first recorded reference to specific medicinal use of the opium poppy are found in ancient Greek and Roman medicine, where it is referenced as a narcotic or purging agent. Then, in early Arabic medicine, it was largely prescribed for ocular maladies and for patients suffering from dysentery (Macht, 1915). Extracts of the opium poppy were incorporated into a number of very popular remedies and antidotes in the early pharmacopeia, and were also commonly used as poisons. Later, opium was often referred to as indispensable to early European physicians. However, while the benefits of opium for pain management and sleep became more recognized again in the 1600s, so did their risks for addiction, tolerance, and death, among other side effects, which were widely reported by physicians in medical literature by the 1800s (Kumar, 2022).

In 1805 Friedrich Wilhelm Adam Sertürner isolated a basic salt from opium and determined that this substance was principally responsible for its sedative properties

(Schmitz, 1985). While it went largely unnoticed in the early years after his publication, this alkaloid was morphine. The isolation of this natural product was then scaled up by another German chemist, Heirich Emmanuel Merck in 1820 (Presley and Lindsley, 2018a), and subsequently, other natural alkaloids of the opium poppy like codeine were isolated. Heroin was the first semisynthetic opioid, first synthesized in 1895 and mass-produced by Bayer starting in 1898, and a waterfall of other semisynthetic and synthetic opioids followed. By 1914, more stringent control of the dispensation and drug content of products containing narcotics had been introduced in the United States by the Food, Drug, and Insecticide Administration (later the FDA). By the mid-20th century, opioid analgesics had been largely relegated to relief of post-operative pain or palliative care for cancer patients. However, in the early 1970s and into the 1980s, the under-treatment of patients experiencing severe pain began to gain more notice, and some advocated for more liberal dosing of opioids (Marks and Sachar, 1973) as well as use in settings outside of cancer or post-operative pain management (Portenoy and Foley, 1986).

Following the establishment of these more liberal prescribing habits, such as the "titrate to effect" methodology, as well as the downplay of their addictive effects, the prevalence of opioid use disorder and opioid overdose deaths began to rise in the late 1990s and early in the 21st century (Kumar, 2022). Deaths due to prescription opioids are estimated to have numbered in the hundreds-of-thousands between 1999 and 2010 (Hedegaard *et al.*, 2017). While the approval of abuse-deterrent formulations of opioids and new prescribing guidelines helped to significantly diminish the widespread prescription of large doses of opioids, individuals who found their access to prescription medications to be limited began transitioning to illicit drugs like heroin (Rudd *et al.*, 2014; Hedegaard *et al.*, 2015). This further accelerated the rise in opioid-linked fatalities, and was often referred to as the 'second wave' of the ongoing opioid crisis in the United States. Currently, the United States is in the grip of a third wave of opioid overdose

fatalities, largely linked to synthetic opioids, fentanyl in particular (O'Donnell *et al.*, 2017). While it is clear that many victims are exposed to fentanyl accidentally, these unintentional exposures along with the COVID-19 pandemic have accelerated the rate of increase in opioid overdose fatalities. Opioid overdose deaths increased by nearly 30% from 2020 to 2021, according to the CDC and its National Vital Statistics System. Despite the known and very apparent dangers of conventional opioid analgesics, there are still no FDA-approved alternatives to analgesics like morphine, codeine, fentanyl, and oxycodone, to treat severe pain. In this context, it is imperative that safer options for pain management become available.

2.2 OPIOID RECEPTORS AND THEIR PHYSIOLOGY

The first proposal of a specific receptor site responsible for analgesia was examined through the use of opioid agonists and antagonists in 1954 (Beckett and Casy, 1954). Following this proposal of a receptor site in the general sense, it was first proposed that opioid agonists and antagonists most likely bind specifically to a receptor or class of receptors in 1965 (Portoghese, 1965), and this interaction was demonstrated in nervous tissue in 1973 (Pert and Snyder, 1973; Simon *et al.*, 1973). It is now known that there are three classes of opioid receptors: μ, δ, and κ opioid receptors, heretofore referred to by MOR, DOR, and KOR, respectively, with potential pharmacological subtypes possible due to alternative splicing or posttranslational modifications (Stein, 2016). Opioid receptors are not only expressed in nervous tissue, but also in other tissues throughout the body as well as immune cells. Though all three classes of receptors are expressed both within and outside of the CNS, MORs and DORs have been shown to have higher expression in the CNS as compared to KORs, which are expressed more universally in peripheral organs like liver, lung, and spleen (Peng *et al.*, 2012).

Opioid receptors are inhibitory G protein-coupled receptors, and the existence of these receptors as well as endogenous agonists is evidence for their integral role in modulation of pain. During pain signaling, ion channels in primary afferent neurons open, allowing the influx of Ca^{2+} and Na^{+} ions (Stein, 2016). If the initial depolarization is large enough, this can generate further depolarization and the generation of an action potential, which carries the signal to the dorsal horn of the spinal cord and eventually to the brain. Activation of opioid receptors by endogenous or exogenous ligands, their dimerization, and subsequent signaling through specific G protein subunits can inhibit a variety of downstream signaling pathways. Downstream signaling involving the G_{α} subunit regulates cyclic AMP production, while the $G_{\beta\gamma}$ subunit modulates the opening of membrane-bound ion channels that help hyper-polarize a cell to prevent the generation of action potentials (Stein, 2016). This can all together decrease neuron excitability or completely inhibit the propagation of action potentials along the journey between primary afferent neurons, where the painful signal originates, and the brain, where the signal is processed. This reduction in excitability has the potential to reduce pain signaling at all levels of the nervous system and results, overall, in the significantly decreased perception of pain.

While pain signaling can be regulated by both the peripheral and central nervous systems, as well as by all three classes of receptors, some common side effects of opioid agonists are regulated by receptors in particular locations and even specific receptor splice variants (Law *et al.*, 2013). For example, respiratory depression, reward, and euphoria are largely mediated by MORs in the brain (Matthes *et al.*, 1996; Pattinson, 2008). Similarly, DORs in the brain appear to be largely responsible for convulsions (Broom *et al.*, 2002), and dysphoria is mediated by KORs (Laurence Lalanne *et al.*, 2014). There is also a large body of evidence that opioid receptors can form heteromdimers (Gomes *et al.*, 2000). Co-localization and heterodimerization of different

classes of opioid receptors in neurons have been demonstrated repeatedly (Jordan and Devi, 1999; Wessendorf and Dooyema, 2001; Wang *et al.*, 2005), and the administration of combinations of opioid agonists elicits pharmacodynamic effects that may be synergistically active and unique to the combinations (Daniels *et al.*, 2005; Lenard *et al.*, 2007; Schuster *et al.*, 2015). This specificity in CNS signaling downstream of different classes and combinations of opioid receptors provides opportunities for the development of novel analgesics with optimal safety profiles.

2.3 CNS DISTRIBUTION OF OPIOIDS

As with any small molecule drug, the activity of opioids both within and outside of the CNS depends on their potency, distribution, and free concentration at the site of action (Hammarlund-Udenaes *et al.*, 2008). Due to the presence of the CNS barriers, including the blood-brain barrier (BBB) and blood-cerebrospinal fluid barrier (BCSFB) among others, many drugs have limited CNS permeability, and this limited delivery has significant impacts on CNS-mediated effects (Abbott, 2013). This is true for opioid agonists as well. Lipophilicity is one factor that can influence the distribution of opioid agonists into the CNS, but lipophilicity, brain penetration, and subsequent pharmacodynamic efficacy are not always directly correlated. Many opioid agonists across receptor specificity are subject to efflux by P-glycoprotein (P-gp) at the blood-brain barrier (Ekblom *et al.*, 1992; Letrent *et al.*, 1999; Zong and Pollack, 2000; Dagenais *et al.*, 2004; Kalvass *et al.*, 2007). However, the degree to which P-gp affects their distribution into the CNS is variable. It is clear that even substrates for efflux like morphine and fentanyl exhibit potent CNS effects, implying that their affinity for the receptor more than makes up for limitations in their delivery to the CNS. Oxycodone, on the other hand, is a substrate for active influx at the CNS barriers, and despite its lower affinity for MORs, it shows similar potency to morphine (Boström *et al.*, 2006). Taken as

a whole, the full consideration of drug delivery as well as drug potency continues to be one of the most important factors in the safety and efficacy of opioid analgesics (Boström *et al.*, 2008).

Given that opioid receptors in the CNS modulate the majority of the most dangerous side effects of opioid agonists that have driven the opioid epidemic, there is increasing attention being paid to the role that peripherally-mediated analgesia could play in the future of pain management (Stein and Machelska, 2011). Both the local and topical administration of opioids has been shown to be effective despite limited systemic exposure (Smith *et al.*, 2015; Uhelski *et al.*, 2020). Furthermore, the systemic administration of peripherally-restricted combinations of opioid agonists with synergistic effects has also been shown to be a very promising avenue for pain management with limited potential for centrally-mediated side effects (Bruce *et al.*, 2019). Together, these studies show how limiting CNS exposure through either limiting systemic exposure, or through the use of peripherally-restricted synergistic combinations can significantly improve the safety profile of opioids. In a very real sense, the CNS barriers play an opposite role in that they enhance the safety and efficacy of some opioids, as opposed to the prohibitive role they play in hindering the development of other types of therapeutics intended for the treatment of CNS disease. Subsequent chapters discuss the CNS distribution of a combination of opioid agonists that are thought to be peripherally-active.

CHAPTER 3

SYSTEMIC DISPOSITION OF AN OPIOID AGONIST COMBINATION WITH SYNERGISTIC ACTIVITY

The content of this Chapter has been published in:

Griffith JI, Kim M, Bruce DJ, Peterson CD, Kitto KF, Mohammad AS, Rathi S, Fairbanks CA, Wilcox GL, Elmquist WF (2021) *Journal of Pharmacology and Experimental Therapeutics* 380(1):34-46.

3.1 INTRODUCTION

Opioid agonists remain the most commonly prescribed treatment for moderate-to-severe pain, and have been in use for centuries (Presley and Lindsley, 2018a). The efficacy of these drugs in chronic and severe pain is well-characterized and has yet to be supplanted in modern clinical practice. However, along with their potent analgesic effects, opioid agonists are accompanied by well-known and sometimes dangerous adverse effects like constipation, sedation, respiratory depression, a liability to dependence, and the development of tolerance (Presley and Lindsley, 2018). In recent decades, rampant over prescription of opioids has led to an epidemic of opioid use disorder and overdose deaths. While subsequent enforcement efforts and prescribing guidance from the Centers for Disease Control and Prevention (CDC) hoped to stem the tide of overdose deaths (Dowell *et al.*, 2016), there are still few alternatives to opioid agonists when it comes to severe pain management. The CDC estimated in 2016 that approximately 20% of adults in the United States suffer from chronic pain (Dahlhamer *et al.*, 2018). A more recent study estimated that 4.8% of adults have high-impact chronic pain, and 13.8% experience pain that limits their daily activities (Pitcher *et al.*, 2019). This experience of pain can result in depression, anxiety, and poor overall quality of life. As a result, 3-4% of the entire US population is prescribed opiates for long-term pain management when the benefits of opioids are thought to outweigh the inherent risks (Dowell *et al.*, 2016). Individuals requiring long-term pain management may include cancer patients and those with postoperative pain, or individuals experiencing neuropathic and chronic pain from a variety of causes. In light of the risks of long-term opioid use, it is imperative that new, effective treatments with minimized risks become available for these patients.

In the search for novel treatments with reduced side effects, combinations of receptor-selective opioid agonists and other compounds have shown potential for potent analgesic and antihyperalgesic effects with reduced liability to tolerance and respiratory depression. Recently published work from Bruce et al. showed that loperamide, a μ-opioid receptor (MOR) agonist, when dosed subcutaneously in a 1:1 combination with the δ-opioid receptor (DOR) agonist oxymorphindole (OMI), exhibited efficacious pain management in the face of inflammatory pain (Bruce *et al.*, 2019). This work is compelling in that efficacious pain management is achieved at many fold lower doses of loperamide, and the combination is peripherally active (Bruce *et al.*, 2019; Uhelski *et al.*, 2020). There is a body of evidence supporting the hypothesis that heterodimerization of MORs with DORs results in downstream signaling that is different than conventional MOR dimerization (Gomes *et al.*, 2000, 2004; Lenard *et al.*, 2007; Schuster *et al.*, 2015). However, the potential for interactions in systemic disposition and CNS distribution that could contribute to the synergy of these two drugs has not been determined. Therefore, there exist two possible mechanisms of action: one having to do with a change in pharmacokinetics, and one due to a change in pharmacodynamics and signaling at and downstream of the MOR/DOR receptor sites (**Figure 3.1**).

In this study, we sought to clarify the mechanism of this synergy by determining whether there is a systemic pharmacokinetic interaction between loperamide and OMI when the two drugs are administered in combination. The primary objective of the current study was to determine if the synergistic effect was related to changes in pharmacokinetics or changes in pharmacodynamics.

Figure 3.1 Elucidating Synergistic Mechanisms for a Combination of Opioid Agonists

Previous publications have shown synergistic activity of loperamide and OMI when co-administered. Two possible mechanisms exist for this synergy: a change in CNS distribution and/or systemic disposition, and heterodimerization of MORs and DORs that result in altered downstream signaling.

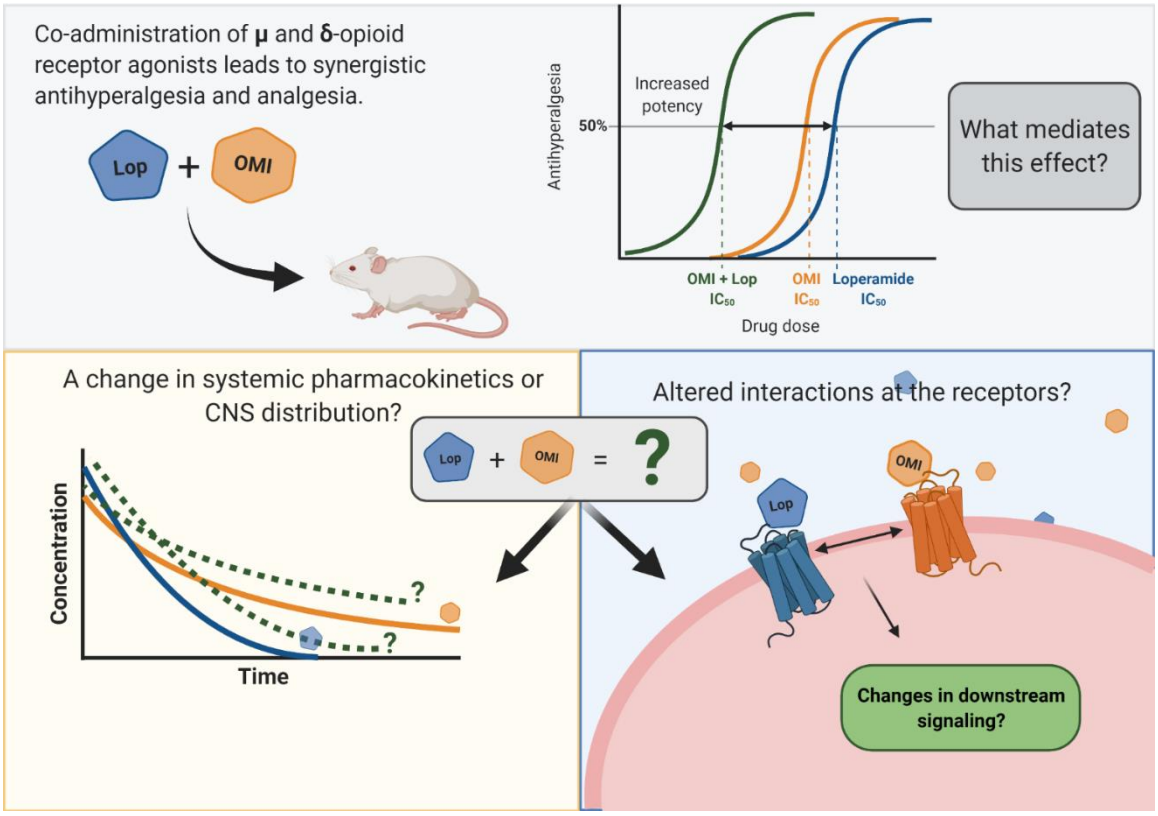

3.2 MATERIALS AND METHODS

3.2.1 Chemicals and Reagents:

Loperamide hydrochloride and naltrindole hydrochloride were obtained from Tocris Bioscience (via Fisher Scientific). [^{6}H]Loperamide was purchased from Alsachim (Illkirch-Graffenstaden, France). Oxymorphindole (OMI), was a gift from the lab of Dr. Phil Portoghese (Portoghese *et al.*, 1988). All other chemical reagents were high-performance liquid chromatography grade and purchased from Thermo Fisher Scientific.

3.2.2 Animals:

For the behavioral experiment, adult ICR-CD1 mice (22-29g, N = 90, male and female) were housed four (male) or five (female) to a cage and maintained on a 12-hour light/dark cycle with *ad libitum* access to water and food. Testing was performed during the light phase of this cycle. For the pharmacokinetic studies, male ICR mice (Envigo, Madison, WI) of age 8-14 weeks were used for initial studies as noted and housed in the Research Animal Resources facility in the Academic Health Center of the University of Minnesota prior to use. All mice for pharmacokinetic studies were maintained on a 12-hour light/dark cycle with *ad libitum* access to water and food. Protocols for all animal experiments received approval by the University of Minnesota Institutional Animal Care and Use Committee and were performed in accordance with the Guide for Care and Use of Laboratory Animals established by the U.S. National Institutes of Health.

3.2.3 Drug Preparation and Administration for Oral ED50 Calculation:

Formulations were prepared as a solution with 5% cremophore and DMSO, and subsequently diluted to administered concentrations with sterile water. Solutions were administered by oral gavage using a 20ga X 30mm sterile plastic feeding tube (Fine

Science Tools, USA). No fluid was noted in the nose, an indication of aspirated solution, in any subject during or following gavage. Thermal nociceptive responses were assessed once prior to CFA administration, a baseline was assessed following CFA administration, and one hour following oral gavage of experimental compound.

3.2.4 Behavioral Measures:

The Hargreaves assay was used to assess peripheral thermal nociception, as described previously (Hargreaves *et al.*, 1988). Briefly, mice were placed in a small plastic box to restrict their movement on a heated glass floor (30°C). Animals were allowed to acclimate to the testing environment for 15 minutes prior to baseline withdrawal assessment. A radiant heat lamp was then shone on the left hind paw until the mouse withdrew the paw, and the paw latency was recorded (baseline) by a plantar stimulator antinociception meter (IITC Lifesciences, USA). A cutoff time of 20 s was established to prevent tissue damage. Three paw withdrawal latencies were recorded with a minimum of 30 s rest time between each test.

After determining naïve paw withdrawal latencies (PWLs), animals were briefly anesthetized using 2.5% isoflurane and 30 µL of an emulsion of 1:1 Complete Freund's Adjuvant (CFA) in saline was injected into the left hindpaw. 3-5 days following this injection, a well-characterized hyperalgesia was present in the left hindpaw, and post-CFA PWLs were assessed (post CFA value) (Newbould, 1963). The experimental compounds (loperamide, OMI, or their combination) were then delivered by oral gavage. One hour following oral gavage, thermal responses were again assessed (experimental value). Each animal received only one dose of compounds or of the combination. The experimenters were not blinded to drug or concentration during compound administration or behavioral testing. One experimenter delivered compound to all subjects, and a separate experimenter performed all PWL assessment.

3.2.5 Data Analysis of Behavioral Measures:

Thermal nociceptive responses following oral gavage of OMI, loperamide, or their combination were analyzed as a percentage of antihyperalgesia (%AH) given by the following equation:

$$\%\,\boldsymbol{AH} = \frac{([\boldsymbol{post\ CFA\ value - baseline}] - [\boldsymbol{experimental\ value - baseline}])}{(\boldsymbol{post\ CFA\ value - baseline}) \times \mathbf{100}}$$

(1)

The ED_{50} of loperamide and loperamide in the presence of oxymorphindole (Lo (+OMI)) were calculated using the graded dose-response curve method (Tallarida and Murray, 1987).

3.2.6 Systemic Pharmacokinetics and CNS Distribution Studies:

Single doses of loperamide, OMI, or a combination of the two drugs were administered to ICR mice via tail vein injection or oral gavage. Dosing formulations for both drugs were first prepared in sterile water for injection (SWFI) with 5% DMSO and 5% Cremophore. This solution was subsequently diluted 4X in SWFI to the final concentrations of 1 mg/mL for IV studies and 6 mg/mL for oral studies (1% DMSO, 1% Cremophore), with the exception of the first OMI IV study, which was diluted 2 mg/mL. The first OMI IV study was conducted with a dose of 10 mg/kg, which was well tolerated. However, when loperamide was initially dosed to two animals at 10 mg/kg IV, it was found to be poorly tolerated, and the dose was lowered to 5 mg/kg. All subsequent IV studies for both drugs were conducted with a dose of 5 mg/kg.

After IV administration, blood, brain, and spinal cord samples were collected at time points from 10 minutes to 16 hours (n=4 mice per time point). After oral administration, samples were collected from 30 minutes to 16 hours (n=4 mice per time point). Mice were euthanized via a CO_2 chamber. Blood was rapidly collected via cardiac puncture using heparinized syringes and transferred into heparinized tubes. Plasma was separated by centrifugation at 7500 rpm for 15 minutes at 4°C. Spinal cords were collected via the hydraulic extrusion method as described by Roberts et al. (Roberts *et al.*, 2005). Briefly, after decapitation, the spinal column rostral of the pelvis was removed. Then, a saline-filled syringe fixed with a blunt-tipped needle was inserted into the caudal end of the spinal column. The plunger was depressed to extrude the spinal cord fully intact. Plasma, brain, and spinal cord were stored at -80°C until LC-MS/MS analysis. Prior to analysis, brain and spinal cord were thawed and homogenized in 2X (w/v) 5% BSA.

3.2.7 LC-MS/MS Analysis:

Given their widely disparate hydrophobicity, separate LC-MS/MS methods were developed for loperamide and OMI. Both methods utilized reverse-phase liquid chromatography via an Aligent 1200 Series HPLC connected to a TSQ Quantum Classic mass spectrometer in positive ion mode. Briefly, both drugs and their internal standards were extracted from plasma, brain homogenate, and spinal cord samples via liquid-liquid extraction with 5X (v/v) ethyl acetate. Samples were vortexed for 5 minutes and centrifuged. Supernatant was collected and completely dried under nitrogen, and samples were reconstituted with mobile phase (MP). For loperamide, the internal standard was [^{6}H]-loperamide, and for OMI, the internal standard was naltrindole. Both methods used a Phenomenex Synergi 4µm Polar-RP column (4µm, 75 x 2mm) for chromatographic separation and a MP flow rate of 0.3 mL/minute. For loperamide, the method was isocratic with a MP composition of aqueous phase (A) 45% distilled water with 0.1% formic acid and organic phase (B) of 55% acetonitrile with 0.1% formic acid and a total run time of 4 minutes. The OMI method utilized gradient elution with initial MP composition of aqueous phase (A) 75% distilled water with 0.1% formic acid and organic phase (B) 25% acetonitrile with 0.1% formic acid. The gradient was as follows: starting at 3 minutes, organic phase was increased to 90% over 0.75 minutes, held at 90% for 1.25 minutes, and decreased back to 25% over 0.5 minutes. It was then held at 25% for 4.5 minutes for a total runtime of 10 minutes. The *m/z* transition for all molecules were as follows: loperamide 478.1 → 267.3, [^{6}H]-loperamide 484.1 → 273.3, OMI 375.1 → 254.1, naltrindole 415.1 → 254.1. For both methods, the standard curve was linear over the range of 0.1-1000ng/mL (weighted $1/Y^2$) with coefficients of variation less than 15%. Data were acquired and analyzed using Xcalibur software. The inter-day variability for loperamide for all concentrations in the standard curve was less than 4%, the intra-day variability was less than 7%, and the limit of quantification was 0.1 ng/mL. For OMI, the

inter-day variability was less than 15%, the intra-day variability was less than 7% and the limit of quantification was 0.1 ng/mL.

3.2.8 Pharmacokinetic Parameter Estimation

Plasma, brain, and spinal cord concentration-time profiles were analyzed using Phoenix WinNonlin version 8.3 (Certara USA Inc., Princeton, NJ). Brain concentrations were corrected for residual blood estimated at 1.4% of brain weight and with blood concentrations approximated by plasma concentrations (Fridén *et al.*, 2010). Pharmacokinetic parameters and metrics were calculated by performing noncompartmental analysis (NCA). Areas under the curve (AUCs) were determined by linear trapezoidal integration, where the AUC to the last time point (AUC_{Last}) was calculated directly. The AUC to time infinity ($AUC_{0\rightarrow\infty}$) was extrapolated from the last time point to infinite time by dividing the concentration at the last time point (C_{Last}) by the terminal elimination rate constant (λ_z) as determined by the last 4 time points. In cases where the terminal slope was not sufficiently negative for the time course of these experiments, AUC_{Last} is reported rather than $AUC_{0\rightarrow\infty}$. Variances for $AUCs_{Last}$ were calculated using the Bailer method as reported in Phoenix WinNonlin (Bailer, 1988). Variances for $AUC_{0\rightarrow\infty}$ were calculated utilizing the Yuan extension of the Bailer method (Yuan, 1993).

Other pharmacokinetic parameters, including systemic clearance (CL), apparent clearance (CL/F), volume of distribution (V_{ss}) and apparent volume of distribution (V/F) as well as the terminal half-life ($t_{1/2}$) were also calculated by NCA in Phoenix software by the following methods:

$$\boldsymbol{CL\ and\ CL/F = \frac{Dose}{AUC_{0\rightarrow\infty}}} \qquad (3)$$

$$V_{ss} = MRT_{inf} \times CL \qquad (4)$$

Where MRT_{inf} is the area under the first moment curve to infinity ($AUMC_{inf}$) divided by the $AUC_{0\rightarrow\infty}$.

$$t_{1/2} = \frac{ln\,(2)}{\lambda_z} \qquad (5)$$

Where λ_z is the terminal first-order elimination rate constant associated with the log-linear portion of the concentration-time profile and is estimated by linear regression of time vs log-concentration.

The brain-to-plasma ratio, or brain tissue partition coefficient (Kp_{Brain}), for each drug was calculated as a ratio of the AUC of the brain concentration-time profile to the AUC of the plasma concentration-time profile (Equation 6). Similarly, the spinal cord-to-plasma ratio, or spinal cord tissue partition coefficient ($Kp_{Spinal\ Cord}$) was calculated as a ratio of the AUCs (Equation 7). The brain partition coefficient of free drug (Kp_{uu}) was calculated by multiplying the Kp_{Brain} by the ratio of unbound fractions in brain and plasma (Equation 8).

$$Kp_{Brain} = \frac{AUC_{Brain}}{AUC_{\ Plasma}} \qquad (6)$$

$$Kp_{Spinal\ Cord} = \frac{AUC_{Spinal\ Cord}}{AUC_{Plasma}} \qquad (7)$$

$$Kp_{uu} = Kp_{Brain} \times \frac{fu_{Brain}}{fu_{Plasma}} \quad (8)$$

The tissue-to-plasma concentration ratio at time t is used to assess the extent of drug distribution over time, and will be notated as Kp_t values for both brain and spinal cord. These were calculated by the following:

$$Kp_t = \frac{Concentration_{tissue}}{Concentration_{plasma}} \quad (9)$$

The oral bioavailability (F) of both drugs was calculated by Equation 9:

$$F = \left\{\frac{[AUC_{(0\rightarrow\infty),plasma}]\ oral}{[AUC_{(0\rightarrow\infty),plasma}]IV}\right\}\left(\frac{Dose_{IV}}{Dose_{oral}}\right) \quad (10)$$

The distributional advantage (DA) achieved in mice lacking efflux transporters at the CNS barriers was calculated by the following equation.

$$DA_{(brain\ or\ spinal\ cord)} = \frac{Kp_{Brain\ or\ spinal\ cord}\ transporter\ knockout\ mice}{Kp_{Brain\ or\ spinal\ cord}\ wild-type\ mice} \quad (11)$$

3.2.9 Statistical Analysis:

Data are represented as mean ± S.D. where applicable. For the behavioral study, the data were analyzed by non-linear regression, fitting an [agonist] vs. response curve to compare ED50 values by GraphPad Prism (version 8.4; Graphpad Software, La Jolla, CA), with a null hypothesis that the ED50s for both data sets were equal. To compare

AUCs among studies and between different tissues, a two-tailed unpaired *t* test was performed in Graphpad Prism with a null hypothesis that AUCs were equal. One-way ANOVA with Tukey's multiple comparisons test was performed to compare AUCs among WT and transporter knockout mice in Graphpad. A significance level of $P < 0.05$ was considered significant in all tests.

3.3 RESULTS

3.3.1 Oral ED_{50} of Loperamide with and without OMI

`The oral ED50 for loperamide was 51.8 mg/kg, and the oral ED50 for loperamide with OMI was 0.68 mg/kg. The best fit models for the dose-response curves resulted in a rejection of the null hypothesis ($p<0.01$), indicating that the potency of loperamide is increased when administered in combination with OMI (**Figure 3.2**). OMI individual ED50 could not be determined from these data.

Figure 3.2 Potency of oral loperamide with and without co-administration of OMI in ICR mice.

Peripherally-mediated thermal nociceptive responses in the Hargreaves assay were assessed. Following CFA-induced inflammation in the hindpaw, subjects were given an oral gavage of loperamide, OMI or combination and post-drug nociceptive responses were taken one hour post-administration. Responses are reported as % anti-hyperalgesia, which was used to generate dose-response curves. The data were analyzed by non-linear regression, fitting an [agonist] vs. response curve to compare ED50 values by GraphPad Prism 8.4.

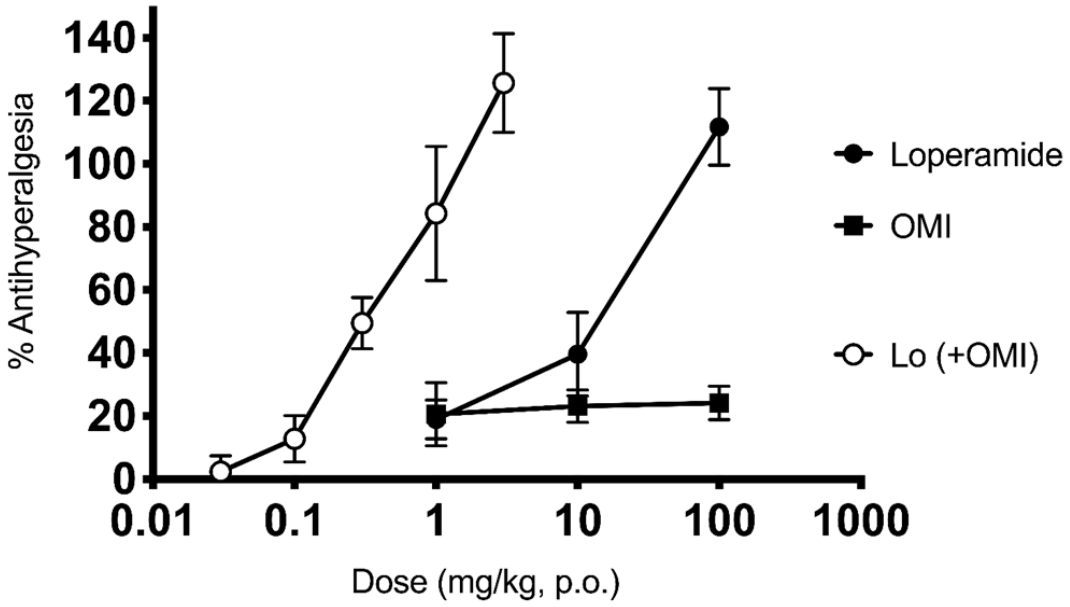

3.3.2 Loperamide Disposition in ICR mice

In order to determine whether the co-administration of OMI and loperamide changes their CNS distribution or systemic pharmacokinetics, the two drugs were dosed alone and in combination. Brain, plasma, and spinal cord were collected and the concentrations of drug in each tissue were determined by LC-MS/MS. The total (bound + unbound drug) plasma, brain, and spinal cord concentration-time profiles for a single IV dose of loperamide alone (5 mg/kg) and loperamide in combination with OMI (5 mg/kg) in ICR mice are shown in **Figures 3.3A and 3.3B**. The plasma, brain, and spinal cord concentrations were below the limit of quantification for these studies at 12 and 16 hr time points, and therefore these were not included. Concentration-time profiles in all tissues exhibited biexponential decline over time. For loperamide alone, brain concentrations were significantly lower than that of plasma ($p < 0.001$), and spinal cord concentrations were lower than that of brain and significantly lower than plasma ($p < 0.001$) for the duration of the time course. For loperamide in combination with OMI, the same trend was observed. The tissue-to-plasma concentration ratios over time (Kp_{tBrain} and $Kp_{t\ Spinal\ Cord}$, **Figures 3.3C and 3.3D**) remain less than 1 for the duration of the time course. Accordingly, the overall Kp_{Brain} and $Kp_{Spinal\ Cord}$ as calculated by AUC ratios were also less than 1 for both discrete dosing and combination studies, which was expected, as loperamide is a P-gp substrate (**Table 3.1**). Loperamide appears to reach a rapid distributional equilibrium in the CNS, as Kp_t did not change over the time course in either brain or spinal cord.

The pharmacokinetic parameters for loperamide alone and in combination with OMI are also listed in **Table 3.1**. There was no apparent difference among the parameters of $t_{1/2}$, CL, or V in the two studies. The difference among AUCs in plasma, brain, and spinal cord for loperamide alone and loperamide in combination with OMI was non-significant ($p = 0.966$, $p = 0.312$, and $p = 0.779$, respectively.)

Figure 3.3 Loperamide IV Pharmacokinetics and CNS Distribution in ICR mice.

(A) Plasma, brain, and spinal cord concentration-time profiles following a single IV dose (5 mg/kg) of loperamide (B) Plasma, brain, and spinal cord concentration-time profiles following a single IV dose of loperamide (5 mg/kg) co-administered with OMI (5 mg/kg) (C) Kp_{tBrain} of loperamide from the pharmacokinetic studies described by A and B (D) $Kp_{tSpinal\ Cord}$ from the pharmacokinetic studies described by A and B.

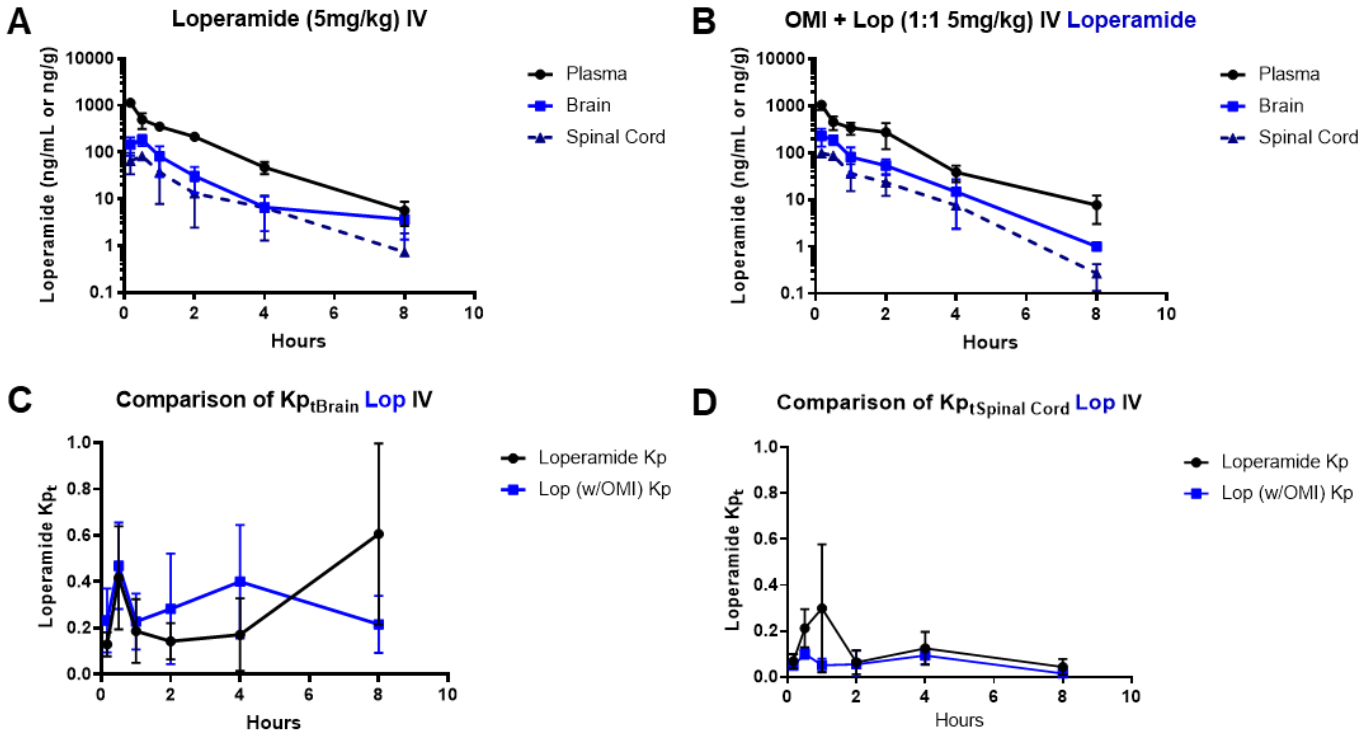

Table 3.1 Summary pharmacokinetic parameters for loperamide and OMI in ICR mice following IV administration alone and in combination.

OMI exposures are dose-normalized. A two-tailed unpaired t-test was performed to compare AUCs among tissues (see results) and between the same tissues in discrete vs. combination studies (*p <0.001).

Results are presented as mean or mean ± S.D.

Parameter	Loperamide Alone (5mg/kg)	Loperamide in Combination (5mg/kg)	OMI Alone (dose-normalized)	OMI in Combination (dose-normalized)
$t_{1/2}$ (h)	1.16	1.23	3.35	3.9
CL (L/h)/kg	3.6	3.6	12	6.6
V L/kg	4.7	4.9	17.6	11.6
$AUC_{0\rightarrow\infty}$ Plasma (h*ng)/mL	1389 ± 140	1374 ± 299	84 ± 6*	149 ± 16*
$AUC_{0\rightarrow\infty}$ Brain (h*ng)/g	257 ± 55	347 ± 65	175 ± 15	219 ± 20
$AUC_{0\rightarrow\infty}$ Spinal Cord (h*ng)/g	163 ± 32	151 ± 28	43 ± 3	63 ± 10
Kp_{Brain}	0.19	0.25	2.0	1.4
$Kp_{Spinal\ Cord}$	0.12	0.11	0.51	0.42

3.3.3 OMI disposition in ICR mice

The total (bound + unbound drug) plasma, brain, and spinal cord concentration-time profiles for single IV dose of OMI (10 mg/kg) and OMI in combination with loperamide (5 mg/kg) in ICR mice are shown in Figures **3.4A and 3.4B**. The plasma, brain, and spinal cord concentrations show a pronounced distributional phase in both the discrete and combination studies. Brain and spinal cord concentrations are greater than plasma in the terminal phase for both studies, and this is apparent in **Figure 3.4C**, where Kp_{tBrain} (calculated as concentration ratios over time) is greater than unity at 2 hours for both OMI alone and OMI in combination. Similarly, in both the discrete dosing and combination studies, the $Kp_{tSpinal\ Cord}$ is greater than unity at 4 hours after administration (**Figure 3.4D**). OMI appears to take longer than loperamide to reach dynamic equilibrium between plasma and the CNS, as the Kp_t for both brain and spinal cord reaches a maximum around 8-12 hours after administration. The overall Kp_{Brain} was 2.0 for OMI dosed alone, and 1.4 for OMI dosed in combination (**Table 3.1**). The overall $Kp_{spinal\ Cord}$ was 0.51 in the discrete dosing study, and 0.42 in the combination study.

There was no difference in the half-life of OMI between the discrete and combination studies. In order to compare the AUCs between discrete dosing and the combination, dose-normalized AUCs were used, as the two studies were performed at difference doses. When dose-normalized AUCs were compared, the plasma $AUCs_{0\rightarrow\infty}$ in the combination study (149 ± 16 h*ng/mL) was significantly higher than the plasma $AUC_{0\rightarrow\infty}$ for OMI alone (84 ± 6 h*ng/mL, $p < 0.001$, **Table 3.1**). There also appeared to be evidence of an increase in the dose-normalized AUC for both brain and spinal cord, though the difference was not statistically significant.

Regarding OMI systemic exposure, because the AUC depends on dose and clearance, assuming linear pharmacokinetics, the most likely explanation for an increase in the AUC is a reduction in the systemic clearance of OMI. This is evident in a

decreased clearance from 12 (L/h)/kg for OMI alone to 6.6 (L/h)/kg for OMI in combination (**Table 3.1**).

Figure 3.4 OMI IV Pharmacokinetics and CNS Distribution in ICR mice.

(A) Plasma, brain, and spinal cord concentration-time profiles following a single IV dose (10 mg/kg) of OMI (B) Plasma, brain, and spinal cord concentration-time profiles following a single IV dose of OMI (5 mg/kg) co-administered with loperamide (5 mg/kg) (C) Kp_{tBrain} of OMI from the pharmacokinetic studies described by A and B (D) $Kp_{tSpinal\ Cord}$ of OMI from the pharmacokinetic studies described by A and B.

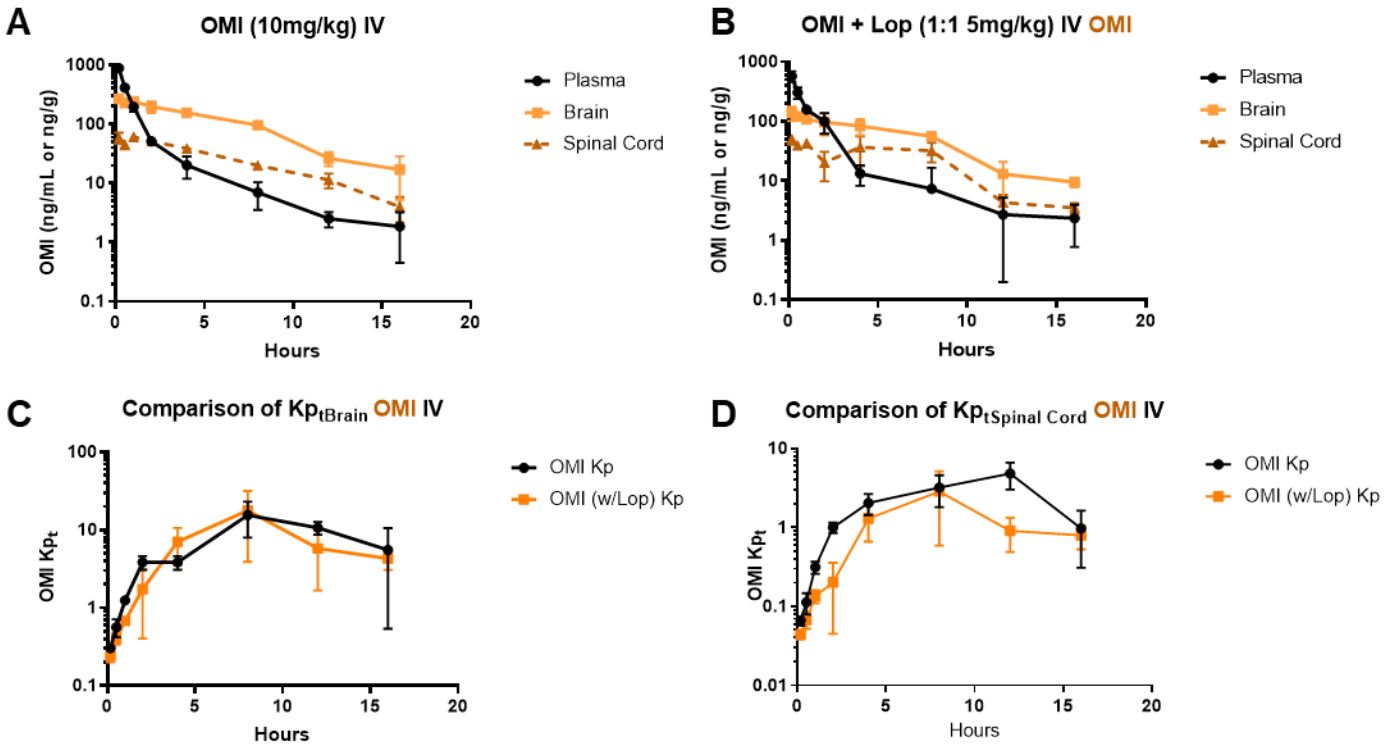

3.3.4 Loperamide PO Systemic Pharmacokinetics and CNS distribution in ICR mice

Loperamide and OMI were also administered orally to assess systemic pharmacokinetics, CNS distribution, and bioavailability of the drugs when dosed in combination. The total plasma, brain, and spinal cord concentration-time profiles for loperamide in mice when dosed at 30mg/kg alone and in combination with OMI (30mg/kg) are shown in **Figures 3.5A and 3.5B**. Similarly to the IV studies, the brain and spinal cord concentrations in the PO study are less than the plasma for the duration of the time course, and therefore the Kp_{tBrain} and $Kp_{tSpinal\ Cord}$ were also less than unity (**Figures 3.5C and 3.5D**). However, these concentration-time profiles in both studies show some evidence of multiple peaks, possibly because loperamide undergoes enterohepatic recycling (Miyazaki *et al.*, 1979). The t_{max} occurred at 1 hour for loperamide alone and at 4 hours for loperamide with OMI. The half-life for loperamide alone and in combination was 7 and 3.1 hours, respectively (**Table 3.2**). The apparent clearance (CL/F) for loperamide when dosed alone was similar to CL/F in the combination study, and the differences in the AUCs between the two studies for plasma, brain, and spinal cord were all nonsignificant (p=0.49, p=0.150, and p=0.720, respectively), and in accord with the IV studies, the bioavailability (F) was also not different (F=0.19 and F=0.25, **Table 3.2**).

Figure 3.5 Loperamide Oral Pharmacokinetics and CNS Distribution in ICR mice.

(A) Plasma, brain, and spinal cord concentration-time profiles following a single oral dose (30 mg/kg) of loperamide (B) Plasma, brain, and spinal cord concentration-time profiles following a single oral dose of loperamide (30 mg/kg) co-administered with OMI (30 mg/kg) (C) Kp_{tBrain} of loperamide from the pharmacokinetic studies described by A and B (D) $Kp_{tSpinal\ Cord}$ from the pharmacokinetic studies described by A and B.

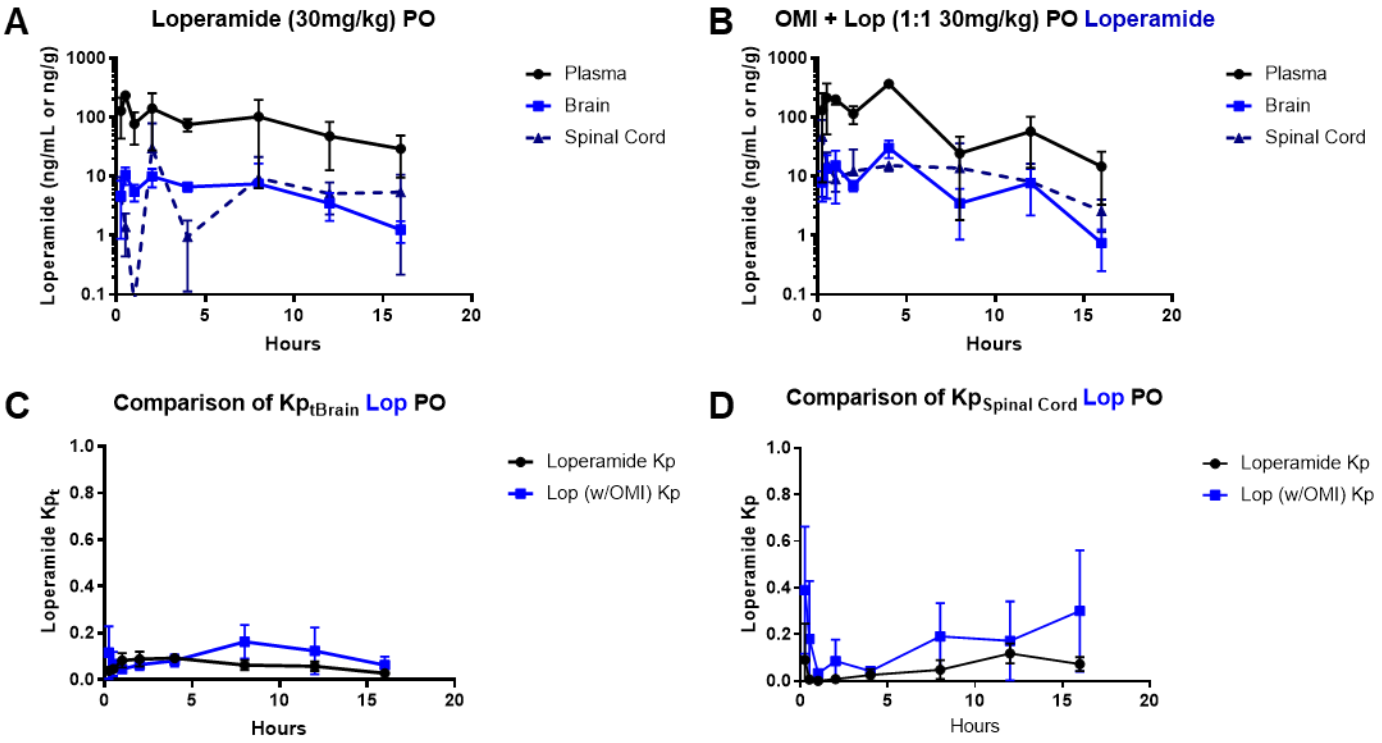

Table 3.2 Summary pharmacokinetic parameters for loperamide and OMI in ICR mice following oral administration alone and in combination.

A two-tailed unpaired t-test was performed to compare AUCs among tissues (see results) and between the same tissues in discrete vs. combination studies (*p=0.014). Results are presented as mean or mean ± S.D.

Parameter	Loperamide Alone (30 mg/kg)	Loperamide in Combination (30mg/kg)	OMI Alone (30 mg/kg)	OMI in Combination (30 mg/kg)
$t_{1/2}$ (h)	7	3.1	2.5	4.5
CL/F (L/h)/kg	19	15.5	22.3	51.2
V/F L/kg	192	70.3	80 L/kg	162
C_{max} (ng/mL)	235	370	345	186
T_{max} (h)	0.5	4	1	0.5
$AUC_{0\rightarrow\infty}$ Plasma (h*ng)/mL	1577 ± 427	1936 ± 290	1386 ± 191*	745 ± 166*
$AUC_{0\rightarrow\infty}$ Brain (h*ng)/g	94 ± 13	162 ± 40	1762 ± 296	1121 ± 262
$AUC_{0\rightarrow\infty}$ Spinal Cord (h*ng)/g	304 ± 220	223 ± 44	744 ± 273	615 ± 262
Kp_{Brain}	0.06	0.08	1.27	1.5
$Kp_{Spinal\ Cord}$	0.19	0.12	0.54	0.82
F	0.19	0.25	0.55	0.17

3.3.5 OMI PO systemic Pharmacokinetics and CNS distribution in ICR mice

The total concentration-time profiles for OMI administered at 30 mg/kg alone and in combination are shown in **Figures 3.6A and 3.6B**. The t_{max} occurred at 1 hour for OMI alone and at 30 minutes for OMI in combination with loperamide. The Kp_{tBrain} for OMI alone and in combination showed a similar trend as in the IV studies (**Figure 3.6C)**, however the concentration in brain did not surpass the concentration in plasma until after 4 hours in the PO studies. The overall brain-to-plasma ratio for OMI was greater than 1 for both the discrete and combination studies, and were similar (Kp_{Brain} = 1.27 and 1.5, respectively, **Table 3.2**). In accordance to the IV studies, the concentrations of OMI in spinal cord were less than brain and only surpassed plasma concentrations at later time points (**Figure 3.6D**). The overall spinal cord-to-plasma ratios were 0.54 for OMI alone and 0.82 in combination with loperamide (**Table 3.2**). The plasma AUC for OMI alone was significantly greater than AUC plasma for OMI in the combination (p=0.014). In accord with the IV studies, the oral bioavailability of OMI when dosed orally with loperamide was reduced from 0.55 to 0.17 (**Table 3.2**). However, when comparing the AUCs for brain and spinal cord for OMI alone and OMI in combination, the AUCs were indistinguishable (p=0.111 and p=0.735, **Table 3.2**).

Figure 3.6 OMI Oral Pharmacokinetics and CNS Distribution in ICR mice.

(A) Plasma, brain, and spinal cord concentration-time profiles following a single oral dose (30 mg/kg) of OMI (B) Plasma, brain, and spinal cord concentration-time profiles following a single IV dose of OMI (30 mg/kg) co-administered with loperamide (30 mg/kg) (C) Kp_{tBrain} of OMI from the pharmacokinetic studies described by A and B (D) $Kp_{tSpinal\ Cord}$ of OMI from the pharmacokinetic studies described by A and B.

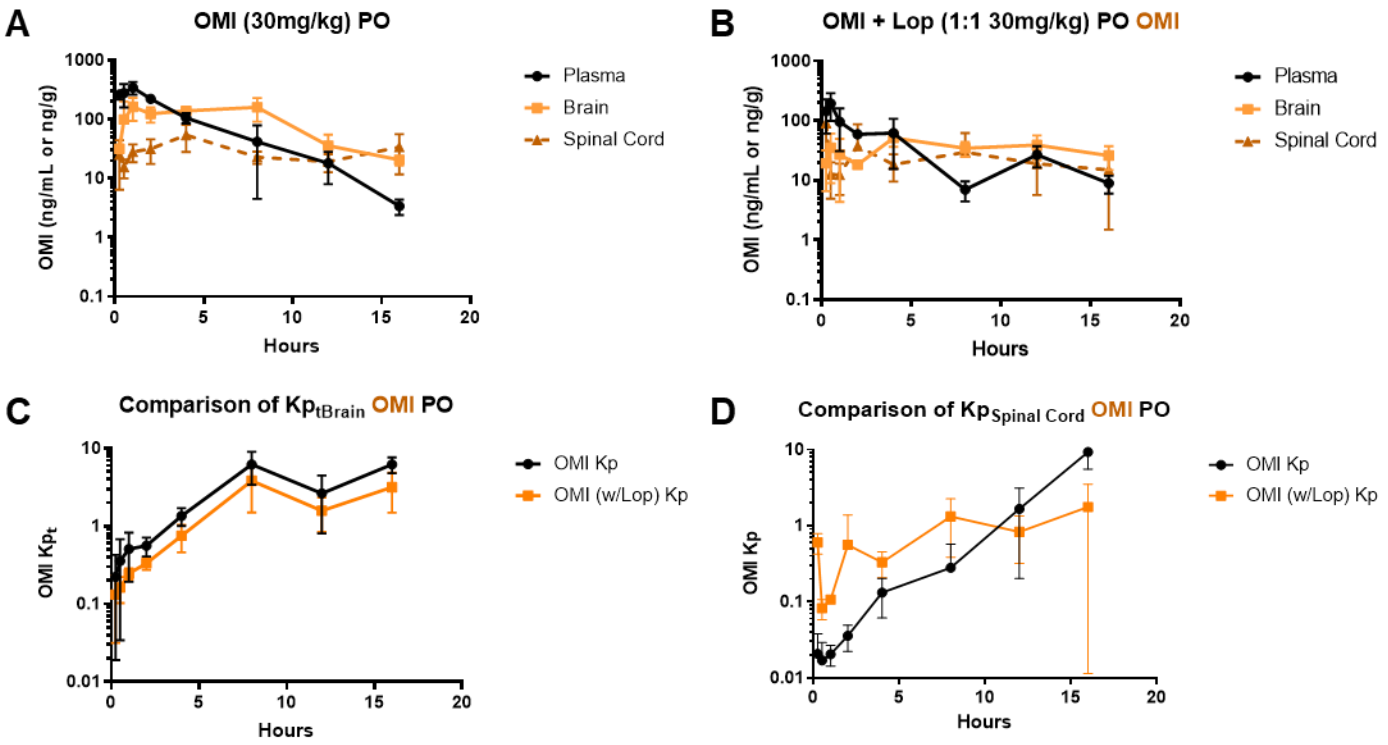

3.4 DISCUSSION

Opioid agonists have a long history of effective use in the treatment of pain. However, along with their benefits come a number of caveats and risks like tolerance, dependence, and death (Presley and Lindsley, 2018b). This has led to demand for more prudent prescription practices and alternatives to the conventional use of opioids. One promising avenue for alternatives is through combinations of biased opioid agonists targeting the μ- and δ-opioid receptors. Loperamide is a MOR-agonist that is already FDA-approved as an antidiarrheal medication, and oxymorphindole is a novel DOR-agonist with high selectivity (Takemori *et al.*, 1992). In combination, these drugs have shown to be peripherally active with synergistic efficacy (Bruce *et al.*, 2019; Uhelski *et al.*, 2020) or at least significantly increased potency of loperamide, depending on the route of administration (**Figure 3.2**). While there are proposed mechanisms of action for this significant increase in potency, it could be due to a change in pharmacokinetics or CNS penetration (**Figure 3.1**). Our pharmacokinetic assessment sought to clarify whether these drugs have a pharmacokinetic interaction. In the present study, we administered loperamide and OMI alone and in combination to ICR mice. The ICR mouse studies provide continuity with previously published pharmacodynamic studies and give information about the systemic disposition of both drugs.

The results from the loperamide IV administration studies in ICR mice indicate that OMI has no significant effect on loperamide systemic pharmacokinetics or CNS distribution that might alter the activity or safety of this drug. With reference to safety, MOR agonists are of particular concern, as the reward signaling and adverse effects of dependence and respiratory depression are mediated by MORs in the CNS (Matthes *et al.*, 1996; Pattinson, 2008). The present studies show no change in the total Kp_{Brain}, $Kp_{Spinal\ Cord}$ of loperamide. Following oral administration of the combination, there is no significant change in loperamide's systemic disposition, CNS distribution, or oral

bioavailability. Given that the combination was administered at doses nearly 10-fold higher than the oral ED_{50} for this pharmacokinetic assessment, the likelihood of a pharmacokinetic interaction that changes the efficacy or safety of loperamide is even lower at the therapeutic oral doses, and would be of little concern for future development of this combination therapy.

In assessing the disposition and CNS distribution of OMI for the first time, it was found that OMI has appreciable CNS penetration, and that the plasma and CNS exposure of OMI is increased in the presence of loperamide. According to the IV administration studies in ICR mice, while the overall exposure in the CNS increases when OMI is administered with loperamide, the increase in CNS exposure is proportional to the increased plasma exposure. Further, given OMI's tolerability in ICR mice at a higher dose of 10 mg/kg IV, and the fact that DORs do not promote the undesirable effect respiratory depression, the distribution of OMI to the CNS is not a present concern with regards to safety. In fact, certain DORs have been shown to modulate some opioid effects such as tolerance; therefore OMI CNS penetration could be an advantage of the combination (Zhu *et al.*, 1999; Pradhan *et al.*, 2009). In the case of oral administration, the systemic exposure of OMI is significantly reduced. This is likely due to the decreased bioavailability of OMI when administered in the combination. According to the pharmacodynamic data, significantly lower oral doses of the combination show increased potency, and therefore a potential reduction in the bioavailability of OMI is not likely to be a limitation of the combination.

Subsequent studies will assess the efflux liability of OMI and determine whether there is a change in the unbound CNS partitioning of either drug when administered in combination. This assessment will further inform the potential for the safe clinical development of this combination for the treatment of pain.

CHAPTER 4

CNS DISPOSITION OF AN OPIOID AGONIST COMBINATION WITH SYNERGISTIC ACTIVITY

The content of this Chapter has been published in:

Griffith JI, Kim M, Bruce DJ, Peterson CD, Kitto KF, Mohammad AS, Rathi S, Fairbanks CA, Wilcox GL, Elmquist WF (2021) *Journal of Pharmacology and Experimental Therapeutics* 380(1):34-46.

3.1 INTRODUCTION

The distribution of opioids to the CNS plays a crucial role in the activity and use of opioid agonists. Sedation, respiratory depression, and addiction are mediated by MOR in the CNS as shown by studies in MOR knockout mice (Matthes *et al.*, 1996; Pattinson, 2008). Alterations in loperamide systemic pharmacokinetics or distribution to the CNS resulting from co-administration with OMI might play a role in the mechanism of action and safety of this combination. Because loperamide has long been known to be a P-glycoprotein (P-gp, ABCB1) substrate for efflux from the CNS as well as the gut epithelium (Schinkel *et al.*, 1996), it is possible that synergistic activity between these two drugs results from alterations in systemic pharmacokinetics or CNS drug distribution. This is especially important since the efflux status of OMI has not been determined. Previous studies have shown that the pharmacodynamics of opioids as well as their off-target effects are dependent on not only the drug's potency and affinity for the target receptor, but also the CNS partitioning and free concentrations at the site of action (Ekblom *et al.*, 1992; Xie and Hammarlund-Udenaes, 1998; Boström *et al.*, 2006, 2008). In this context, it is imperative to characterize the total CNS distribution, efflux liability, and unbound partitioning of these two opioids.

In this study, we sought to determine the substrate status of oxymorphindole, and to assess whether its efflux substrate status could be a factor that may influence the safety or efficacy of this combination of opioid agonists.

4.2 MATERIALS AND METHODS

4.2.1 Chemicals and Reagents:

Loperamide hydrochloride and naltrindole hydrochloride were obtained from Tocris Bioscience (via Fisher Scientific). [^{6}H]Loperamide was purchased from Alsachim (Illkirch-Graffenstaden, France). Oxymorphindole (OMI), was a gift from the lab of Dr. Phil Portoghese (Portoghese *et al.*, 1988). All other chemical reagents were high-performance liquid chromatography grade and purchased from Thermo Fisher Scientific. Rapid equilibrium dialysis plates and inserts (8kDa molecular weight cutoff) were also purchased from Thermo Fisher Scientific.

4.2.2 Animals:

Both male and female Friend Leukemia Virus strain B (FBV) mice of age 8-14 weeks of four different genotypes were used for transporter knockout studies. These genotypes included wild-type, *Bcrp*$^{-/-}$ (Bcrp knockout, BKO), *Mdr1a/b*$^{-/-}$ (P-gp knockout, PKO), and *Bcrp*$^{-/-}$ *Mdr1a/b*$^{-/-}$(triple knockout, TKO) mice (breeder pairs from Taconic Biosciences, Inc., Germantown, NY). Colonies of the FVB mice were maintained and housed in the RAR facility at the Academic Health Center of the University of Minnesota, and animal genotypes were regularly verified by tail snip (TransnetYX, Cordova, TN). All mice for pharmacokinetic studies were maintained on a 12-hour light/dark cycle with *ad libitum* access to water and food. Protocols for all animal experiments received approval by the University of Minnesota Institutional Animal Care and Use Committee and were performed in accordance with the Guide for Care and Use of Laboratory Animals established by the U.S. National Institutes of Health.

4.2.3 CNS Distribution Studies:

Single doses of loperamide, OMI, or a combination of the two drugs were administered to FVB mice via tail vein injection. Dosing formulations for both drugs were first prepared in sterile water for injection (SWFI) with 5% DMSO and 5% Cremophore. This solution was subsequently diluted 4X in SWFI to the final concentrations of 1 mg/mL for IV studies and 6 mg/mL for oral studies (1% DMSO, 1% Cremophore).

Following IV administration, blood, brain, and spinal cord samples were collected at time points from 10 minutes to 16 hours (n=4 mice per time point). Mice were euthanized via a CO_2 chamber. Blood was rapidly collected via cardiac puncture using heparinized syringes and transferred into heparinized tubes. Plasma was separated by centrifugation at 7500 rpm for 15 minutes at 4°C. Spinal cords were collected via the hydraulic extrusion method as described by Roberts et al. (Roberts *et al.*, 2005). Briefly, after decapitation, the spinal column rostral of the pelvis was removed. Then, a saline-filled syringe fixed with a blunt-tipped needle was inserted into the caudal end of the spinal column. The plunger was depressed to extrude the spinal cord fully intact. Plasma, brain, and spinal cord were stored at -80°C until LC-MS/MS analysis. Prior to analysis, brain and spinal cord were thawed and homogenized in 2X (w/v) 5% BSA.

4.2.4 LC-MS/MS Analysis:

Given their widely disparate hydrophobicity, separate LC-MS/MS methods were developed for loperamide and OMI. Both methods utilized reverse-phase liquid chromatography via an Aligent 1200 Series HPLC connected to a TSQ Quantum Classic mass spectrometer in positive ion mode. Briefly, both drugs and their respective internal standards were extracted from plasma, brain homogenate, and spinal cord samples via liquid-liquid extraction with 5X (v/v) ethyl acetate. Samples were vortexed for 5 minutes and centrifuged. Supernatant was collected and completely dried under nitrogen, and samples were reconstituted with mobile phase (MP). For loperamide, the internal standard was [^{6}H]-loperamide, and for OMI, the internal standard was naltrindole. Both methods used a Phenomenex Synergi 4µm Polar-RP column (4µm, 75 x 2mm) for chromatographic separation and a MP flow rate of 0.3 mL/minute. For loperamide, the method was isocratic with a MP composition of aqueous phase (A) 45% distilled water with 0.1% formic acid and organic phase (B) of 55% acetonitrile with 0.1% formic acid and a total run time of 4 minutes. The OMI method utilized gradient elution with initial MP composition of aqueous phase (A) 75% distilled water with 0.1% formic acid and organic phase (B) 25% acetonitrile with 0.1% formic acid. The gradient was as follows: starting at 3 minutes, organic phase was increased to 90% over 0.75 minutes, held at 90% for 1.25 minutes, and decreased back to 25% over 0.5 minutes. It was then held at 25% for 4.5 minutes for a total runtime of 10 minutes. The *m/z* transitions for all molecules were as follows: loperamide 478.1 → 267.3, [^{6}H]-loperamide 484.1 → 273.3, OMI 375.1 → 254.1, naltrindole 415.1 → 254.1. For both methods, the standard curve was linear over the range of 0.1-1000ng/mL (weighted $1/Y^2$) with coefficients of variation less than 15%. Data were acquired and analyzed using Xcalibur software. The inter-day variability for loperamide for all concentrations in the standard curve was less than 4%, the intra-day variability was less than 7%, and the limit of quantification was 0.1 ng/mL. For OMI, the

inter-day variability was less than 15%, the intra-day variability was less than 7% and the limit of quantification was 0.1 ng/mL.

4.2.5 Pharmacokinetic Parameter Estimation

Plasma, brain, and spinal cord concentration-time profiles were analyzed using Phoenix WinNonlin version 8.3 (Certara USA Inc., Princeton, NJ). Brain concentrations were corrected for residual blood estimated at 1.4% of brain weight and with blood concentrations approximated by plasma concentrations (Fridén *et al.*, 2010). Pharmacokinetic parameters and metrics were calculated by performing noncompartmental analysis (NCA). Areas under the curve (AUCs) were determined by linear trapezoidal integration, where the AUC to the last time point (AUC_{Last}) was calculated directly. The AUC to time infinity ($AUC_{0\rightarrow\infty}$) was extrapolated from the last time point to infinite time by dividing the concentration at the last time point (C_{Last}) by the terminal elimination rate constant (λ_z) as determined by the last 4 time points. In cases where the terminal slope was not sufficiently negative for the time course of these experiments, AUC_{Last} is reported rather than $AUC_{0\rightarrow\infty}$. Variances for $AUCs_{Last}$ were calculated using the Bailer method as reported in Phoenix WinNonlin (Bailer, 1988). Variances for $AUC_{0\rightarrow\infty}$ were calculated utilizing the Yuan extension of the Bailer method (Yuan, 1993).

Other pharmacokinetic parameters, including systemic clearance (CL), apparent clearance (CL/F), volume of distribution (V_{ss}) and apparent volume of distribution (V/F) as well as the terminal half-life ($t_{1/2}$) were also calculated by NCA in Phoenix software by the following methods:

$$\boldsymbol{CL\ and\ CL/F = \frac{Dose}{AUC_{0\rightarrow\infty}}} \qquad (3)$$

$$V_{ss} = MRT_{inf} \times CL \qquad (4)$$

Where MRT_{inf} is the area under the first moment curve to infinity ($AUMC_{inf}$) divided by the $AUC_{0\rightarrow\infty}$.

$$t_{1/2} = \frac{ln\,(2)}{\lambda_z} \qquad (5)$$

Where λ_z is the terminal first-order elimination rate constant associated with the log-linear portion of the concentration-time profile and is estimated by linear regression of time vs log-concentration.

The brain-to-plasma ratio, or brain tissue partition coefficient (Kp_{Brain}), for each drug was calculated as a ratio of the AUC of the brain concentration-time profile to the AUC of the plasma concentration-time profile (Equation 6). Similarly, the spinal cord-to-plasma ratio, or spinal cord tissue partition coefficient ($Kp_{Spinal\ Cord}$) was calculated as a ratio of the AUCs (Equation 7). The brain partition coefficient of free drug (Kp_{uu}) was calculated by multiplying the Kp_{Brain} by the ratio of unbound fractions in brain and plasma (Equation 8).

$$Kp_{Brain} = \frac{AUC_{Brain}}{AUC_{\ Plasma}} \qquad (6)$$

$$Kp_{Spinal\ Cord} = \frac{AUC_{Spinal\ Cord}}{AUC_{Plasma}} \qquad (7)$$

$$Kp_{uu} = Kp_{Brain} \times \frac{fu_{Brain}}{fu_{Plasma}} \quad (8)$$

The tissue-to-plasma concentration ratio at time t is used to assess the extent of drug distribution over time, and will be notated as Kp_t values for both brain and spinal cord. These were calculated by the following:

$$Kp_t = \frac{Concentration_{tissue}}{Concentration_{plasma}} \quad (9)$$

The oral bioavailability (F) of both drugs was calculated by Equation 9:

$$F = \left\{\frac{[AUC_{(0\rightarrow\infty),plasma}]\ oral}{[AUC_{(0\rightarrow\infty),plasma}]IV}\right\}\left(\frac{Dose_{IV}}{Dose_{oral}}\right) \quad (10)$$

The distributional advantage (DA) achieved in mice lacking efflux transporters at the CNS barriers was calculated by the following equation.

$$DA_{(brain\ or\ spinal\ cord)} = \frac{Kp_{Brain\ or\ spinal\ cord}\ transporter\ knockout\ mice}{Kp_{Brain\ or\ spinal\ cord}\ wild-type\ mice} \quad (11)$$

4.2.6 Rapid Equilibrium Dialysis (RED) for Free Fraction in Mouse Plasma and Brain Homogenate:

Free fractions of loperamide, OMI, and the combination in mouse plasma and brain homogenate were determined using RED devices according to the manufacturer's protocol (Thermo Fisher). For brain homogenate, brain tissue was homogenized in 2

volumes (w/v) of PBS (pH 7.4) using a mechanical homogenizer. Both plasma and brain homogenate were spiked with loperamide, OMI, or a 1:1 combination to a final concentration of 5µM (for each drug) with 0.025% DMSO. Drug-matrix solutions (300µL) were then added to the sample chamber, and then 500µL of PBS (0.025% DMSO) was added to the buffer chamber. The plate was then sealed with adhesive film and incubated for 24 hours at 37°C in an orbital shaker set to 600 rpm. At 24 hours, samples were collected from both chambers and stored at -20°C until LC-MS/MS analysis. The undiluted free fraction (f_u) for both drugs was calculated with the following equation, as reported previously (Kalvass and Maurer, 2002).

$$f_u = \frac{1/D}{\left(\left(\frac{1}{f_{u,diluted}}\right) - 1\right) + 1/D} \qquad (2)$$

Where D is the dilution factor, or 3 as noted above.

4.2.7 Statistical Analysis:

Data are represented as mean ± S.D. where applicable. To compare AUCs among studies and between different tissues, a two-tailed unpaired *t* test was performed in Graphpad Prism with a null hypothesis that AUCs were equal. One-way ANOVA with Tukey's multiple comparisons test was performed to compare AUCs among WT and transporter knockout mice in Graphpad. A significance level of $P < 0.05$ was considered significant in all tests.

4.3 RESULTS

4.3.1 Loperamide disposition in transgenic FVB mice with and without OMI

To determine the contribution of P-gp and BCRP to the pharmacokinetics and CNS distribution of OMI and loperamide alone and in combination, 5mg/kg of both drugs and the combination were administered IV to wild-type (WT), BCRP knockout (BKO), P-gp knockout (PKO), and triple knockout (TKO) FVB mice. Concentration-time profiles for loperamide alone are shown in **Figure 4.1**. Loperamide disposition in the wild-type mice when administered alone is similar to its disposition in the ICR mice (**Chapter 3)**, and the plasma AUCs for loperamide IV in ICR and wild-type FVB studies are not significantly different ($p = 0.56$), indicating no significant strain differences. The concentration-time profiles in the BKO mice also have similar kinetics and distribution to WT mice (**Fig. 4.1A and 4.1B**), with brain and spinal concentrations lower than that of plasma. However, in the PKO and TKO mice, brain and spinal cord concentrations are higher than plasma for the duration of the time course. The terminal slopes for brain and spinal cord in these genotypes were not sufficiently negative to accurately extrapolate to time infinity, and therefore AUC_{Last} is reported for these tissues rather than $AUC_{0\rightarrow\infty}$. Upon comparison, the brain AUCs in the PKO and TKO mice were significantly higher than that of the WT mice ($p_{adj} < 0.001$, and $p_{adj} = 0.009$, respectively) as well as BKO mice ($p_{adj} < 0.001$ and $p_{adj} = 0.015$, respectively), but the brain AUCs in the PKO and TKO mice were not significantly different. The spinal cord AUCs in the PKO and TKO mice were also significantly higher than in the WT ($p_{adj} = 0.001$ and $p_{adj} = 0.003$, respectively) and the BKO mice ($p_{adj} = 0.001$ and $p_{adj} = 0.004$, respectively). This agrees with the prior characterization of loperamide as a P-gp substrate (Schinkel *et al.*, 1996). These data, for the first time, characterize the contribution of P-gp to efflux of loperamide from mouse spinal cord.

Additionally, the plasma terminal phase in both the PKO and TKO mice shows a reduced slope (**Figure 4.1C and 4.1D**). When the plasma $AUC_{0\rightarrow\infty}$ was compared among the 4 genotypes, it was found that the WT AUC was not significantly different from the BKO mice ($p_{adj} = 0.988$) or the TKO mice ($p_{adj} = 0.3151$). However, the plasma AUC in PKO mice was significantly greater than in the WT mice ($p_{adj} = 0.001$), and the PKO and TKO mice were not significantly different ($p_{adj} = 0.152$). Therefore, the systemic clearance was reduced in mice lacking P-gp.

The concentration-time profiles and overall PK parameters for loperamide when administered with OMI show the same trends as the discrete dosing studies in all four genotypes (**Figure 4.2A-D, Table 4.1**). Again, the distribution of loperamide into the CNS is significantly increased in mice lacking P-gp. The half-life for loperamide also appears to be increased in mice lacking P-gp, and the clearance to be reduced. Similarly to the ICR mouse studies in the previous chapter, the addition of OMI did not significantly alter the plasma, brain, or spinal cord AUCs in the WT FVB mice (**Table 4.1**, $p = 0.914$, $p = 0.139$, $p = 0.617$, respectively).

When the Kp_{tBrain} and $Kp_{tSpinal\ Cord}$ for loperamide alone are plotted over time, it is apparent that the mice with functional P-gp have similar tissue-to-plasma ratios (**Figure 4.3A and 4.3B**). This is also reflected in the distributional advantage (DA) for loperamide in both brain (DA_{Brain}) and spinal cord ($DA_{Spinal\ Cord}$), which is around 2 in the BKO mice (**Table 4.2**). Alternatively, the mice lacking P-gp have much higher tissue-to-plasma ratios over time for both brain and spinal cord (**Figure 4.3A and 4.3B**), with distributional advantages around and above 40 (**Table 4.2**). These same patterns are mirrored in the tissue-to-plasma ratios for loperamide in the combination study, where mice with functional P-gp have lower tissue-to-plasma ratios than the mice lacking P-gp (**Figure 4.3C and 4.3D**). Interestingly, the DA for brain and spinal cord may be reduced when loperamide is dosed in combination with OMI (**Table 4.2**).

Figure 4.1. Loperamide IV Pharmacokinetics and CNS Distribution in FVB mice

Plasma, brain, and spinal cord concentration-time profiles following a single IV dose of loperamide (5mg/kg) in (A) wild-type, (B) BCRP knockout, (C) P-gp knockout, and (D) triple knockout FVB mice.

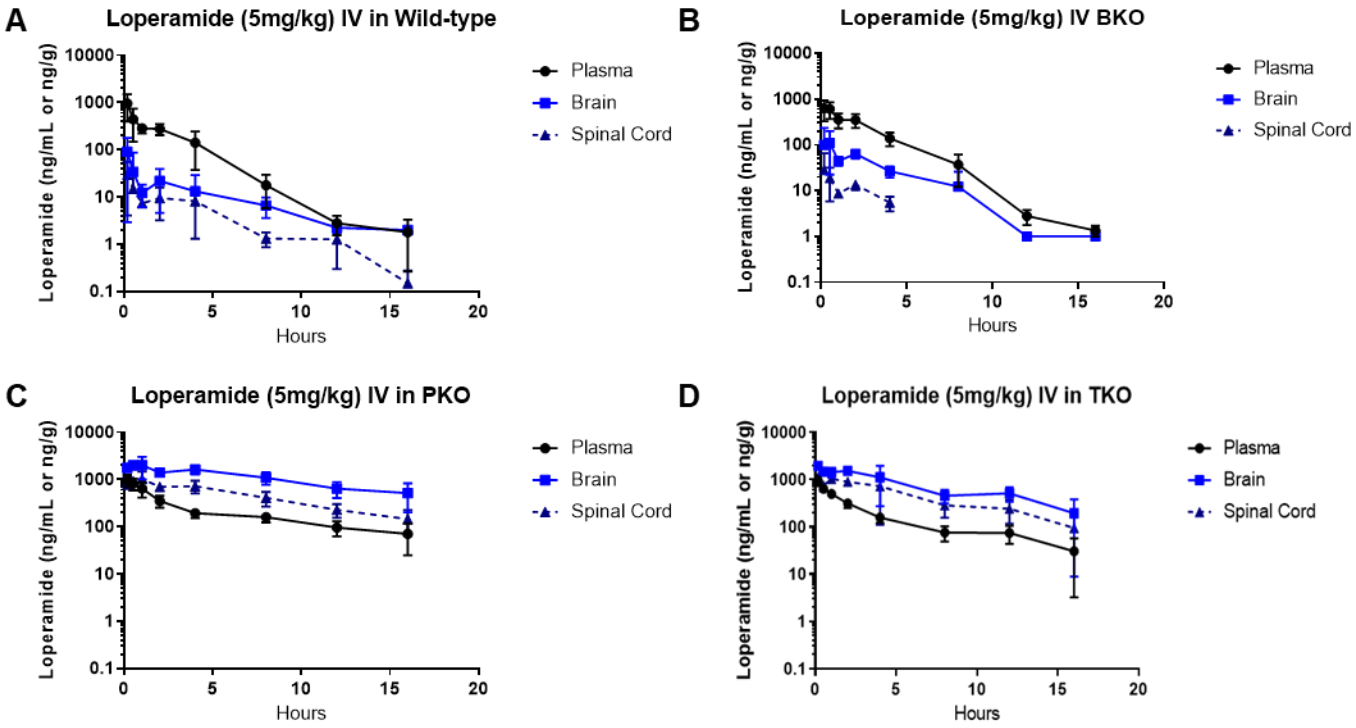

Figure 4.2 Loperamide IV Pharmacokinetics and CNS distribution with Co-administration of OMI

Plasma, brain, and spinal cord concentration-time profiles following a single IV dose of loperamide (5mg/kg) co-administered with OMI (5mg/kg) in (A) Wild-type, (B) BCRP knockout, (C) P-gp knockout, and (D) triple knockout FVB mice.

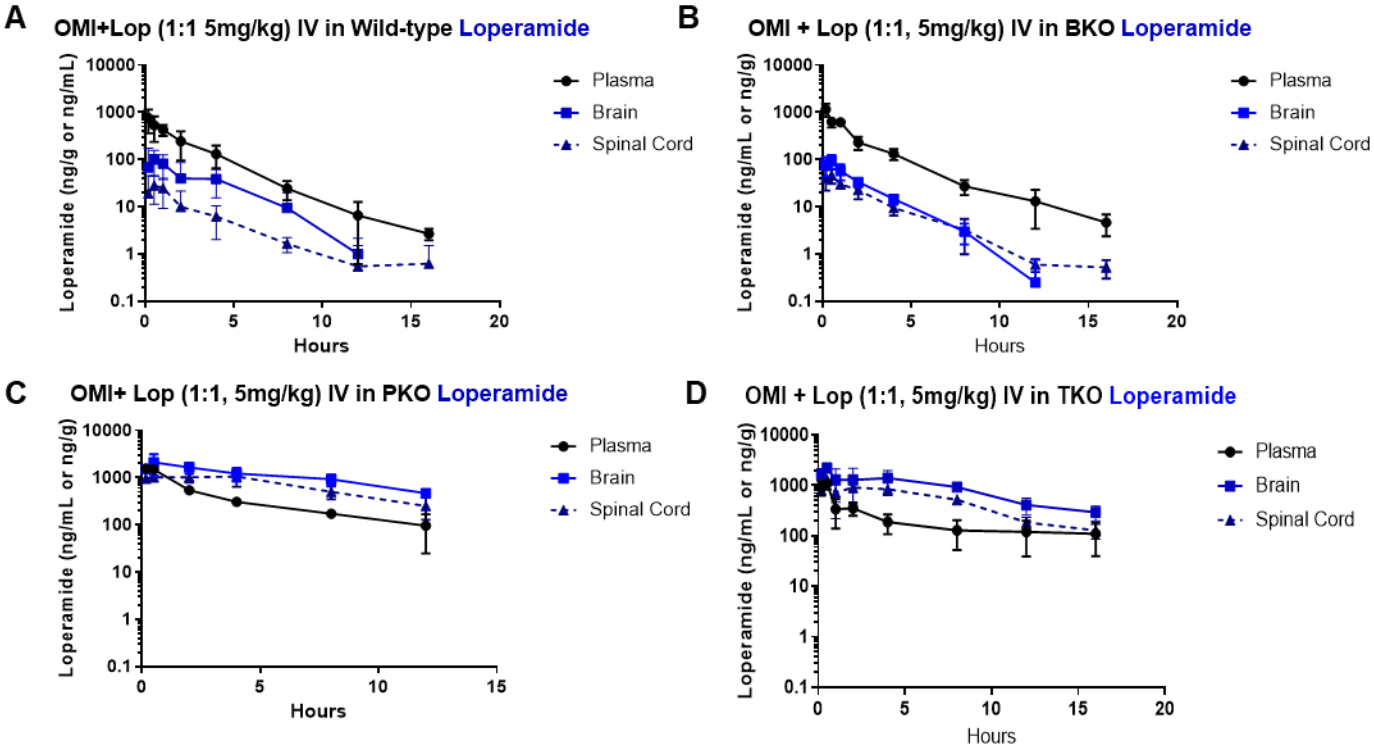

Figure 4.3 Loperamide CNS Partitioning in FVB Transporter Knockout mice

(A) Kp_{tBrain} of loperamide in WT, BKO, PKO and TKO FVB mice (B) $Kp_{tSpinal\ Cord}$ of loperamide in WT, BKO, PKO and TKO FVB mice (C) Kp_{tBrain} of loperamide when co-administered with OMI in WT, BKO, PKO and TKO FVB mice (D) $Kp_{tSpinal\ Cord}$ of loperamide when co-administered with OMI in WT, BKO, PKO and TKO FVB mice .

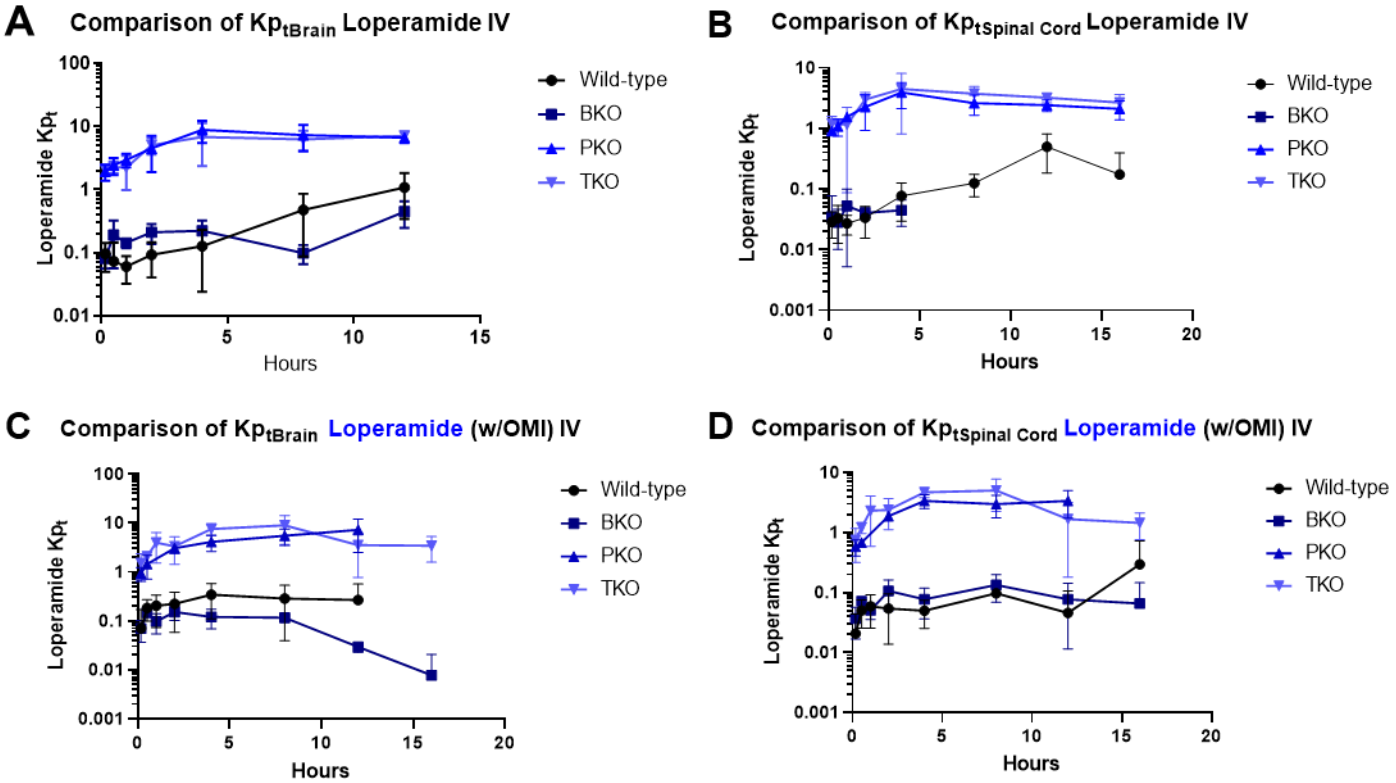

Table 4.1 Summary Pharmacokinetic Parameters of Loperamide Wild-type and Transgenic FVB Mice Following IV Administration with and without OMI

A two-tailed unpaired t-test was performed to compare AUCs among tissues within the same study (see results) and between the same tissues in discrete vs. combination studies. A one-way ANOVA with Tukey's multiple comparisons test was used to compare AUCs for the same tissue among different genotypes.

Results are presented as mean or mean ± S.D where applicable.

Table 4.1 Continued

Drug	Parameter	Wild-type	BKO	PKO	TKO
Loperamide alone	$t_{1/2}$ (h)	1.85	1.7	7.8	5.6
	CL (L/h)/kg	2.9	2.6	1.2	1.8
	V (L/kg)	6.6	7.0	10.6	10.1
	$AUC_{0\rightarrow\infty}$ or (last) Plasma (h*ng)/mL	1,686 ± 413	1,909 ± 312	4,302 ± 781	2,838 ± 273
	$AUC_{0\rightarrow\infty}$ or (last) Brain (h*ng)/g	173 ± 78	397 ± 105	17,503 ± 5,100	13,832 ± 3,503
	$AUC_{0\rightarrow\infty}$ or (last) Spinal Cord (h*ng)/g	70 ± 25	82 ± 9.6	8,752 ± 1,978	7,823 ± 2,403
	Kp_{Brain}	0.10	0.21	4.1	4.9
	$Kp_{Spinal\ cord}$	0.05	0.11	2.0	2.7
Loperamide in Combination	$t_{1/2}$ (h)	2.05	2.4	4.17	9.54
	CL (L/h)/kg	2.9	2.4	0.98	1.02
	V (L/kg)	6.9	5.67	4.46	13.2
	$AUC_{0\rightarrow\infty}$ or (last) Plasma (h*ng)/mL	1,744 ± 333	2,080 ± 207	5,266 ± 923	4,860 ± 1,377
	$AUC_{0\rightarrow\infty}$ or (last) Brain (h*ng)/g	460 ± 188	216 ± 27	13,350 ± 2,012	14,566 ± 2,713
	$AUC_{0\rightarrow\infty}$ or (last) Spinal Cord (h*ng)/g	90.2 ± 31.3	137 ± 26	10,516 ± 1,966	9,185 ± 1,400
	Kp_{Brain}	0.26	0.10	2.5	3.0
	$Kp_{Spinal\ cord}$	0.05	0.07	2.0	1.89

Table 4.2 Distributional advantage for brain and spinal cord in Transgenic FVB mice

Determined by a ratio of Kps in each tissue to the corresponding Kp in wild-type FVB mice.

Genotype	Tissue	Loperamide alone	Lop in Combination	OMI alone	OMI in Combination
BKO	DA_{Brain}	2.1	0.38	1.2	0.71
	$DA_{Spinal\ Cord}$	2.2	1.4	0.53	0.53
PKO	DA_{Brain}	41	9.6	8.1	2.5
	$DA_{Spinal\ Cord}$	40	40	25	3.9
TKO	DA_{Brain}	49	11	8.4	3.4
	$DA_{Spinal\ Cord}$	54	38	14	6

4.3.2 OMI disposition in FVB transgenic FVB mice with and without loperamide

When OMI was administered alone in WT and BKO FVB mice, it showed similar distribution kinetics, with the brain and spinal cord concentrations surpassing that of plasma at the later time points (**Figure 4.4A and 4.4B**). However, the PKO and TKO mice showed higher concentrations of OMI in brain and spinal cord throughout the time course. The terminal slopes for brain and spinal cord in these genotypes were not sufficiently negative to accurately extrapolate to time infinity, and therefore AUC_{Last} is reported for these tissues rather than $AUC_{0\rightarrow\infty}$ (**Table 4.3**). When the AUCs were compared, differences among brain and spinal cord AUCs in WT and BKO mice were not distinguishable ($p_{adj} = 0.551$ and $p_{adj} = 0.999$, respectively). The PKO and TKO mice, however, did have significantly higher AUCs than the WT mice and the BKO mice for both brain and spinal cord ($p_{adj} < 0.001$ for all cases).

For OMI discrete dosing, there was no difference in the plasma AUC or the half-life in any of the genotypes, implying that the systemic clearance and volume of distribution of OMI were not altered significantly by a lack of P-gp or BCRP (**Table 4.3**). The concentration-time profiles for OMI in combination with loperamide were similar to OMI alone for all 4 genotypes (**Figure 4.5A-D**). As observed in the ICR OMI IV studies in **Chapter 3**, the clearance of OMI is reduced by approximately half when administered in combination with loperamide (**Table 4.3**), and as previously stated, the AUC_{Brain} for OMI in WT FVB mice is significantly higher when dosed in combination with loperamide, but the overall Kp_{Brain} did not change. Also, as previously stated, the dose-normalized plasma AUCs for OMI IV in ICR and wild-type FVB are not significantly different ($p = 0.19$), indicating no significant strain differences. Interestingly, the reduction in clearance in the presence of loperamide that is observed in the ICR mice and WT FVB mice is also consistent across all FVB genotypes when comparing OMI discrete dosing and the

combination. This indicates that neither P-gp nor BCRP are likely to be involved in the mechanism of the interaction resulting in reduced systemic clearance of OMI.

When the Kp_{tBrain} and $Kp_{tSpinal\ Cord}$ were compared over time, it was apparent that the mice with functional P-gp trend closely together at ratios near 1, lower than that of the PKO and TKO mice (**Figure 4.6A-D**). The DA_{Brain} for OMI in the knockouts was around 1 for the BKOs and 8 in the two genotypes lacking P-gp. The $DA_{Spinal\ Cord}$ was less than 1 in the BKOs and greater than 8 in the P-gp knockouts and triple knockouts (**Table 4.2**). All of these data indicate that OMI is a P-gp substrate but not a BCRP substrate.

Figure 4.4 OMI IV Pharmacokinetics and CNS Distribution in FVB mice

Plasma, brain, and spinal cord concentration-time profiles following a single IV dose of OMI (5mg/kg) in (A) wild-type, (B) BCRP knockout, (C) P-gp knockout, and (D) triple knockout FVB mice.

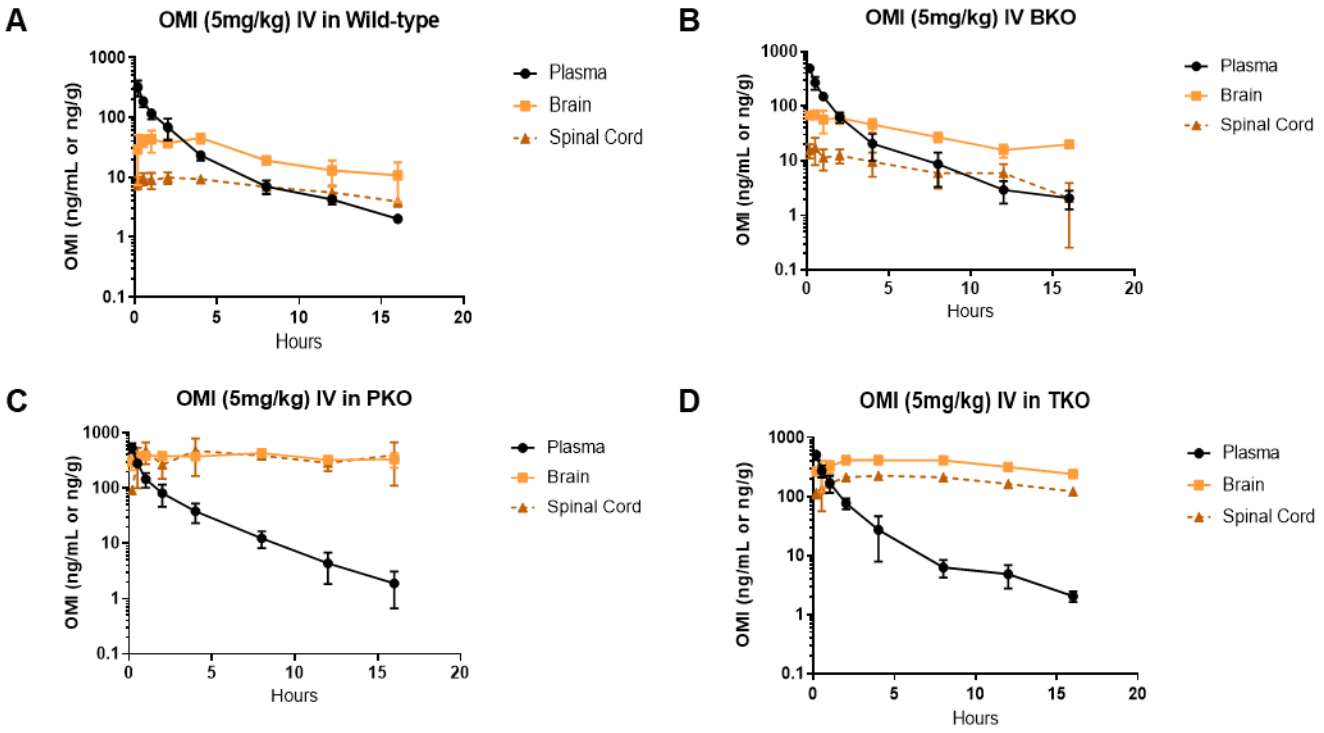

Figure 4.5 OMI IV Pharmacokinetics and CNS Distribution in FVB Mice with Co-administration of Loperamide

Plasma, brain, and spinal cord concentration-time profiles following a single IV dose of OMI (5mg/kg) co-administered with loperamide (5mg/kg) in (A) Wild-type, (B) BCRP knockout, (C) P-gp knockout, and (D) triple knockout FVB mice

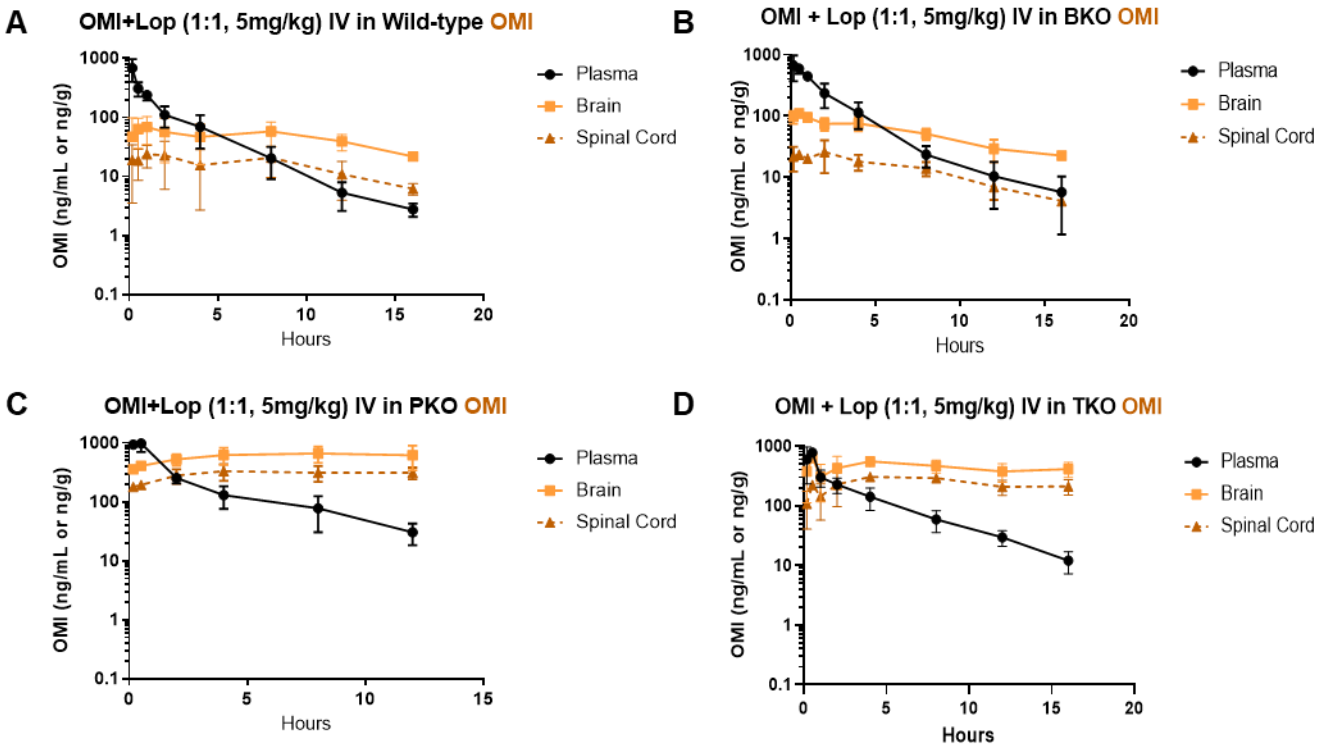

Figure 4.6 OMI CNS Partitioning in FVB Transporter Knockout mice.

(A) Kp_{tBrain} of OMI in WT, BKO, PKO and TKO FVB mice (B) $Kp_{tSpinal\ Cord}$ of OMI in WT, BKO, PKO and TKO FVB mice (C) Kp_{tBrain} of OMI when co-administered with loperamide in WT, BKO, PKO and TKO FVB mice (D) $Kp_{tSpinal\ Cord}$ of OMI when co-administered with loperamide in WT, BKO, PKO and TKO FVB mice.

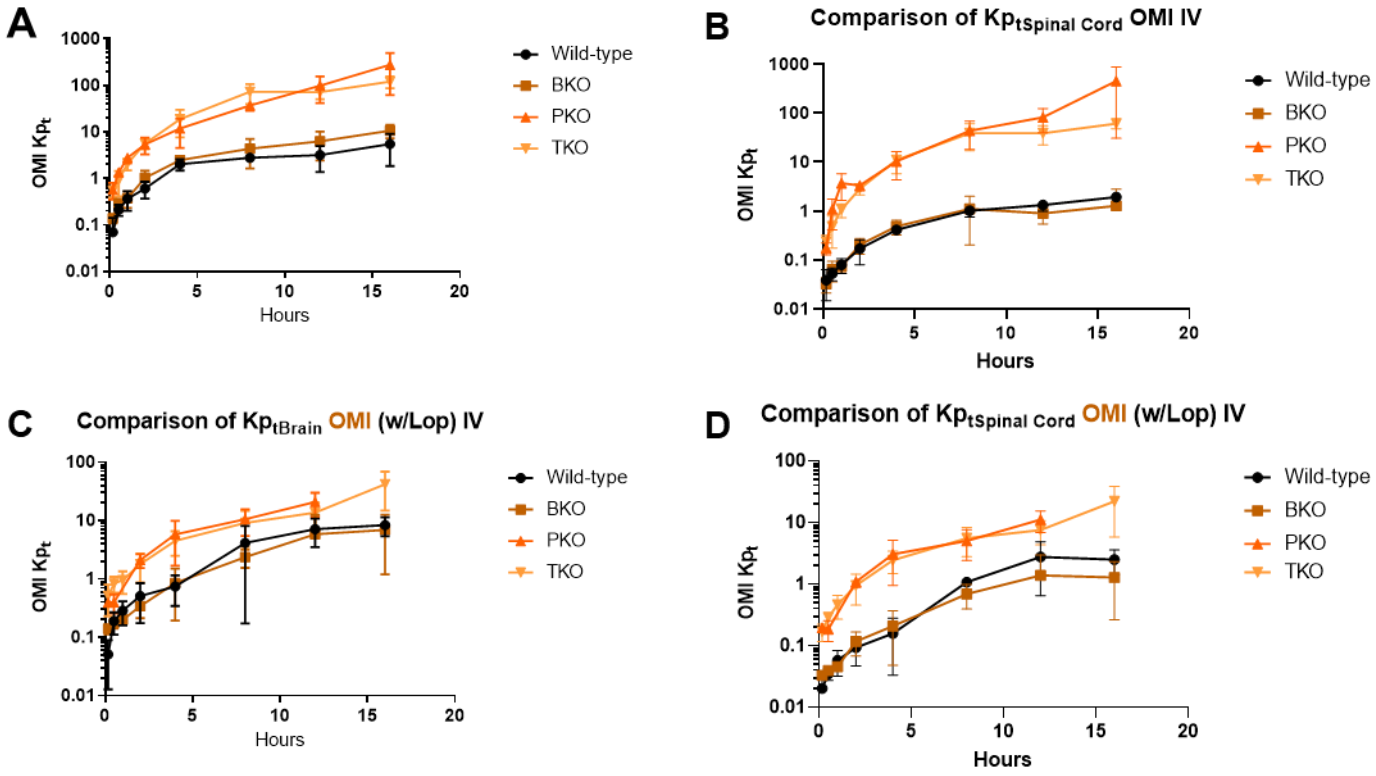

Table 4.3 Summary pharmacokinetic parameters determined by noncompartmental analysis of total drug concentrations of OMI in WT, BKO, PKO, and TKO FVB mice following a single IV dose (5 mg/kg) and following co-administration with loperamide (5 mg/kg).

A two-tailed unpaired t-test was performed to compare AUCs among tissues within the same study (see results) and between the same tissues in discrete vs. combination studies. A one-way ANOVA with Tukey's multiple comparisons test was used to compare AUCs for the same tissue among different genotypes.

Results are presented as mean or mean ± S.D where applicable.

Table 4.3 Continued

Drug	Parameter	Wild-type	BKO	PKO	TKO
OMI alone	$t_{1/2}$ (h)	2.9	2.9	2.6	2.8
	CL (L/h)/kg	9.8	8.0	6.7	7.4
	V (L/kg)	24.9	16.6	15.5	15.5
	$AUC_{0\rightarrow\infty}$ or (last) Plasma (h*ng)/mL	508 ± 57	623 ± 86	735 ± 43	670 ± 42
	$AUC_{0\rightarrow\infty}$ or (last) Brain (h*ng)/g	500 ± 116	760 ± 66	5976 ± 184	5665 ± 159
	$AUC_{0\rightarrow\infty}$ or (last) Spinal Cord (h*ng)/g	172 ± 16	121 ± 27	5689 ± 607	2952 ± 62
	Kp_{Brain}	1.0	1.2	8.1	8.4
	$Kp_{Spinal\ cord}$	0.34	0.18	7.6	4.3
OMI in Combination	$t_{1/2}$ (h)	2.5	2.6	3.48	3.37
	CL (L/h)/kg	5.0	3.0	1.8	2.6
	V (L/kg)	13	8.7	5.8	10.1
	$AUC_{0\rightarrow\infty}$ or (last) Plasma (h*ng)/mL	1002 ± 167	1541 ± 245	2613 ± 258	1893 ± 130
	$AUC_{0\rightarrow\infty}$ or (last) Brain (h*ng)/g	1115 ± 136	1076 ± 77	6993 ± 581	7128 ± 458
	$AUC_{0\rightarrow\infty}$ or (last) Spinal Cord (h*ng)/g	326 ± 71	248 ± 32	3584 ± 260	3913 ± 203
	Kp_{Brain}	1.1	0.71	2.7	3.7
	$Kp_{Spinal\ cord}$	0.33	0.16	1.37	2.0

4.3.3 Rapid Equilibrium Dialysis (RED) for Free Fraction in Mouse Plasma and Brain Homogenate

The free fraction in plasma and brain was determined by rapid equilibrium dialysis. The unbound brain partition coefficient (Kp_{uu}) was determined using the brain partition coefficients from wild-type FVB mouse studies as all of these studies were carried out at the same dose. The unbound fractions and Kp_{uu} are reported in **Table 4.4**. There was a significant increase in the unbound fraction of loperamide in plasma in the presence of OMI ($p<0.001$). However, there was no detectable difference in the unbound fraction of loperamide in brain homogenate with the presence of OMI. The fraction unbound of OMI was much higher than that of loperamide in both plasma and brain ($p<0.001$ in both cases), but there was no change in the unbound fraction of OMI in the presence of loperamide in either plasma ($p=0.165$) or in brain homogenate ($p=0.222$). The Kp_{uu} for both drugs was unchanged by the presence of the other. The Kp_{uu} for loperamide alone was 0.1 vs 0.11 in the presence of OMI, and the Kp_{uu} for OMI alone was 0.44 vs 0.42 in the presence of loperamide. This indicates that the brain penetration of both drugs is not significantly altered by a change in protein binding when they are administered in combination.

Table 4.4 Unbound Fractions of Loperamide and OMI in Brain and Plasma

Unbound partition coefficients determined using rapid equilibrium dialysis (RED) in 5 replicates. Data from WT FVB mice were used to determine unbound tissue partition coefficients.

Results are presented as mean ± S.D.

* indicates $p < 0.05$.

Drug	Plasma fu (mean ± S.D.)	Brain fu (mean ± S.D.)	Kpuu (wild-type FVB mice)
Loperamide	0.0183 ± 0.0011*	0.0154 ± 0.0022	0.10
Loperamide (w/OMI)	0.0357 ± 0.0053*	0.0140 ± 0. 0016	0.11
OMI	0.192 ± 0.0754	0.0841 ± 0.0142	0.44
OMI (w/loperamide)	0.253 ± 0.0482	0.0951 ± 0.0187	0.42

2.4 DISCUSSION

The analgesic and antihyperalgesic efficacy and safety of opioids is not only determined by their affinity for their target receptor. The CNS penetration of these drugs plays a central role in their safety, and often their CNS penetration is greatly impacted by active transport at the CNS barriers (Ekblom *et al.*, 1992; Xie and Hammarlund-Udenaes, 1998; Boström *et al.*, 2006, 2008). Though there is evidence that the synergistic activity of the combination of loperamide and OMI is largely mediated at target receptors in the peripheral nervous system (Bruce *et al.*, 2019; Uhelski *et al.*, 2020), it was imperative that the CNS disposition of loperamide and oxymorphindole be determined, as it could play a role in both the safety of the combination as well as its efficacy. The previous chapter of this dissertation focused on ICR mice and showed that there were no systemic pharmacokinetic interactions that might play a role in this synergy or safety. While loperamide CNS penetration has been previously shown to be impaired by P-gp (Schinkel *et al.*, 1996), the efflux liability of OMI was unknown. We determined the efflux liability and the unbound CNS partitioning of these two drugs alone and in combination in wild-type and transgenic FVB mice lacking either one of the efflux transporters P-gp, BCRP, or both.

In agreement with the previous studies showing that loperamide is a P-gp substrate, we found that loperamide total CNS penetration was limited by P-gp, but not BCRP. The spinal cord penetration of loperamide was previously undetermined, but our studies show that P-gp plays a significant role in excluding loperamide from spinal cord. As for OMI, the current study indicates that OMI is a substrate of P-gp, but not a substrate of BCRP. Additionally, because neither drug shows increased CNS tissue partitioning after co-administration in the studies described herein, there is no evidence that P-gp is saturated when the drugs are co-administered.

A large body of research shows that efflux transport systems at the BBB are robust even in cases where the BBB is disrupted either by the presence of a tumor or by artificial means (Goutal *et al.*, 2018; de Gooijer *et al.*, 2021; Griffith *et al.*, 2021). While some studies have shown that the administration of loperamide with P-gp modulators and inhibitors like quinidine could pose the risk of classical opioid effects (Sadeque *et al.*, 2000), post-marketing assessments of loperamide when administered in combination with a variety of other P-gp substrates show that MOR-associated adverse effects are unlikely to occur, implying that loperamide's access to the CNS is not enhanced to a therapeutically significant extent (Vandenbossche *et al.*, 2010).

While the CNS exposure of OMI may be increased after IV administration of the combination due to a reduction in its systemic clearance as shown in the **Chapter 3**, the unbound CNS partitioning of both drugs is unchanged in the combination. Given the fact that the drugs appear to have no significant interaction at the CNS barriers, the most likely mechanism for the interaction between loperamide and OMI is an alteration in pharmacodynamics at receptors in the peripheral nervous system. A large body of research has shown co-localization of MOR and DOR receptors and evidence of heterodimerization, especially in inflammatory pain states (Gomes *et al.*, 2004; Bruce *et al.*, 2019). Previous studies have shown that the synergy between specific MOR- and DOR-agonists requires protein kinase C epsilon (PKCε), and that DOR agonism is retained only in the case of biased signaling where specific agonists promote DOR and MOR phosphorylation but not DOR and MOR internalization (Pradhan *et al.*, 2009; Schuster *et al.*, 2015; Derouiche *et al.*, 2020). The mechanism of synergy for OMI and loperamide is therefore most likely that MORs and DORs form heteromers that remain localized at the cell membrane of primary afferents and retain PKCε-dependent signaling.

This conclusion regarding the peripherally-mediated activity of OMI and loperamide is another promising step in the development of peripherally-restricted opioids for the management of chronic and severe pain that significantly reduce the potential for tolerance, dependence, and overdose deaths. No peripherally-restricted opioids have been approved for the treatment of chronic pain, but their development is of increasing interest. A number of bi-specific agonists have been proposed, and previous work shows that bispecific agonists with a specific linker length have pronounced synergy and modulation of undesirable side effects (Daniels *et al.*, 2005; Lenard *et al.*, 2007; Ding *et al.*, 2018; Lei *et al.*, 2020). This strategy is attractive for future drug development, and accounting for biased signaling of peripherally-restricted combinations of MOR and DOR agonists will likely lead to the development of safer and more effective analgesics.

CHAPTER 5

ADDRESSING BBB HETEROGENEITY: A NEW PARADIGM FOR DRUG DELIVERY TO BRAIN TUMORS

The content of this chapter has been published in:

Griffith JI, Rathi S, Zhang Wenqiu, Zhang Wenjuan, Drewes LR, Sarkaria JN, Elmquist WF (2020) *Pharmaceutics* 11;12(12):1205

5.1 INTRODUCTION

The blood-brain barrier (BBB) remains one of the greatest obstacles to effective pharmaceutical interventions in the treatment of central nervous system (CNS) disease, including brain tumors. While it is true that some loss of neurovascular and barrier integrity may occur in and around brain tumors, the magnitude of this change is not consistent , and new pharmaceutical strategies for the treatment of brain tumors have yet to show significant efficacy in the clinic (Pitz *et al.*, 2011; Arvold *et al.*, 2016; Sarkaria *et al.*, 2018a). This lack of efficacy is largely attributed to insufficient drug delivery due to the presence of the BBB. The dense vascular network of the brain works to strictly regulate transport of substances into and out of the brain parenchyma in order to maintain ionic homeostasis, nutrient supply, and removal of waste for optimal neuronal function. In recent decades, research has revealed that the BBB is composed of specialized endothelial cells (ECs), which are surrounded and supported by pericytes and astrocytes, and are regulated by neuronal signaling, forming what is referred to as the neurovascular unit (NVU)(Abbott *et al.*, 2010). A lack of vesicular transport across these specialized ECs and the presence of active efflux proteins help to further restrict the access of drugs to the CNS (Terasaki and Ohtsuki, 2005). Currently, treatment for the majority of brain tumors involves maximal surgical resection, if possible, followed by radiation, and in the case of glioblastoma multiforme (GBM), concomitant temozolomide (TMZ) (Arvold *et al.*, 2016). However, these treatments often prove to be palliative, and malignant brain tumors are nearly always fatal within 5 years of initial diagnosis (Nayak *et al.*, 2012; Thakkar *et al.*, 2014).

While treatments for peripheral malignancies have improved dramatically in recent decades with the advent of earlier diagnosis, improved imaging, targeted small molecule inhibitors, and large molecule biologics, the treatment of brain tumors has lagged far behind, and their incidence is on the rise (Nayak *et al.*, 2012). Therefore, it is

imperative to understand how the NVU/BBB may be altered in the case of brain tumors and how to design pharmaceutical interventions specifically to overcome this challenge while maintaining neurovascular integrity as much as possible. To this end, a number of strategies have been proposed to improve drug delivery to the brain and brain tumors. Invasive strategies to bypass the NVU/BBB include convection-enhanced delivery (CED) and direct injection. Noninvasive strategies might include focused ultrasound (FUS) and hyperosmotic disruption of the NVU/BBB, as well as inhibition of efflux transporters, nanoparticle-based strategies, and the use of the endogenous transport mechanisms across the brain EC by receptor-mediated transcytosis. In this review, we will introduce brain barrier anatomy and physiology, discuss the heterogeneous impacts of tumor growth and signaling on NVU/BBB integrity, and provide brief overviews of the strategies investigated to deliver drugs to CNS tumors.

5.2 HETEROGENEOUS BLOOD-TUMOR BARRIER PERMEABILITY

The understanding of the BBB's physical and biochemical barrier functions, including the expression of tight junction proteins, restricted paracellular transport, and active efflux mechanisms, have been well established. However, determining the integrity of the NVU/BBB in and around tumors, and how this affects tumor treatment, has been less straightforward. In the case of both primary and metastatic tumors, the NVU/BBB is subject to changes due to tumor growth and signaling, and these alterations in NVU/BBB integrity and physiology result in what will hereafter be referred to as the blood-tumor barrier (BTB). The BTB may be characterized by an inflammatory environment with increased numbers of activated astrocytes, vascular endothelial growth factor (VEGF)-induced reduction in the expression of tight junction proteins like claudin-5, breakdown of the basal lamina, and tumor cell interference in associations between endothelial cells and astrocytic end feet (**Figure 5.1**) (Argaw *et al.*, 2009; Watkins *et al.*,

2014; Arvanitis *et al.*, 2020). There is also evidence for a change in the phenotype of BTB-associated pericytes, which may show decreased platelet-derived growth factor receptor-β (PDGFR-β) expression in addition to increased desmin expression (Lyle *et al.*, 2016). As a result of these changes, the BTB can be, on average, somewhat 'leakier' (more permeable) than the normal NVU/BBB in absence of disease (Adkins *et al.*, 2016; Arvanitis *et al.*, 2020; Gampa *et al.*, 2020). The predominant question with regards to BBB-breakdown and the treatment of brain tumors has therefore been: is breakdown of the NVU/BBB in the case of brain tumors significant enough to allow for the accumulation of efficacious drug concentrations?

Figure 5.1 The Blood-tumor Barrier (BTB)

The BTB is characterized by increased cytokine and VEGF signaling from the tumor, which may lead to decreased expression of TJ proteins like claudin-5. Alterations in pericyte phenotype as well as disruption of astrocytic associations with endothelial cells may contribute to decreased barrier integrity. However, this is not a uniform phenomenon within or among tumors, and the expression of efflux transporters limits drug permeation into the tumor. Evidence exists showing decreased permeability of the BTB in regions distant to the core of the tumor, which more closely resemble 'unaffected' brain.

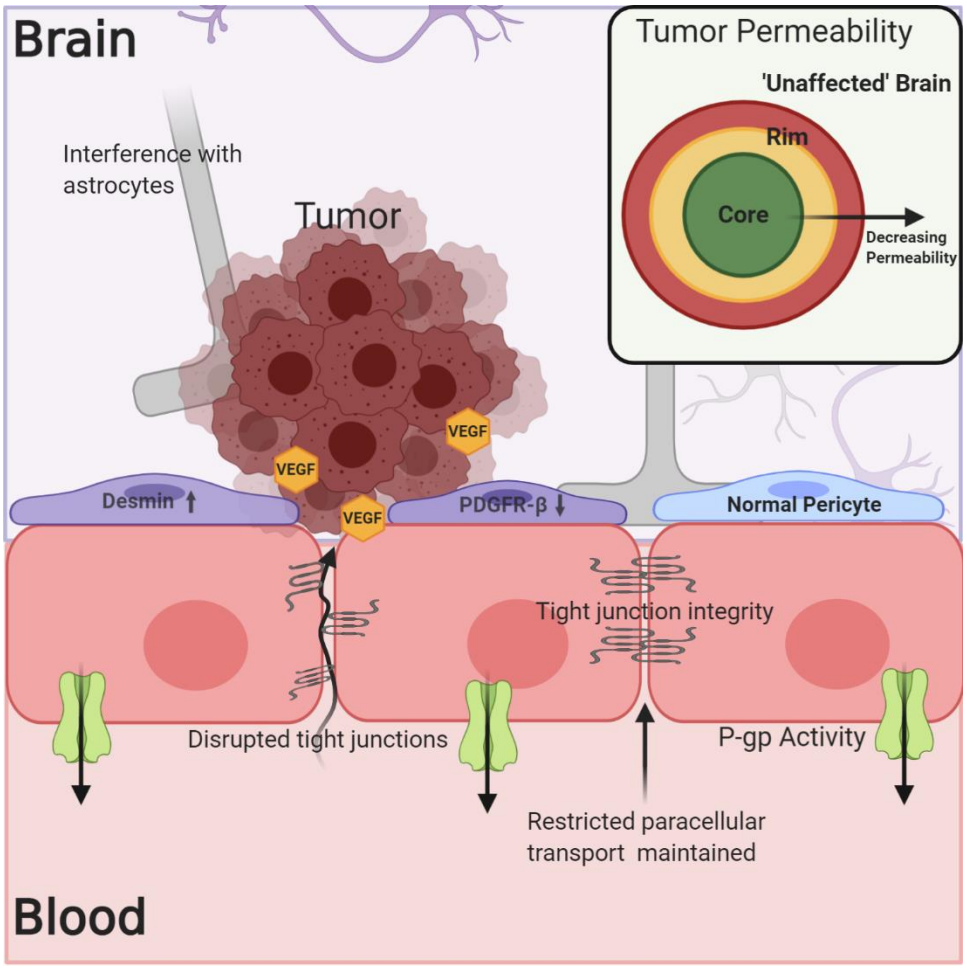

As this question has been repeatedly investigated, various preclinical tumor models routinely lead to conflicting results. In some cases, tumor vascular permeability, assessed by the accumulation of fluorescent tracers, has been previously correlated with growth patterns, tumor size, or peripheral tumor of origin (Zhang *et al.*, 1992). In other cases, including a variety of brain-trophic metastatic breast cancer models developed at the National Institutes of Health (NIH), no correlation between tumor size and permeability has been found (Lockman *et al.*, 2010; Adkins *et al.*, 2016). These studies also found that the variability of BTB permeability among tumors in the same animal and even among regions of the same tumors, as assessed by the accumulation of fluorescent tracers and small molecules like paclitaxel, doxorubicin, and lapatinib, could be as much as 100-fold (Lockman *et al.*, 2010; Taskar *et al.*, 2012; Terrell-Hall *et al.*, 2017). More recent studies in HER2+ brain trophic breast cancer metastasis models have shown poor correlation between drug accumulation and tracer accumulation, as well as inconsistent drug uptake and variable efficacy of biologics like trastuzumab and other antibody-based therapies (Askoxylakis *et al.*, 2016; Terrell-Hall *et al.*, 2017; Gril *et al.*, 2020). Another model of lung cancer brain metastases found two-fold increases in permeability to small molecules like 3H-mannitol, but concluded that this small relative increase in addition to functional P-gp was still a significant limitation to systemic drug therapy (On *et al.*, 2013). In addition, a number of studies utilizing transporter knockout mice and patient-derived xenograft (PDX) models of GBMs and brain metastases have shown that efficacy of systemic administration of various small molecules is consistently limited by the presence of the NVU/BBB and BTB, active efflux, and the fact that vascular permeability is widely variable within and around the tumor region (Agarwal and Elmquist, 2012; Lakoma *et al.*, 2015; Parrish *et al.*, 2015; Pokorny *et al.*, 2015; Mittapalli *et al.*, 2016; Kim *et al.*, 2018; Gampa *et al.*, 2019, 2020). This variability has also been

confirmed by elegant correlated ultramicroscopy and MRI techniques in preclinical tumor models (Breckwoldt *et al.*, 2019). These studies point to the conclusion that relying on the potential for increased BTB permeability is unlikely to result in efficacious treatment through the systemic administration of novel therapies and their subsequent regulatory approval for such applications.

Though the aforementioned evidence has been largely preclinical, it agrees with clinical observations as well, when considered in the appropriate context. Increased permeability of the BTB relative to normal brain is observed clinically, as increased uptake of tracers in magnetic resonance imaging (MRI) and positron emission tomography (PET) imaging allows for definitive diagnosis of brain tumors and informs many aspects of their treatment (Fink *et al.*, 2015). However, especially in the case of diffuse and invasive tumors like GBM, it has also been shown that non-enhancing, infiltrating regions of brain tumors often exist outside of the region of T1-weighted contrast enhancement (Kelly *et al.*, 1987; Watanabe *et al.*, 1992). This indicates that some portions of the malignant tumor are protected by a relatively uncompromised NVU/BBB. The patterns of treatment failure are strongly correlated with and attributed to these non-enhancing regions, and maximal resection including these regions improves survival (Sanai and Berger, 2008; Brown *et al.*, 2016; Pessina *et al.*, 2017). Increasingly, early phase studies in which patients receive drug prior to tumor resection and biopsy are being utilized to determine the real extent of antineoplastic drug permeability to the BTB (Pitz *et al.*, 2011; Sarkaria *et al.*, 2018a). Though fold-increases in drug concentrations relative to normal brain may be observed at the core of the tumor, this still may not be adequate to cause cell death, and it is unlikely that these drug concentrations are representative of concentrations in the entirety of the tumor, as the infiltrative boundaries of the tumor are likely to have a more competent and intact BTB, closer to that of ‘unaffected brain’ (Agarwal *et al.*, 2012; Pokorny *et al.*, 2015; Sanai *et*

al., 2018; Gampa *et al.*, 2020). This is evidenced in drug concentrations from biopsies of non-contrast-enhancing regions (Milano *et al.*, 2010).

As there has been great success with novel treatments of peripheral disease, the culmination of decades of brain tumor research leads to the conclusion that it is imperative that molecules and delivery strategies be designed foremost with an intact NVU/BBB in mind. As an example, GNE317, a small molecule which was designed specifically to avoid active efflux, showed significantly higher activity in a model of brain metastases of lung cancer than another counterpart PI3K inhibitor not designed to penetrate the BBB (Salphati *et al.*, 2012; Osswald *et al.*, 2016). Other brain-penetrant inhibitors like osimertinib, an EGFR inhibitor, have also shown better preclinical and potential clinical efficacy (Ballard *et al.*, 2016; Reungwetwattana *et al.*, 2018). While designing small lipophilic molecules in an attempt to optimize tumor penetration and minimize active efflux is certainly one potential method towards effective treatments for brain tumors, there are a vast number of other drug delivery strategies and novel molecules in development for this application. These strategies will be discussed in the following sections.

5. 3 INVASIVE TECHNOLOGIES

The NVU/BBB poses numerous challenges for efficient drug delivery to the brain and brain tumors, as discussed in the previous section. To address these challenges, various invasive and non-invasive strategies have been developed to improve the delivery of therapeutic agents to the brain. Invasive technologies are based on local delivery of therapeutics to the brain, bypassing the NVU/BBB entirely. They include drug delivery to the cerebrospinal fluid (CSF) via intrathecal or intraventricular injections, and interstitial delivery via biodegradable wafers or catheters (**Figure 5.2**).

Figure 5.2 Invasive Strategies for Drug Delivery to Brain Tumors

Various invasive technologies to increase drug delivery to brain by bypassing the BBB include intrathecal injection via a lumbar puncture, as well as varius intracranial techniques. These include A) intracerebroventricular injection using the Ommaya reservoir, B) CED by way of intracerebral catheter placement, and C) placement of drug-loaded polymeric wafers.

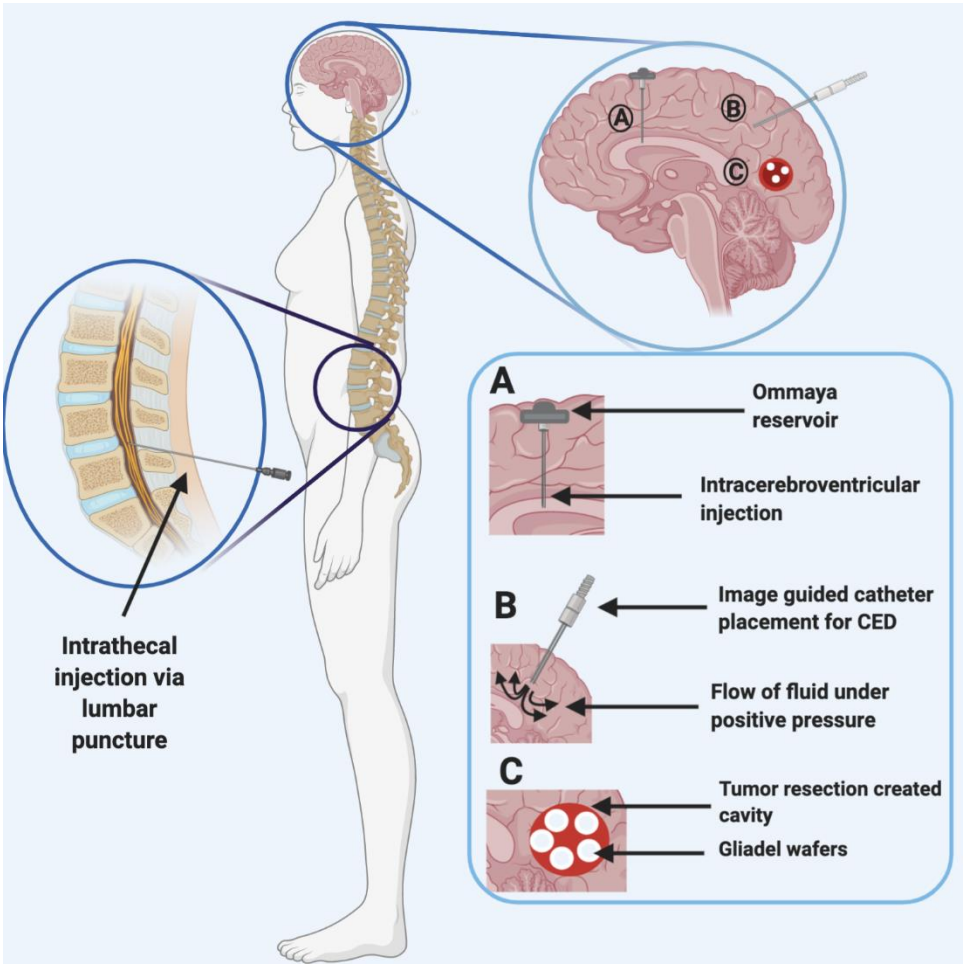

Intrathecal and intraventricular injections

Intrathecal (IT) administration involves direct injection of therapeutics into the CSF that fills the thecal space and encompasses intrathecal-lumbar injection, but can also be used to describe intracerebro-ventricular or intracisternal magna injections (Fowler *et al.*, 2020). Chemotherapy may be administered directly into the lumbar thecal sac via lumbar puncture or infused into the lateral ventricle through a subcutaneous reservoir and a ventricular catheter, allowing drug to distribute into the target sites via diffusion (Costa and Kumthekar, 2018). Drug delivery via lumbar puncture may require multiple administrations, is highly invasive, causes discomfort to the patient, and is not likely to allow for effective drug delivery to brain tumors. Alternatively, intraventricular infusions are often administered via the Ommaya reservoir, invented in 1963 by Ayub Ommaya, which is inserted into one of the lateral ventricles (**Figure 5.2**) (Ommaya, 1963; Witorsch *et al.*, 1965). Clinically, it is essential to ensure correct placement of the catheter in the ventricle, and to this end, new state of the art technology using smartphones is being developed as a guide for accurate neuronavigation and catheter placement, which may make these procedures more accessible for a variety of clinics (Ozerov *et al.*, 2018).

From amongst small molecules, methotrexate and cytarabine are frequently prescribed for IT administration. However, there are numerous reports of neurotoxicity and other complications such as transverse myelopathy associated with the IT administration of these drugs (Chen *et al.*, 2003; Jabbour *et al.*, 2007; Partap *et al.*, 2011; Chotsampancharoen *et al.*, 2016; Nair, 2016; Y Pan *et al.*, 2016). Therefore, though high concentrations can be attained in the CSF using IT injections, reducing the total dose and risk of systemic toxicity, this method of administration has its drawbacks. The rate of drug distribution is slow and inversely proportional to the molecular weight, meaning large molecules often have very low or undetectable concentrations distant

from the site of injection (Ferguson and Woodbury, 1969). Additionally , rapid CSF turnover as compared to the rate of diffusion results in faster clearance of the therapeutics from the site of administration (Bergman *et al.*, n.d.; Collins, 1983). For years, there has been a common misconception that distribution of drug into the CSF is indicative of NVU/BBB permeability, and that delivery of drug to CSF would ensure delivery to the deeper brain tissues. However, it is now more widely accepted that this is not the case, and the reader is directed to a review of this topic (Pardridge, 2016).

Convection Enhanced Delivery

Convection enhanced delivery (CED) is one of the most explored techniques to bypass the NVU/BBB and was developed in the early 1990s by Edward Oldfield's group at the NIH (Bobo *et al.*, 1994). CED involves infusion of fluids locally under pressure into the interstitial space in brain or tumor using stereotactically-placed catheters. CED primarily utilizes bulk flow, and diffusion is a minor component. While diffusion relies on concentration gradient, and macromolecules penetrate only up to a few millimeters under diffusive forces, the distribution pattern attained with CED can be described by Darcy's law, in which the velocity of the molecule is dependent on the pressure gradient and hydraulic conductivity of the medium (Mehta *et al.*, 2017; Saka *et al.*, 2019).

CED is being widely studied in pre-clinical and clinical studies for GBM as well as diffuse intrinsic pontine glioma (DIPG). Various nanotechnology-based drug delivery systems like liposomes, nanoparticles, polymeric micelles, etc. are being administered via CED to increase the volume of the brain tissue accessible to these systems that are otherwise limited by poor diffusion (Grahn *et al.*, 2009; Yokosawa *et al.*, 2010; Zhang *et al.*, 2016, 2017; Jahangiri *et al.*, 2017; Nordling-David *et al.*, 2017; Lin *et al.*, 2018; Pang *et al.*, 2019). Models of CED could help inform treatment design and optimization of other parameters like volume of infusate, duration of infusion, catheter design and placement,

and can guide treatment design (Rechberger *et al.*, 2020). A model was recently developed to understand the flow and distribution of carmustine and paclitaxel solutions as well as doxorubicin loaded liposomes post-CED (Zhan *et al.*, 2017; Zhan and Wang, 2018).

CED is a promising technique and has potential to overcome the limitations posed by systemic delivery. Successful translation of this technique to the clinic would have varied applications to treat a multitude of CNS disorders. For CED to reach its full therapeutic potential, characteristic challenges like catheter design and placement, prevention of reflux, tracking infusate delivery, reduction in mechanical tissue damage and edema, and the potential requirements of multiple infusions need to be addressed. Other challenges associated with CED include cost of the procedure, specific clinical expertise, and post-procedural imaging (Jahangiri *et al.*, 2017).

5.4 NON-INVASIVE TECHNOLOGIES

Apart from these invasive methods, other non-invasive techniques have been investigated to transiently disrupt the neurovasculature to enhance drug delivery to the CNS. These methods may have better patient compatibility compared to invasive approaches such as CED and IT injection, and will perhaps allow lower dosage thus reducing toxicity compared to traditional systemic administration routes like intravenous injection.

Osmotic Blood-Brain Barrier Disruption

The tight junctions of the cerebrovascular endothelium can be transiently and reversibly disrupted by the infusion of a hyperosmolar solution into a cerebral artery, putatively because of the shrinkage of endothelial cells and following splitting of tight

junctions. The resulting intracellular spaces increase the paracellular diffusion and facilitate the delivery of therapeutic, diagnostic, and functional agents relevant to CNS disease. This method was first proposed by Rapoport *et al* in 1972 who exposed the pia arachnoid surface of the cerebral cortex of healthy rabbits to different osmotic concentrations resulting in osmotically-induced and reversible cell shrinkage (**Figure 5.3**) (Rapoport *et al.*, 1972). In practice, this method involves the infusion of 1.4 M mannitol, which has been FDA-approved for administration to patients (Neuwelt, 1980). Besides mannitol, other hypertonic solutions used for transient barrier disruption include arabinose, lactamide, saline, urea and several radiographic contrast agents (Kroll and Neuwelt, 1998). The first Phase I clinical trial osmotic BBB disruption (BBBD) for enhanced drug delivery to brain was initiated 1979 (Levin *et al.*, 1979). Using this technique in experimental and clinical treatment of brain tumors, permeability enhancements of greater magnitude were observed for tumors with low rather than high initial permeability relative to that of normal brain (Rapoport, 2000)

Although the disruption is transient and is fully reversed within several hours (Rapoport *et al.*, 1980; Siegal *et al.*, 2000), one risk of osmotic BBB disruption is the additional mass effect in the brain, resulting from a 1.5% increase in brain fluid content (Kemper *et al.*, 2004; Bellavance *et al.*, 2008). Assessment of the extent of tumor and associated mass effect prior to osmotic BBB disruption is important for optimizing protocols and minimizing the risks of this procedure (Doolittle *et al.*, 2000).

Figure 5.3 Blood-brain Barrier Disrupting Strategies for Drug Delivery to Brain Tumors

Drug delivery to brain may be increased by noninvasive BBBD techniques including A) osmotic disruption and B) focused ultrasound. In osmotic disruption, infusion of a hyperosmolar solution via a cerebral artery results in endothelial cell shrinkage, temporarily disrupting tight junctions. Focused ultrasound uses an infusion of inert gas-filled microbubbles which, upon application of focused ultrasound, may burst and temporarily disrupt tight junction proteins. Advantages and disadvantages of both are listed.

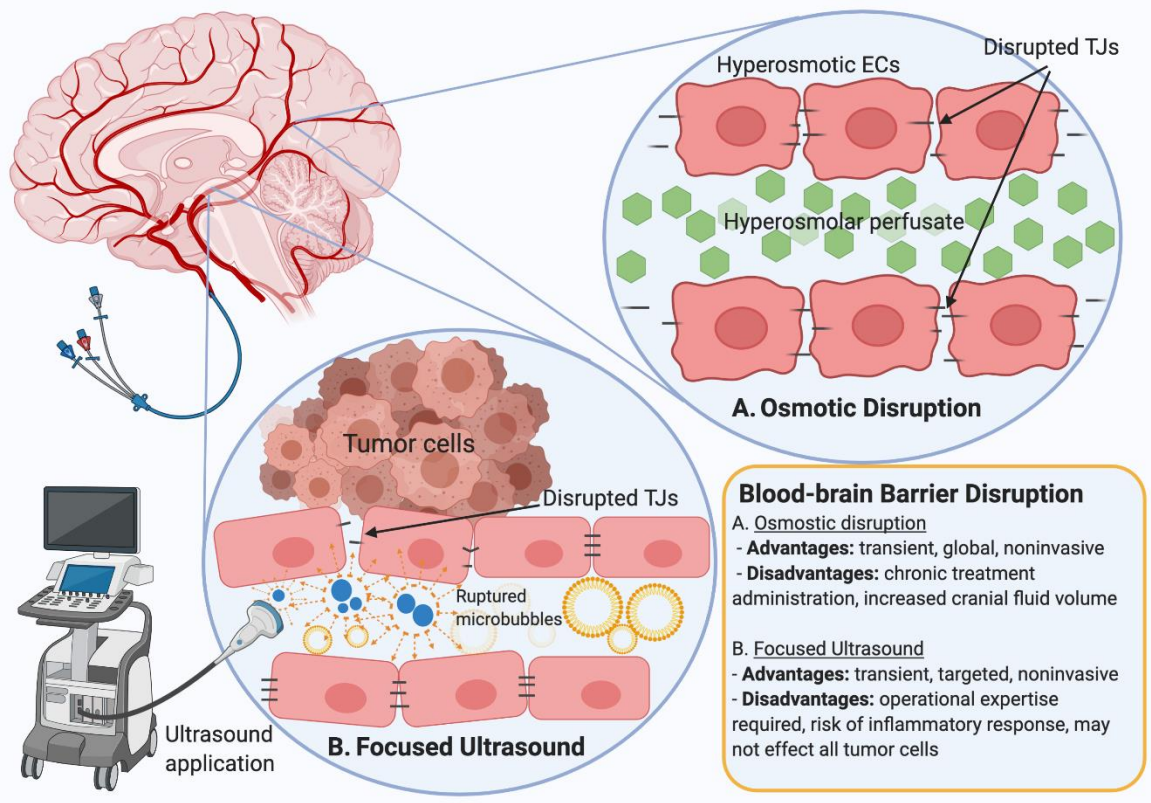

Focused Ultrasound

A localized disruption of the neurovasculature using focused ultrasound (FUS) has been suggested as an anatomically or functionally-targeted method for drug delivery from the vasculature into the brain parenchyma. FUS-induced BBB opening in the presence of microbubbles is local, transient and reversible, usually within several hours (Sheikov *et al.*, 2008). Its feasibility and efficacy to promote the delivery of therapeutic agents into the brain has been examined extensively since 1997 when Kullervo Hynynen and Ferenc Jolesz first demonstrated the potential feasibility of BBBD through the intact human skull utilizing short, high-intensity ultrasound (Hynynen and Jolesz, 1998). More recently, with the application of magnetic resonance-compatible transducers, image-guided FUS has allowed targeted localization to brain tumors and reduced the risk of off-target effects (Choi *et al.*, 2007; Treat *et al.*, 2007; Lipsman *et al.*, 2018).

Therapeutic FUS is generally applied in conjunction with intravenously administered microbubbles (**Figure 5.3**). These microbubbles are lipid, protein, or polymer-shelled, inert gas-filled bubbles which are usually between 0.5 to 10 μm in diameter (Himuro, 2007). They are currently FDA-approved for use as contrast agents in ultrasound imaging and are utilized in the context of drug delivery to help reduce the energy threshold required for BBBD (Timbie *et al.*, 2015). The energy threshold is, to some extent, determined by the size of microbubbles, and typically the smaller the diameter of these microbubbles, the higher the pressure required for effectiveness (Tung *et al.*, 2011). It is important to carefully control the energy level of FUS, as high pressure and frequency may cause an inflammatory response and/or tissue damage, such as hemorrhage and apoptotic neuronal damage(Tsai *et al.*, 2018). Extensive research into the safety and feasibility of FUS has been initiated in a variety of CNS diseases, and recently, clinical studies have been conducted to determine the safety and efficacy of the

application of FUS with intravenously injected microbubbles in human brain tumors (Carpentier *et al.*, 2016; Idbaih *et al.*, 2019; Mainprize *et al.*, 2019).

This approach for BBBD has been shown to be relatively safe, but it also has limitations (Burgess and Hynynen, 2013). Despite the early increase in drug delivery to CNS, recent studies with large molecules showed that enhanced permeability is diminished after 5 days (Arvanitis *et al.*, 2018). This could be one explanation for why many animal studies on FUS conducted with trastuzumab showed nonsignificant difference regarding survival when comparing FUS- and nonFUS-treated groups (Park *et al.*, 2012; Kobus *et al.*, 2016). Repeated FUS treatment before drug administration may therefore be required, which increases risk. Other obstacles in a wide clinical FUS application include issues with repeatability of the FUS procedure and dependence on MRI and specially-trained operators (Burgess *et al.*, 2016).

Overall, FUS-mediated BBBD has provided a promising approach to therapeutic delivery to brain tumors and other CNS diseases such as Alzheimer's and Parkinson's diseases (Miller and O'Callaghan, 2017). Meanwhile, successful and wider clinical translation requires more extensive and thorough examination of possible safety issues due to repeated BBBD, the repeatability of FUS treatment, and optimization of ultrasound parameter settings.

5.5 NANOPARTICLES AND TARGETED DELIVERY

Nanoparticles are a large category of nanoscale particles (1-1000 nm) with the capacity to adsorb, entrap, or to be modified with various therapeutic agents. These particles are promising strategies to improve brain drug delivery (Lockman *et al.*, 2002). This section is focused on nanoparticle strategies to overcome low neurovascular permeability and increase drug delivery into brain tumors.

Biological Vectors:

Viral vectors

Viral vectors have been repeatedly used in GBM gene therapy clinical trials (Caffery *et al.*, 2019). Viral vectors have the ability to naturally infect cells with nucleic acids with high transfection efficiency (Dong, 2018). Currently, several viruses have been developed into vectors for brain delivery, including retroviruses, adenoviruses and adeno-associated viruses (AAVs) (Lang *et al.*, 2003; Huang *et al.*, 2013; Guhasarkar *et al.*, 2016; Caffery *et al.*, 2019; Pandit *et al.*, 2019). Although viral vectors have been studied for over two decades, they have only resulted in marginal increases in overall survival. The limitations of using viral vectors for drug delivery include poor brain tumor penetration, highly invasive administration methods, and a prevailing risk of oncogenesis and lethality of viral vectors (Lang *et al.*, 2003; Huang *et al.*, 2013; Guhasarkar *et al.*, 2016; Caffery *et al.*, 2019; Pandit *et al.*, 2019).

Exosomes

Exosomes are small endogenous extracellular vesicles (40–100 nm in diameter), which are secreted by various types of cells and have drug loading and signal-carrying capacity (Liao *et al.*, 2019). Exosomes can be loaded with various kinds of cargos, such as nucleic acids, proteins, and small molecules due to their bubble-like structure (Yang

et al., 2015; Ha *et al.*, 2016). Exosomes are generally stable in circulation and lack significant immunogenicity (Ha *et al.*, 2016; Pandit *et al.*, 2019). They transport cargos among cells and may even cross BBB via endogenous pathways of intercellular communication (Yang *et al.*, 2015; Ha *et al.*, 2016; Liao *et al.*, 2019; Pandit *et al.*, 2019). In addition, exosomes have also played important roles in cancer immunotherapy by virtue of the biological signals enclosed in exosomes (Liu *et al.*, 2017; Liao *et al.*, 2019). However, the technologies and strategies to isolate and purify exosomes must be further developed to ensure quality control, and other side effects such as the potential tumor induction risk of tumor cell-derived exosomes has to be taken into account (Ha *et al.*, 2016; Dong, 2018; Liao *et al.*, 2019).

Cell delivery

Cell-based drug delivery is another exciting strategy for delivery of therapeutics across the BBB via the innate mobility of cells. There are two cell types that have been evaluated as therapeutic carriers: immune cells and stem cells. In particular, neural stem cells (NSCs), mesenchymal stem cells (MSCs) and neutrophils have been studied for cell-based therapy (Aboody *et al.*, 2008; Xue *et al.*, 2017; Sheets *et al.*, 2018).These cell carriers can deliver a variety of therapeutics, including genes, cytokines, enzymes, and nanoparticles across the BBB and are naturally recruited to the sites of brain tumors by an inflammation-mediated pathway (S. Hersh *et al.*, 2016). Detailed mechanisms of the cell carrier's delivery can be found in recommended reviews (S. Hersh *et al.*, 2016; Parodi *et al.*, 2019).The major difficulties associated with this strategy are the limited therapeutics loading and potential toxicity of the cargos to the cell carriers themselves. What's more, the spatial and temporal release of the therapeutic agents from the cell carriers must be well-controlled during drug delivery in order to achieve expected efficacy (Batrakova *et al.*, 2011; S. Hersh *et al.*, 2016).

Synthetic Vehicles

Synthetic nanoparticles have been broadly investigated to deliver drugs to brain. The physicochemical properties of the nanoparticles, including the size, surface charge, and lipophilicity are important in the brain passive diffusion process. A growing interest in the application of inorganic nanoparticles, especially metallic nanoparticles and metallic oxide nanoparticles, in CNS delivery has emerged among the BBB research community (Sawicki *et al.*, 2019; Luther *et al.*, 2020). Iron oxide nanoparticles, such as maghemite (γ-Fe_2O_3) and magnetite (Fe_3O_4), are extensively explored due to the inherent magnetic properties coupled with tunable size and surface functionality (Prades *et al.*, 2012; Múzquiz-Ramos *et al.*, 2015; Azcona *et al.*, 2016). Mesoporous silica nanoparticles (MSNPs) are nanoscale silica particles with a good loading capacity due to the porous structure and easily modified surface, which are the most commonly applied silica-based delivery vehicles (Tang *et al.*, 2012). These inorganic nanoparticles are produced on the scale of nanometers in order to increase their ability to cross BBB, providing photodynamic or contrast imaging functions due to the materials properties (Luther *et al.*, 2020) . However, the potential for neurotoxicity and unspecific distribution are serious barriers to the broad application of metallic nanoparticles (Sawicki *et al.*, 2019).

Actively targeted nanoparticles account for the majority of brain drug delivery systems currently under investigation. Surface modified nanoparticles are transported into brain, bypassing the BBB by three main routes: adsorptive-mediated transcytosis (AMT), receptor-mediated transcytosis (RMT), and transporter-mediated transcytosis (TMT) (Kreuter, 2013; Parodi *et al.*, 2019). Adsorptive-mediated brain targeting largely depends on the electrostatic interaction between the positively-charged drug delivery systems and the negatively-charged BBB (Jallouli *et al.*, 2007). However, this nonspecific targeting is the inherent limitation of AMT since the negatively-charged membranes present throughout all the vascular system (Parodi *et al.*, 2019). What's

more, positive nanoparticles have more tendency to adsorb surrounded proteins and form protein corona (Mendes *et al.*, 2018). RMT and TMT target brain more specifically than AMT through ligand-receptor recognition. These receptor-mediated strategies will be further introduced in the following section. The transporters for TMT are usually transporters of nutrient materials like sugars, vitamins, hormones, and amino acids (Li *et al.*, 2011; Rip *et al.*, 2014; Parodi *et al.*, 2019). These actively-targeted nanoparticles target brain tumor more specifically and therefore have higher accumulation and lower systemic side effects. However, some concerns such as protein adsorption and corona formation around the nanoparticles, potential neurotoxicity, and the difficulty of manufacturing due to the complex structures need to be further addressed (Johnsen *et al.*, 2017; Parodi *et al.*, 2019).

Receptor-Mediated Transcytosis (RMT)

The final strategy to be discussed in this section is the use of endogenous active transport mechanisms to improve drug delivery to brain tumors, in particular, RMT. This transport is accomplished by three basic steps: binding of the cargo to the target receptor on the luminal side of the brain EC, endocytosis, sorting, and transport across the EC cytoplasm, and finally release of the cargo from the basolateral membrane of the EC into the brain interstitium (**Figure 5.4**). As discussed in reference to the heterogeneity of BTB permeability, it may be beneficial to address the treatment of brain tumors by utilizing a 'whole brain' delivery strategy to address intact NVU/BBB (Agarwal *et al.*, 2011). RMT-based strategies can be viewed as such an approach, because they are generally designed to target transport mechanisms that are functional throughout the extensive vasculature of the brain. Successful brain delivery using RMT requires that target receptors have high relative expression on the luminal side of the brain endothelium, must mediate transcytosis, and should have high turnover (Yu *et al.*, 2011;

Oller-Salvia *et al.*, 2016a). Importantly, the receptor-binding moiety should also have relatively low affinity for the target in order to optimize drug delivery and release in the brain parenchyma, and to limit trafficking to the lysosome (Yu *et al.*, 2011; Haqqani *et al.*, 2018).

Figure 5.4 Receptor-Mediated Transcytosis for Drug Delivery to Brain Tumors

Receptor-mediated transcytosis is one of the most common techniques to increase delivery of large molecules, nanoparticles, and brain-impermeant drugs to brain tumors. Cargo bound to endothelial membrane-bound receptors is pulled into ECs and sorted in the early endosome. Bivalent-binding and high-affinity cargo-receptor complexes are often trafficked to the lysosome for degradation, whereas cargoes bound with lower affinity are more likely to be trafficked for transport across the cell. The cargo is then released on the abluminal side of the endothelium, and the receptor may be recycled back to the luminal membrane.

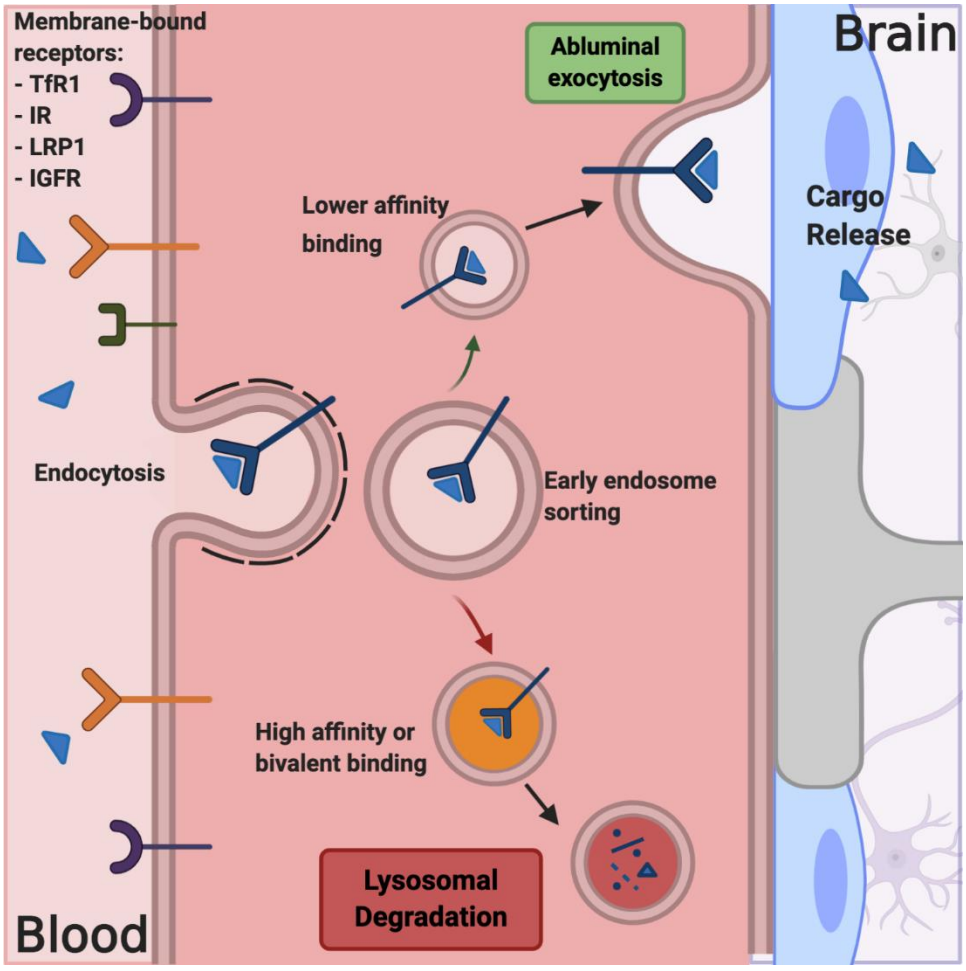

Common receptor targets include thransferrin receptors (TfR1), insulin receptors (IRs), insulin-like growth factor receptors (IGFRs), the low-density lipoprotein-related protein receptor 1 (LRP1), and nicotinic acetylcholine receptors (nAchRs). This strategy has been widely explored in the brain barriers-research community for use in a number of CNS diseases from brain tumors to lysosomal storage disorders, Alzheimer's disease, Parkinson's disease, and others. As noted in the previous sections, these various RMT-based delivery mechanisms are often combined with other technologies like BBBD, CED, nanoparticle formulations, gene delivery, and novel biologics. Herein, we will classify delivery constructs into two categories: shuttle peptides, and antibody-based constructs.

BBB Shuttle Peptides

Shuttle peptides are relatively short sequences of amino acids (<50 AAs) that bind to a receptor on the luminal side of the EC to induce endocytosis of the cargo. They are often based on the known sequences from receptor-binding domains of endogenously transported substances like insulin, ApoE and transferrin, but they may also be discovered by phage display biopanning. These peptides can be directly bound to cargo or associated via noncovalent interactions (Oller-Salvia *et al.*, 2016b). Covalently bound shuttle peptides are more likely to have known and relatively consistent stoichiometry, kinetics, and affinity. On the other hand, some investigation into noncovalent associations that may be more prone to cargo release might be more rapidly translated across a number of different drugs for various applications (Sarkar *et al.*, 2014; Aasen *et al.*, 2019). However, their binding affinity for cargo and optimal stoichiometry must be determined. Benefits to shuttle peptides in general include their relatively small size, simplicity of synthesis and purification, versatility, and discovery through biopanning. Limitations include their liability to proteolytic degradation and

relatively short half-life in circulation, which may be ameliorated somewhat by cyclization (Bird *et al.*, 2010).

All of the aforementioned receptors have been targeted for drug delivery. Though there is debate as to the location of LRP1 expression on brain ECs (Richardson and Morgan, 2004; Pardridge, 2020), a number of shuttle peptides have been developed to target this receptor, including the agiopeps and K16ApoE. The K16ApoE peptide consists of 16 lysine residues and the LRP1-binding domain of ApoE (G. *et al.*, 2013; Sarkar *et al.*, 2014). While this has shown some evidence of improved drug delivery to brain, the therapeutic window is narrow, and may not be suitable for clinical translation due to acute toxicities observed in mice (Aasen *et al.*, 2019). Angiopep-2 is one of the most well-characterized shuttle peptides for brain delivery, and is derived from the Kunitz domain of aprotinin (Demeule *et al.*, 2008). Angiopep-2 has been widely utilized as a targeting moiety for nanoparticle formulations of antineoplastic agents like TMZ and docetaxel, as well as siRNA, monoclonal antibodies (mAbs) and various radiosensitizing agents for the treatment of CNS tumors (Regina *et al.*, 2015; Tian *et al.*, 2015; Luo *et al.*, 2017; Shi *et al.*, 2018; Wang *et al.*, 2018; Zhu *et al.*, 2018; Hoyos-Ceballos *et al.*, 2020). The most developed shuttle peptide construct is likely ANG1005, an Angiopep-paclitaxel conjugate recently investigated in clinical trials for the treatment of brain metastases from breast cancer as well as meningiomas (Thomas *et al.*, 2009; P. *et al.*, 2016; Kumthekar *et al.*, 2020). Other shuttle peptides include Peptide-22, which binds to LDLR, and glutathione, which binds to the GSH transporter. GSH-coated pegylated nanoparticles show increased CNS penetration, and have been investigated in clinical trials for the delivery of doxorubicin to brain tumors (Brandsma *et al.*, 2014; Gaillard *et al.*, 2014). TfR1 has also been widely investigated as a delivery mechanism, due to its expression on tumor cells as well as brain ECs (Recht *et al.*, 1990). T7 targets TfR1, and is a shuttle peptide that has been investigated to deliver antisense oligonucleotides to

gliomas (Kuang *et al.*, 2013; Kim *et al.*, 2020). Delivery of radiosensitizing gold nanoparticles to brain tumors has been shown to be enhanced by Tfpep (Dixit *et al.*, 2015), and another TfR1 directed peptide, THR, was recently compared with other previously mentioned peptides for the delivery of AAVs and gold nanoparticles to brain, but without specific applications towards the treatment of brain tumors (Prades *et al.*, 2012; Zhang *et al.*, 2018). A vast variety of BBB shuttle peptides have been explored, and we direct the reader to an excellent review of the topic for further reading (Oller-Salvia *et al.*, 2016a).

Antibody-based delivery systems

Antibody-based therapies are one of the most rapidly-evolving fields in pharmaceutics due to their plasma stability, long half-life, and specificity. Antibodies, specifically immunoglobulin G (IgGs) are large, bivalent molecules (~150kDa) composed of two identical heavy chains and two identical light chains bound by disulfide bonds. These proteins have proved to be incredibly effective in the treatment of peripheral tumors, but they do not generally cross the BBB from blood into brain (Zhang and Pardridge, 2001; Schlachetzki *et al.*, 2002; Abuqayyas and Balthasar, 2013). In fact, without enhanced delivery mechanisms, drug accumulation in the brain is likely to be much less than 1% (Abuqayyas and Balthasar, 2013; St-Amour *et al.*, 2013). However, there is still significant interest in delivering these drugs to brain (Gan *et al.*, 2017; Kumar *et al.*, 2018; Cavaco *et al.*, 2020; Gril *et al.*, 2020; Pardridge, 2020), and antibodies are also well-suited to serve the same purpose as shuttle peptides to promote RMT. With the recent blossoming of innovative protein engineering and use of antibody fragments, the somewhat ‘modular’ structure of IgGs has been exploited to modify and utilize different domains. This allows them to be optimized for use as brain-targeted therapies and brain delivery vehicles.

A variety of therapeutic antibodies as well as antibody-decorated NPs have been targeted to the brain via the TfRs and IRs for treatments of CNS diseases, most notably Alzheimer's disease and brain tumors (Zhang *et al.*, 2002; Boado *et al.*, 2016). In recent years, a nanocarrier of p53 gene therapy decorated with anti-TfR1 single-chain variable fragments (scFvs), SGT-53, has been successful in preclinical studies and has moved into clinical trials (Xu *et al.*, 2002; Senzer *et al.*, 2013; SS Kim *et al.*, 2019). Though a study in adult refractory CNS tumors was terminated, actively recruiting studies for children with refractory solid tumors, and planned clinical trials in refractory CNS tumors in pediatric patients (NCT02354547, NCT03554707) are still ongoing. Other imaginative antibody constructs explore bispecific or multivalent targeting (Stanimirovic *et al.*, 2014; Verdino *et al.*, 2018). Recent work from AbbVie demonstrates the targeting of multivalent, dual-variable-domain IgGs (DVD-Igs) with dual affinity for precision targeting. These molecules can bind two targets, TfR1 for RMT, and HER2 for prospective targeting to HER2+ brain tumors, while maintaining the Fc domain unchanged, allowing for beneficial FcRn recycling (Karaoglu Hanzatian *et al.*, 2018). Further, recently published work from Denali Therapeutics demonstrates a novel protein transport vehicle (TV) with affinity for TfR1 incorporated into the Fc region of the IgG, allowing for retention of bivalent binding to the therapeutic target (Kariolis *et al.*, 2020; Ullman *et al.*, 2020). Though these are not explicitly intended to treat brain tumors, they are an exciting contribution.

5.5 CONCLUSION AND FUTURE PERSPECTIVES

In the past decade, there has been a tremendous increase in the understanding of the physiology of the BBB. However, this has not translated to efficacious treatment of CNS disorders ranging from epilepsy to brain tumors. In the case of both primary and metastatic brain tumors, the BBB is disrupted heterogeneously, leading to the formation of the blood-tumor barrier (BTB). The BTB harbors considerable structural and functional heterogeneity within the tumor microenvironment and varies across different cancer subtypes (Arvanitis *et al.*, 2020). It compels us to question if the leakiness can be used to our advantage to deliver drugs in desired concentrations that the target site.

While some reports have shown positive correlation between increased permeability in the tumor to tumor size and growth patterns, there are reports, including those from NIH, that demonstrate no correlation between the two. These inconsistencies highlight the problem of heterogeneity of the BBB breakdown, and this challenge is encountered in the clinical setting as well. Diagnosis of brain tumors using fluorescent tracers is facilitated by the increased permeability of the BTB, but why does it not extrapolate to the treatment modalities like chemotherapy? Instead of relying on the altered BBB permeability to delivery cytotoxic cargo to the tumor cells, it would be better to prepare the delivery systems to face the most challenging barrier – the intact BBB, and strategize the delivery to efficiently target the tumor cells and reduce any off-target toxicity.

Over years of research, various strategies have been developed to invasively or non-invasively overcome the BBB. The invasive strategies bypass the BBB altogether and deliver the therapeutic agents directly into the brain parenchyma or into the CSF. These strategies prevent systemic exposure of the drug, thereby limiting its toxicity and side-effects. They have been widely explored in the clinical setting and there are numerous on-going clinical trials, demonstrating the huge potential of this strategy. However, invasive procedures need highly specialized instruments and personnel. From

a patient's perspective, non-invasive strategies are preferred. Various non-invasive BBB-disrupting strategies and nanoparticle drug delivery systems which bypass the BBB by a number of transport routes are discussed in the review. Transient disruption of the BBB using focused ultrasound enables delivery of a wide range of therapeutics in the brain, ranging from small molecules to large molecules. It is imperative to understand the kinetics and time duration of the temporary disruption to effectively plan the delivery of therapeutics. The first decade of the 21st century saw the "nanoparticle boom" and nanoparticles proved to be able to deliver conventional drugs, recombinant proteins, vaccines, and nucleotides. This versatile carrier system can be modified to target various transcytosis pathways to ensure improved drug delivery using the enhanced permeation retention (EPR) effect (Tzeng and Green, 2013).

Understanding the physiology of the BBB at a cellular and molecular level helps design delivery systems that selectively target the receptors and transporters on the cell surface of BBB. A challenge while developing these constructs is to avoid off-target effects. Ensuring delivery at the site of action is critical to achieve the desired concentrations at that site and minimal off-target effects. Thus, understanding the pharmacokinetics of the delivery systems would be imperative for their progress from the pre-clinical research settings to the clinical scenario.

In conclusion, there is now a better understanding of the BBB/BTB physiology that has led to the development of a multitude of strategies to target the tumor cells present beyond these barriers. As has been demonstrated on numerous occasions in the past, a "one size fits all" approach is not effective. Rational combination of drugs and their delivery is now designed to attain optimal concentrations in brain tumors. In this way, a comprehensive treatment regime will be established

CHAPTER 6

PAYLOAD DISTRIBUTION AND PHARMACOKINETICS FOLLOWING ADMINISTRATION OF AN ANTIBODY-DRUG CONJUGATE VIA CONVECTION-ENHANCED DELIVERY

6.1 INTRODUCTION

Antibody-drug conjugates (ADCs) are a rapidly developing class of therapeutics and have ushered in a new paradigm for the treatment of numerous cancers. These drugs are comprised of cytotoxic payload molecules conjugated to a tumor-targeting antibody via a chemical linker. ADCs are formulated to be stable in the systemic circulation, and the payload is released upon binding and internalization of the ADC into a target-expressing cell. Therefore, they combine the highly-specific targeting and extended exposure of an antibody with potent toxins, significantly increasing the therapeutic index. These drugs have sometimes been called the “guided missiles” of oncology (Fu *et al.*, 2022), and the ability to customize combinations of cytotoxic payload, linker, and antibody to be highly specific to the application has been a great asset to their development. To date, nine ADCs have been approved by the United States Food and Drug Administration (Tong *et al.*, 2021), and numerous clinical trials of ADCs are ongoing.

In contrast to the success of these drugs in the treatment of peripheral cancers like non-small cell lung cancer, breast cancer, and blood cancers, ADCs have shown little clinical benefit in the treatment of CNS tumors, specifically glioblastoma (GBM). The survival rates for GBM remain dismal, with a 5-year survival rate of only 6.8% despite extensive research and development efforts in recent decades (Ostrom *et al.*, 2019). In this context, depatuxizumab mafodotin, an EGFRviii-directed ADC containing the potent microtubule inhibitor monomethyl auristatin F (MMAF), recently failed to reach the primary endpoint in the pivotal Phase 2/3 clinical trials (van den Bent *et al.*, 2019). The specific targeting of this ADC to an epitope unique to aberrant EGFR expression eliminated the liability to skin and gastrointestinal side effects commonly associated with EGFR inhibitors and antibodies (Reilly *et al.*, 2015; Phillips *et al.*, 2016). However, the trials were plagued by corneal epitheliopathy, known to be associated with MMAF and

mytansinoid toxins (Eaton *et al.*, 2015). Subsequent preclinical studies have shown that the lack of efficacy in GBM was likely due in large part to limited and heterogeneous delivery to the tumors (Marin *et al.*, 2021).

Heterogeneous distribution of systemically administered drugs to brain tumors has been one of the critical hurdles to overcome in the treatment of CNS cancers. While there was a persistent misconception that the increased permeability of the blood-brain barrier (BBB) in brain tumors will allow for their imaging via contrast-enhanced MRI, might also result in efficacious drug delivery; this misconception has been repeatedly disproven (Lockman *et al.*, 2010; Sarkaria *et al.*, 2018b; de Gooijer *et al.*, 2021). Increased permeability in and around brain tumors is highly variable (Talele *et al.*, 2022), and the BBB continues to play a significant role in the clinical failure of many CNS therapeutics across a spectrum of treatments (Griffith *et al.*, 2020). As such, it is imperative to consider an intact blood-brain barrier when developing drugs to treat CNS tumors.

For an intact BBB, the distribution of protein therapeutics into brain interstitial fluid (ISF) is size-dependent and relatively poor for full-length IgGs (Yuan *et al.*, 2022). The large molecular weight of ADCs, over 150,000 kDa, makes their permeability into brain tumors following systemic administration highly dependent on significant BBB breakdown. Given the limitations of systemic delivery, there is an increasing appetite to deliver these drugs directly to the brain parenchyma. Convection-enhanced delivery (CED) is one potential strategy for direct-to-tumor administration of drugs. CED involves the placement of a catheter directly into the brain parenchyma and utilizes convective flow to increase the distribution of drug beyond the region that might be accessible with a point injection and diffusion alone (D'Amico *et al.*, 2021). This strategy may also limit dose-limiting peripheral side effects, as higher concentrations can be administered to the tumor region at lower doses overall. Even though CED has been investigated for the

delivery of large molecules to brain since 1994 (Bobo *et al.*, 1994), the systemic pharmacokinetics of drugs, ADCs in particular, following administration via CED are not described in the literature in conjunction with CNS distribution, as exposures are assumed to be low.

This study investigates the CNS and systemic pharmacokinetics of payload molecules following administration of ABBV-221 via CED. ABBV-221 is comprised of an affinity-matured derivative of the antibody utilized in depatuxizumab mafodotin, which is conjugated to MMAE via a cleavable valine-citrulline (vc) linker (Phillips *et al.*, 2018). The benefits of MMAE as a payload are that it has not been shown to elicit the ocular side effects associated with MMAF, and it is cell-permeable. This allows MMAE to induce bystander killing, which could be an asset in the treatment of genetically heterogeneous GBM (F Li *et al.*, 2016). Recent studies have shown that MMAE distributes widely into peripheral tissues following IV administration of the free drug (Chang *et al.*, 2021). However, the pharmacokinetic disposition of the payload following CED is difficult to predict from these studies, as it has also been characterized to be a substrate for P-glycoprotein (P-gp) efflux *in vitro* (Liu-Kreyche *et al.*, 2019), and P-gp plays an important role in the CNS pharmacokinetics of many small molecules (Durmus *et al.*, 2015; Parrish *et al.*, 2015; Talele *et al.*, 2021; Griffith *et al.*, 2022). Our hypothesis is that the administration of ABBV-221 via CED will provide long-term retention of the payload, MMAE, in the CNS with more limited exposure of the brain to the free drug as compared to the CED administration of free MMAE alone.

One aspect of the current study was to characterize the systemic and CNS disposition of MMAE following IV and CED administration of the free drug (unbound to antibody). This work also conclusively describes the contribution of efflux at the CNS barriers to MMAE CNS disposition, and characterizes the systemic and CNS pharmacokinetics of the payload following systemic and CED administration of ABBV-

221 over 24 hours. The work herein provides valuable information regarding the potential for the safe administration of ABBV-221 and other MMAE-containing ADCs via CED for the treatment of brain tumors.

6.2 MATERIALS AND METHODS

6.2.1 Chemicals, Reagents and Tissues:

Monomethylauristatin E ((2*S*)-*N*-[(2*S*)-1-[[(3*R*,4*S*,5*S*)-1-[(2*S*)-2-[(1*R*,2*R*)-3-[[(1*S*,2*R*)-1-hydroxy-1-phenylpropan-2-yl]amino]-1-methoxy-2-methyl-3-oxopropyl]pyrrolidin-1-yl]-3-methoxy-5-methyl-1-oxoheptan-4-yl]-methylamino]-3-methyl-1-oxobutan-2-yl]-3-methyl-2-(methylamino)butanamid) was obtained from MedChemExpress (# HY-15162, Monmouth Junction, NJ). Monomethylauristatin F ((2*S*)-2-[[(2*R*,3*R*)-3-methoxy-3-[(2*S*)-1-[(3*R*,5*S*)-3-methoxy-5-methyl-4-[methyl-[(2*S*)-3-methyl-2-[[(2*S*)-3-methyl-2-(methylamino)butanoyl]amino]butanoyl]amino]heptanoyl]pyrrolidin-2-yl]-2-methylpropanoyl]amino]-3-phenylpropanoic acid) was also purchased from MedChemExpress (# HY-15579). EGFR-specific antibody-drug conjugate (ABBV-221) with a DAR = 2 was provided by AbbVie (Lot # 2881143, North Chicago, IL) and stored in single-use aliquots at -80°C prior to use. Brentuximab vedotin was a kind gift of Dr. Christopher Moertel. Lyophilized papain protease from papaya latex (# P4762) was purchased from Sigma Aldrich (St. Louis, MO). Human brain biopsy samples were obtained from the Mayo Clinic. All other chemical reagents were high-performance liquid chromatography grade and purchased from Thermo Fisher Scientific (Waltham, MA).

6.2.2 Animals:

MMAE IV pharmacokinetic studies were performed using both male and female Friend Leukemia Virus strain B (FBV) mice of age 8-14 weeks of two different genotypes. These genotypes included wild-type *and* $Bcrp^{-/-}$ $Mdr1a/b^{-/-}$(triple knockout, TKO) mice (breeder pairs from Taconic Biosciences, Inc., Germantown, NY). Colonies of the FVB mice were maintained and housed in the RAR facility at the Academic Health Center of the University of Minnesota, and animal genotypes were regularly verified by

tail snip (TransnetYX, Cordova, TN). Mice for MMAE IV pharmacokinetic studies were maintained on a 12-hour light/dark cycle with *ad libitum* access to water and food. For ABBV-221 in vitro stability studies, brains from CBL6 *CES1C*$^{-/-}$ mice were used. Colonies of *CES1C*$^{-/-}$ mice were similarly maintained and housed in the RAR facility at the Academic Health Center of the University of Minnesota (breeder pairs obtained from Jackson Labs, Bar Harbor, ME) Protocols for these animal experiments received approval by the University of Minnesota Institutional Animal Care and Use Committee and were performed in accordance with the Guide for Care and Use of Laboratory Animals established by the U.S. National Institutes of Health.

For ABBV-221 intraperitoneal (IP) and CED studies as well as MMAE CED studies, wild-type FVB mice of ages 8-10 weeks were used (Charles River Laboratories). These mice were housed for at least 48 hours prior to use on a 12-hour light/dark cycle with *ad libitum* access to water and food. All animals were given 1 mL saline 24 hours prior to the start of dosing, and mice in CED studies were also given 2oz of diet gel (Clear H2O 72-07-5022) 24 hours prior to surgery. All animal studies were approved by the Mayo Institutional Animal Care and Use Committee in accordance with the Guide for Care and Use of Laboratory Animals established by the U.S. National Institutes of Health.

6.2.3 MMAE Intravenous Pharmacokinetic Studies

A single dose of MMAE at 0.5 mg/kg was administered to wild-type (WT) and triple-knockout (*Bcrp*$^{-/-}$ *Mdr1a/b*$^{-/-}$, TKO) FVB mice via tail vain injection. The dosing formulation was prepared in physiological saline with 1% DMSO. Following IV administration, mice were euthanized via a CO_2 chamber, and blood and brain were rapidly collected at time points from 5 minutes to 8 hours (n=4 mice per time point). Blood was collected via cardiac puncture using heparinized syringes and transferred into

heparinized tubes. Plasma was separated by centrifugation at 7500 rpm for 15 minutes at 4°C, and all samples were stored at -80°C until LC-MS/MS analysis. Prior to analysis, brain was thawed and homogenized in 2X (w/v) 5% BSA.

6.2.4 ABBV-221 Intraperitoneal Pharmacokinetic Study

A single dose of ABBV-221 at 5 mg/kg was administered via intraperitoneal injection to wild-type FVB mice. The dosing formulation was prepared in sterile PBS. Following administration, mice were euthanized via a CO_2 chamber, and blood and brain were rapidly collected at time points from 40 minutes to 24 hours after administration (n=5 mice per time point) as stated above. Samples were similarly stored at -80°C until LC-MS/MS analysis, and prior to sample preparation, brain was thawed and homogenized in 2X (w/v) 5% BSA.

6.2.5 ABBV-221 and Free MMAE Convection Enhanced Delivery Pharmacokinetic Studies

In separate studies, single doses of ABBV-221 (60µg) or MMAE (570ng) were administered via CED. The dose of MMAE was chosen to approximate the amount of MMAE administered with 60µg of ABBV-221 with DAR = 2. Dosing formulations for both studies were prepared in sterile PBS. For all CED infusions, mice were anesthetized with 100 mg/kg ketamine and 10 mg/kg xylazine. After skin disinfection, a 1-cm midline incision extending from just behind the eyes to level of the ears was made using a sterile scalpel. Mice were secured on a stereotactic stage with automated thermal support (Stoelting #53800M). The internal cannula (P1 #8IC315IS5SPC, cut 4mm projection) and guide cannula (P1 #8IC315GS5SPC, cut 3.5mm projection) were connected to PE

tubing and secured with a single connector-assembly (P1 #C313C/SPC). The whole unit was secured vertically with a cannula holder (World Precision Instruments #505254). Drug solution was primed through the internal cannula, cannula tubing, and 22-gauge 25 μL Hamilton syringe (Hamilton # 80400) and the syringe was placed in the Legato 130 syringe pump (KD Scientific #788130). The cannula holder with attached internal cannula was lowered into the brain until the plastic pedestal was flush with the mouse skull. A ramped infusion protocol was used with rate of infusion as follows: 3 μL at 0.2 μL/min, then 5 μL at 0.5 μL/min, and then 12 μL at 0.8 μL/min (Beffinger *et al.*, 2019). Blood and brain were rapidly collected as stated above at time points ranging from 40 minutes to 24 hours after the start of the infusion, and brains were separated into right and left hemispheres.

6.2.6 MMAE Forced Deconjugation

Ezymatic cleavage was used to cleave the valine-citrulline (vc) linker of ABBV-221 and liberate MMAE payload for quantitation using LC-MS/MS analysis. Enzymatic cleavage was accomplished using papain cysteine protease from papaya latex (Y Li *et al.*, 2016; Singh and Shah, 2017). Brain homogenate or plasma samples (50uL) were spiked with internal standard (MMAF). To these samples, a 1:1 volume of freshly prepared papain solution (4mg/mL in DI H_2O) was added to achieve a final concentration of 2mg/mL of enzyme. These samples were incubated for 20-22 hours at 40°C with continuous shaking at 160 rpm. Following incubation, the reaction was stopped with the addition of 5X volume acetonitrile to precipitate protein. Samples were vortexed and centrifuged, and supernatant was collected and dried under vacuum. Finally, samples were reconstituted in 100uL 95:5 H_2O:ACN with 0.1% formic acid for injection. The

standard curve was constructed using free MMAE, and the method was initially validated using brentuximab vedotin, another antibody-drug conjugate containing MMAE (DAR = 4) conjugated to the antibody using a vc linker. Briefly, a single-use brentuximab vedotin stock (500µg/mL) was diluted to a concentration of 50 µg/mL, which equates to an approximate concentration of 939 ng/mL of MMAE according to **Equation 6.1** (Liu *et al.*, 2015). Serial dilutions were performed to span the approximate range of the MMAE standard curve, and these samples were treated as above.

$$\frac{\boldsymbol{Conc.of\ conjugated\ payload}\ (\frac{\boldsymbol{ng}}{\boldsymbol{mL}})}{\boldsymbol{Conc.of\ ADC}\ (\frac{\boldsymbol{ng}}{\boldsymbol{mL}})} = \boldsymbol{DAR} \times \frac{\boldsymbol{MW\ of\ conjugated\ payload}\ (\frac{\boldsymbol{g}}{\boldsymbol{mol}})}{\boldsymbol{MW\ of\ ADC}\ (\frac{\boldsymbol{g}}{\boldsymbol{mol}})} \quad (6.1)$$

Following the forced deconjugation of MMAE from brentuximab vedotin in two separate runs on consecutive days, linear regressions of the predicted vs. observed concentrations of MMAE showed slopes of approximately 1.2, with an R squared = 0.997 or greater in both cases. The slopes and intercepts from both runs were not significantly different, and the intercept was approximately 6 ng/mL in both cases (**Figure 6.1**). It was concluded from these data that the stock concentrations may have been higher than expected according to the package insert for brentuximab vedotin, but that the method produced reasonably complete deconjugation of MMAE from the antibody with consistent results. Therefore, this method was employed to quantify total MMAE in samples following the administration of ABBV-221.

Figure 6.1 Predicted vs Observed Concentrations of MMAE

MMAE was cleaved from brentuximab vedotin using papain cysteine protease. Following cleavage, protein was precipitated to separate free MMAE. Concentrations of MMAE were predicted using the average DAR of brentuximab vedotin, and predicted vs observed concentrations were assessed via simple linear regression

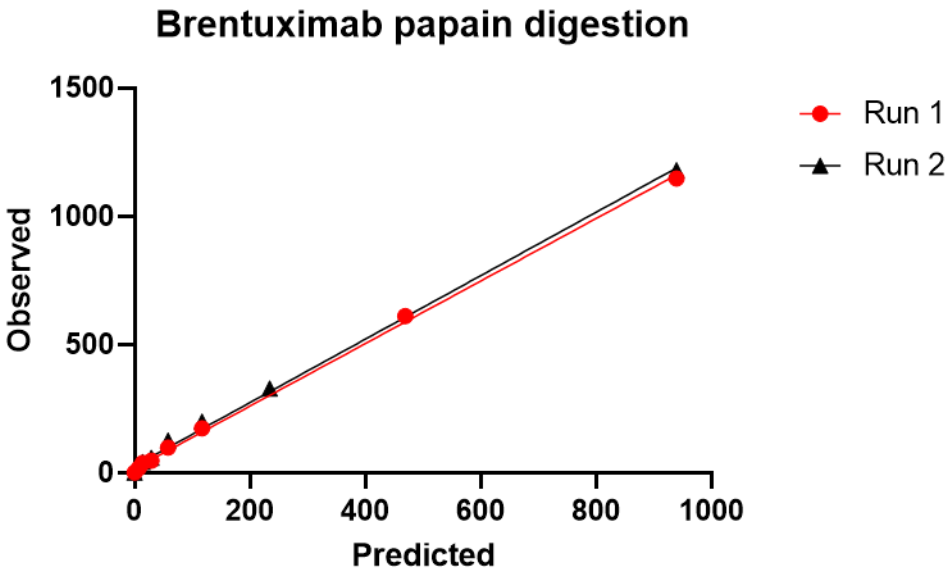

Run 1 slope = 1.21 R^2 = 0.999
Run 2 slope = 1.23 R^2 = 0.997

6.2.7 MMAE LC-MS/MS Analysis

MMAE was analyzed using reverse-phase chromatography tandem mass spectrometry. The system was comprised of a Dionex UltiMate 3000 UPLC coupled to a Thermo Scientific TSQ Vantage mass spectrometer utilizing electrospray ionization in positive ion mode. For sample preparation, free MMAE (MMAE that was not conjugated to an antibody at the time of sample collection) was separated from plasma as follows: internal standard (ISTD, MMAF) was added to samples or spiked blank matrix for standards and QCs, and 5X volume of acetonitrile was added for protein precipitation. Samples were then vortexed for 5 minutes and centrifuged, and supernatant was collected and dried using a speedvac. Samples were then reconstituted in mobile phase (MP) for injection. For total MMAE analysis, MMAE was first liberated from antibody utilizing the forced deconjugation protocol described above.

Chromatographic separation was performed utilizing a Phenomenex Synergi 4µm Polar-RP column (4µm, 75 x 2mm) at a flow rate of 0.5mL/min over a gradient with the initial MP composition of aqueous phase (A) 95% distilled water with 0.1% formic acid and (B) 5% acetonitrile with 0.1% formic acid. The gradient was as follows: starting at 30 seconds, organic phase was increased to 95% over 1.5 minutes, held at 95% for 1.5 minutes, and decreased back to 5% over 0.1 minute. It was then held at 5% for 1.8 minutes. The m/z transitions monitored for MMAE and ISTD were as follows: MMAE 718.4 →152.15 and 718.4 → 686.4, and MMAF 732.4 → 170.15 and 732.4 → 700.4. The standard curve was linear over a range of 0.05-500 ng/mL with weighting of $1/Y^2$ and coefficients of variation of less than 15%. The QC concentrations encompassed the standard curve with concentrations of 0.4, 4, 40, and 400 ng/mL.

6.2.8 Pharmacokinetic Parameter Estimation

Plasma, brain, and spinal cord concentration-time profiles were analyzed using Phoenix WinNonlin version 8.4 (Certara USA Inc., Princeton, NJ). Brain concentrations were corrected for residual blood estimated at 1.4% of brain weight and with blood concentrations approximated by plasma concentrations (Fridén *et al.*, 2010). Pharmacokinetic parameters and metrics were calculated by performing noncompartmental analysis (NCA). Areas under the curve (AUCs) were determined by linear trapezoidal integration, where the AUC to the last time point (AUC_{Last}) was calculated directly. Variances for $AUCs_{Last}$ were calculated using the Bailer method as reported in Phoenix WinNonlin (Bailer, 1988).

Other pharmacokinetic parameters reported for the MMAE IV studies were also calculated in Phoenix WinNonlin using noncompartmental analysis as follows:

$$\boldsymbol{CL = \frac{Dose}{AUC_{0\rightarrow\infty}}} \qquad (6.2)$$

$$\boldsymbol{V = MRT_{inf} \times CL} \qquad (6.3)$$

Where MRT_{inf} is the area under the first moment curve to infinity ($AUMC_{inf}$) divided by the $AUC_{0\rightarrow\infty}$.

$$\boldsymbol{t_{1/2} = \frac{ln\,(2)}{\lambda_z}} \qquad (6.4)$$

Where λ_z is the terminal first-order elimination rate constant.

The brain-to-plasma ratio, or brain tissue partition coefficient (Kp_{Brain}), for free and total MMAE was calculated as a ratio of the AUC of the brain concentration-time profile to the AUC of the plasma concentration-time profile (Equation 5).

$$\boldsymbol{Kp_{Brain}} = \frac{\boldsymbol{AUC_{Brain}}}{\boldsymbol{AUC\ _{Plasma}}} \qquad (6.5)$$

6.2.9 Statistical Analysis

Data are represented as mean ± S.D. where applicable. To compare AUCs among free and total MMAE as well as among tissues, a two-tailed unpaired *t* test was performed in Graphpad Prism with a null hypothesis that AUCs were equal. In order to compare preparations of brentuximab vedotin to validate the forced deconjugation protocol, simple linear regression was performed and slopes and intercepts of the lines were compared using Graphpad Prism. A significance level of $p < 0.05$ was considered significant in all tests.

6.3 RESULTS

6.3.1 MMAE Intravenous Pharmacokinetic Studies

MMAE was administered to wild-type and TKO mice via tail vein injection. The concentration-time profiles for MMAE in brain and plasma in wild-type and TKO mice are shown in **Figure 6.2**. In wild-type mice, MMAE displayed a rapid distribution followed by an elimination phase with a half-life of 5.5 hours (**Table 6.1**). The volume of distribution for MMAE is large, 18.4 L/kg. The concentration-time profile in brain shows that brain concentrations reach a rapid dynamic equilibrium with the plasma, and subsequently shows a similar elimination phase (**Figure 6.2A**). The exposure in the plasma of wild-type mice was significantly higher than in brain ($p<0.001$), with an overall brain-to-plasma ratio of 0.1 (**Table 6.1**).

In TKO mice (**Figure 6.2B**), the plasma showed a similar concentration-time profile as the wild-type mice, and there was no difference in plasma exposure between the two genotypes ($p=0.498$). However, the brain exposure of MMAE was significantly higher in the TKO mice ($p<0.001$), resulting in an overall Kp = 1.2 (**Table 6.1**).

Figure 6.2 MMAE IV Pharmacokinetic Studies

Concentration-time profiles of MMAE in plasma and brain following administration at 0.5 mg/kg in (A) wild-type and (B) triple knockout (TKO) mice.

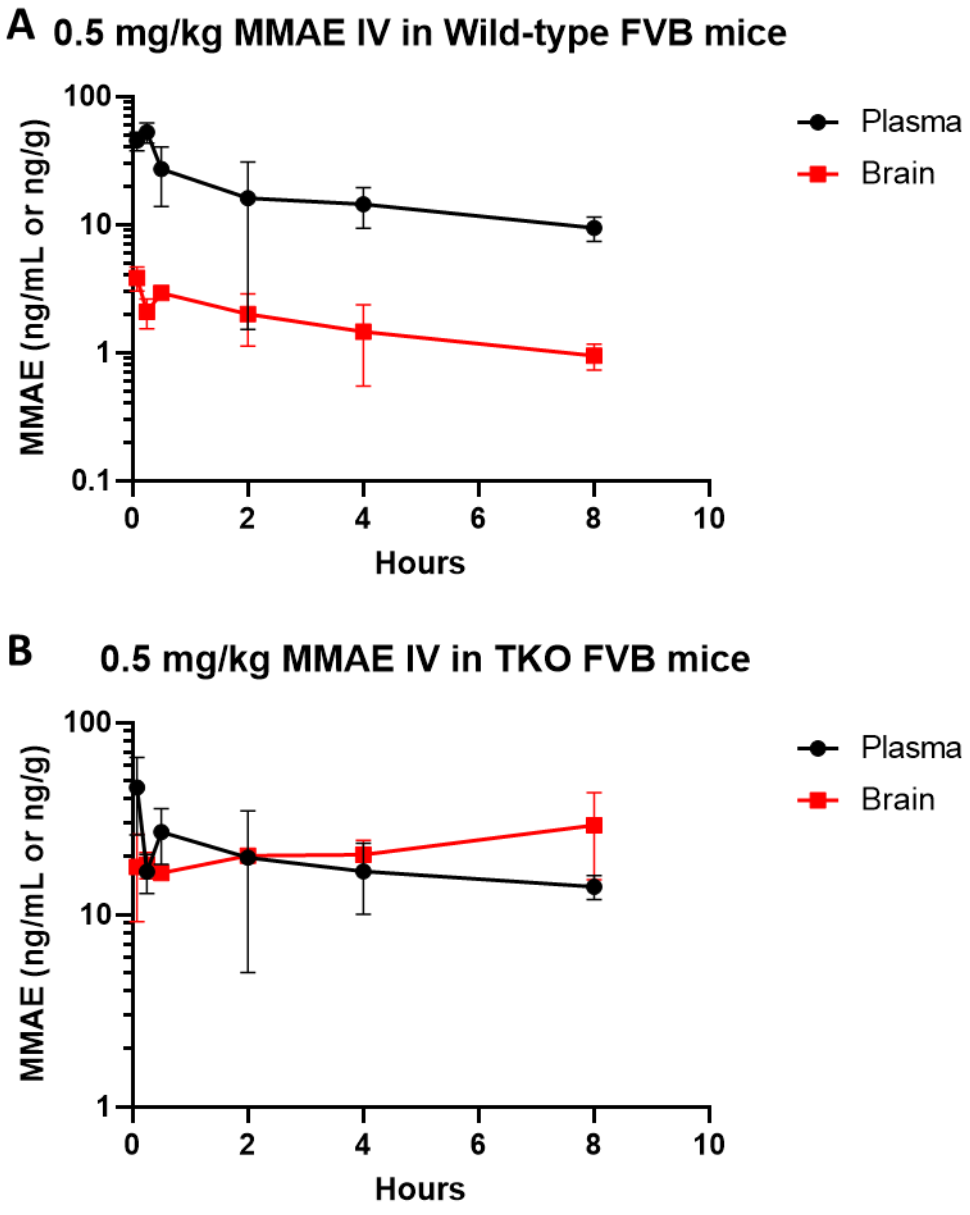

Table 6.1 Summary Pharmacokinetic parameters of MMAE

Pharmacokinetic parameters for MMAE were estimating using NCA following the administration of 0.5 mg/kg MMAE IV to wild-type and TKO mice.

Data are presented as mean ± SD where applicable

Parameter	Wild-type	TKO
$t_{1/2}$ (h)	5.5	8.5
CL (L/h)/kg	2.4	1.6
V L/kg	18.4	19.4
$AUC_{0\rightarrow tlast}$ Plasma (h*ng)/mL	133 ± 16	149 ± 18
$AUC_{0\rightarrow\infty}$ Brain (h*ng)/g	14 ± 1.5	177 ± 15
Kp_{Brain}	0.1	1.2

6.3.2 ABBV-221 Intraperitoneal Pharmacokinetic Study

ABBV-221 was administered at a dose of 5 mg/kg IP to wild-type FVB mice. The concentration-time profiles for free MMAE (drug not conjugated to antibody at the time of sample collection) and total MMAE (free + conjugated drug at the time of sample collection) are shown for both plasma and brain in **Figure 6.3**. Total MMAE in plasma indicates rapid absorption of the ADC from the peritoneum, with the peak concentration of total MMAE, near 400 ng/mL, occurring at 1 hour. Total MMAE plasma concentrations did not decline for 24 hours post-dose. Total MMAE concentrations in the brain could not be calculated when accounting for 1.4% microvascular volume, as total concentrations in plasma were at all times >200-fold higher than the brain concentrations. The correction resulted in concentrations less than zero. The unconjugated concentrations of MMAE in plasma and brain were consistently less than 2 ng/mL, with exposures significantly lower than total MMAE in the plasma ($p<0.001$). While there was no statistically detectable difference between the exposure of free MMAE in brain and plasma as plotted in **Figure 6.3A,** only 9 out of 25 mice had quantifiable free MMAE concentrations in the brain, as opposed to 20 out of 25 mice with quantifiable free concentrations of MMAE in the plasma. This is shown in **Figure 6.3B**, in which all concentrations in each time point are plotted. AUCs were determined using the data in **Figure 6.3A**, as a minimum of 3 of 5 samples showed concentrations above LOQ for each tissue at the time points indicated.

Figure 6.3 ABBV-221 IP Pharmacokinetic Study

(A) Concentration-time profiles for free and total MMAE in plasma and brain following IP administration of ABBV-221, where only concentrations above LOQ are plotted and (B) Free concentrations of MMAE in plasma and brain, including concentrations below LOQ with lines connecting the mean concentration for each time point when points below LOQ are included.

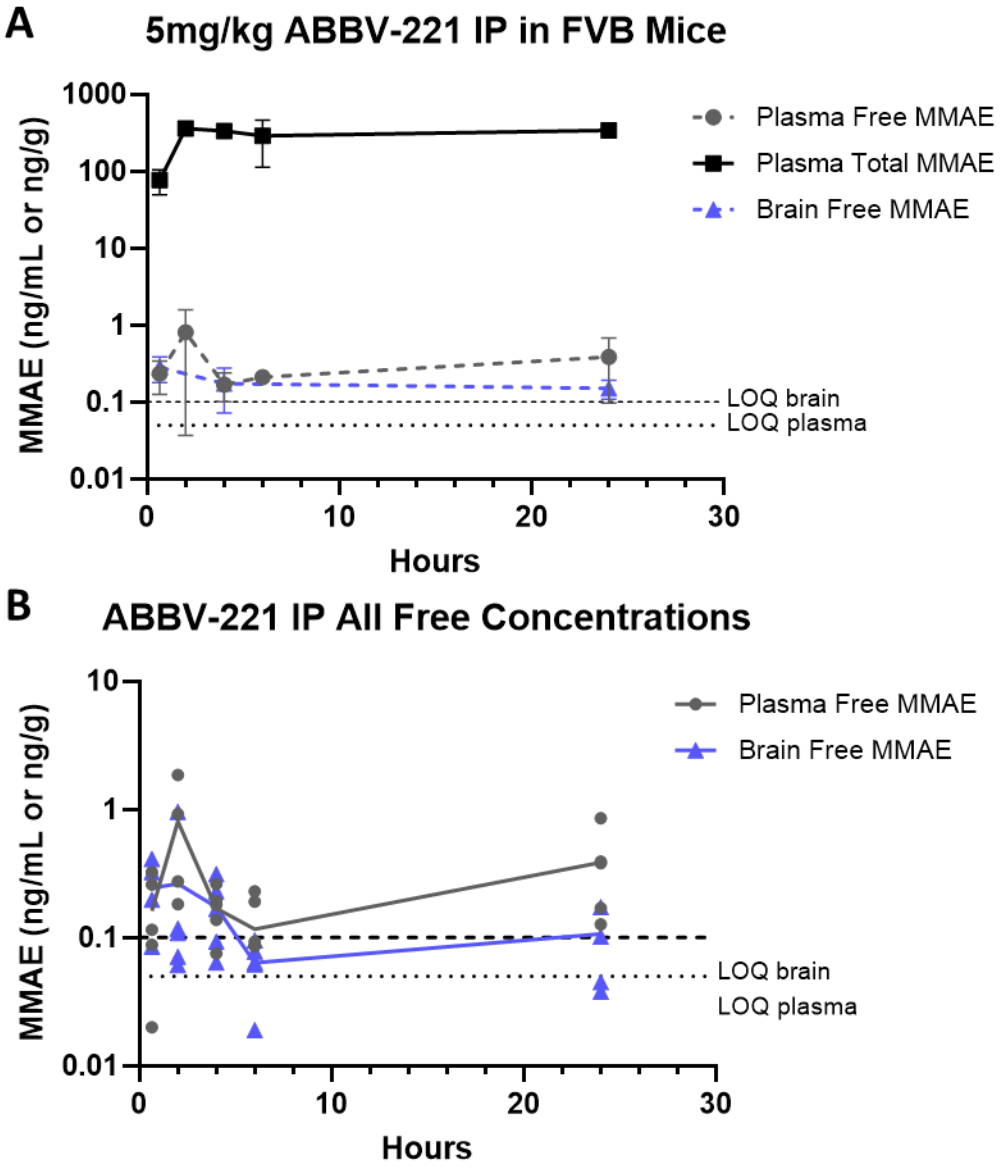

Table 6.2 Free and Total MMAE Tissue Exposures Following IP Administration of ABBV-221

AUC_{last} for free and total MMAE in plasma and brain following IP administration of 5 mg/kg ABBV-221. Mean concentrations to determine AUCs did not include concentrations below LOQ, as a minimum of 3 samples showed concentrations above LOQ. Total MMAE concentrations in brain could not be determined when taking into account the total MMAE in the microvasculature, and so the AUC was not calculated. Data are presented as mean ± SD.

Tissue	AUC_{last} (h*ng/mL or h*ng/g)
Plasma Free MMAE	11.3 ± 4
Plasma Total MMAE	7274 ± 817
Brain Free MMAE	5.0 ± 0.5
Brain Total MMAE	NC

6.3.3 MMAE CED Pharmacokinetic Study

MMAE was administered at a dose of 570ng over 40 minutes via CED into the right hemisphere of wild-type FVB mice. The concentration-time profiles for MMAE in plasma, right hemisphere, and left hemisphere are shown in **Figure 6.4**. Concentrations of MMAE in the right hemisphere were consistently 10-fold higher than those in the left hemisphere. Concentrations in the both hemispheres were relatively constant over the 4-hour study. Concentrations in the plasma were 100-fold lower than that of the right hemisphere and 10-fold lower than left hemisphere at 40 minutes, rapidly declined thereafter, and rate of decline decreased after 2 hours post-infusion. As shown in **Table 6.3**, overall exposures of MMAE in the right hemisphere were 10-fold higher than the left hemisphere ($p<0.001$), and over 1500-times higher than the plasma ($p<0.001$). Overall exposure of MMAE in the left hemisphere was 100-fold higher than the plasma ($p=0.003$).

Figure 6.4 MMAE CED Pharmacokinetic Study

Concentration-time profiles for MMAE in right and left hemispheres as well as plasma following CED administration of 570 ng.

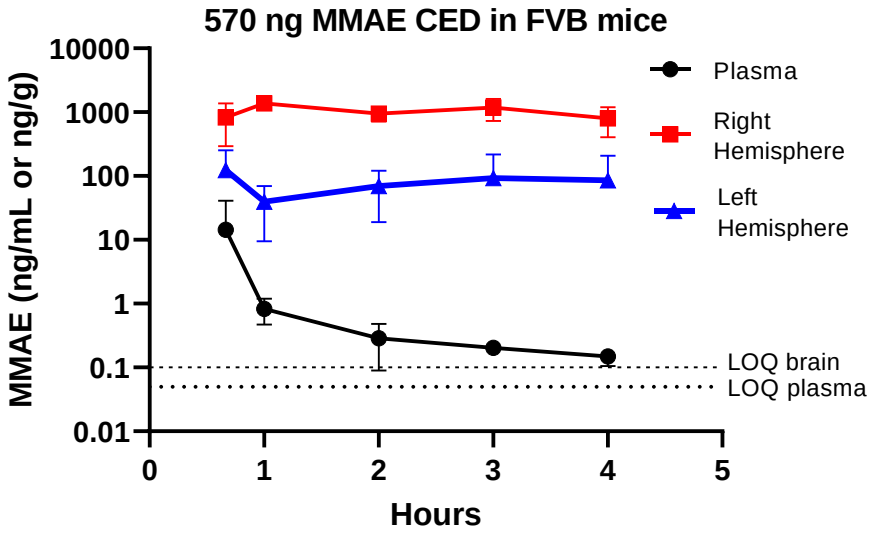

Table 6.3 MMAE Tissue Exposures Following CED of MMAE

Overall AUCs for MMAE calculated from plasma, right hemisphere, and left hemisphere concentration-time profiles.

Data are presented as mean ± SD

Tissue	AUC_{last} (h*ng/mL or h*ng/g)
Plasma	2.4 ± 0.6
Right Hemisphere	3860 ± 311
Left Hemisphere	293 ± 80

6.3.4 ABBV-221 CED Pharmacokinetic Studies

A dose of 60µg of ABBV-221 was administered over 40 minutes to the right hemisphere of wild-type FVB mice via CED. Plasma, right hemisphere, and left hemisphere concentration-time profiles for both free and total MMAE are shown in **Figure 6.5.** The AUCs for all concentration-time profiles in **Figure 6.5** can be found in **Table 6.4**, and a matrix of p-values for all AUC comparisons for this experiment is shown in **Table 6.5**. In **Figure 6.5A**, total MMAE concentrations in the right hemisphere show a decline of approximately 2-fold within the first 4 hours after the end of the CED infusion, after which the rate of decline decreased. The total MMAE plasma concentrations rise over time, generally surpassing that of the right hemisphere by 24 hours, while the total MMAE concentrations in the left hemisphere are consistently around one order of magnitude lower than the right hemisphere for the duration of the time course. Total MMAE exposures in plasma and right hemisphere were indistinguishable (**Table 6.4**), but the left hemisphere had a significantly lower exposure of total MMAE than both the right hemisphere (**Table 6.5**, $p=0.002$) and the plasma ($p<0.001$).

The free concentrations in the right hemisphere rose to a peak at 6 hours, with concentrations at the peak of approximately 13 ng/mL, which remain constant to 24 hours. The overall exposure of the right hemisphere to free MMAE was 10-fold lower than the total MMAE exposure (**Table 6.4,** $p<0.001$). Similarly, the free concentrations in the left hemisphere rose to a peak of approximately 5 ng/mL and maintained this concentration for the remainder of the time course (**Figure 6.5**). While the overall exposures were not statistically distinguishable due to variability and the exclusion of some samples below LOQ, the free concentrations of MMAE in the right hemisphere were consistently higher than the left, with a 3-fold higher AUC (**Table 6.5,** $p=0.153$). The free concentrations of MMAE in plasma were consistently low, with quantifiable

concentrations (above the LOQ) in only 7 of 24 animals. Because of this, there were only 3 (or more) quantifiable concentrations at 4 hours, and therefore a mean concentration could only be determined at the 4 hour time point, approximately 0.2 ng/mL. All measured concentrations were plotted in **Figure 6.5B** to visualize the variability at these low concentrations. In this figure, it is apparent that the majority of the free MMAE plasma concentrations are below the LOQ, and that the right hemisphere free MMAE concentrations are consistently higher than the left.

Figure 6.5 ABBV-221 CED Pharmacokinetic Study

(A) Concentration-time profiles for free and total MMAE in plasma and brain following CED administration of 60µg ABBV-221, where only concentrations above LOQ are plotted and (B) Free concentrations of MMAE in plasma and brain, including concentrations below LOQ with lines connecting the mean concentration for each time point when points below LOQ are included.

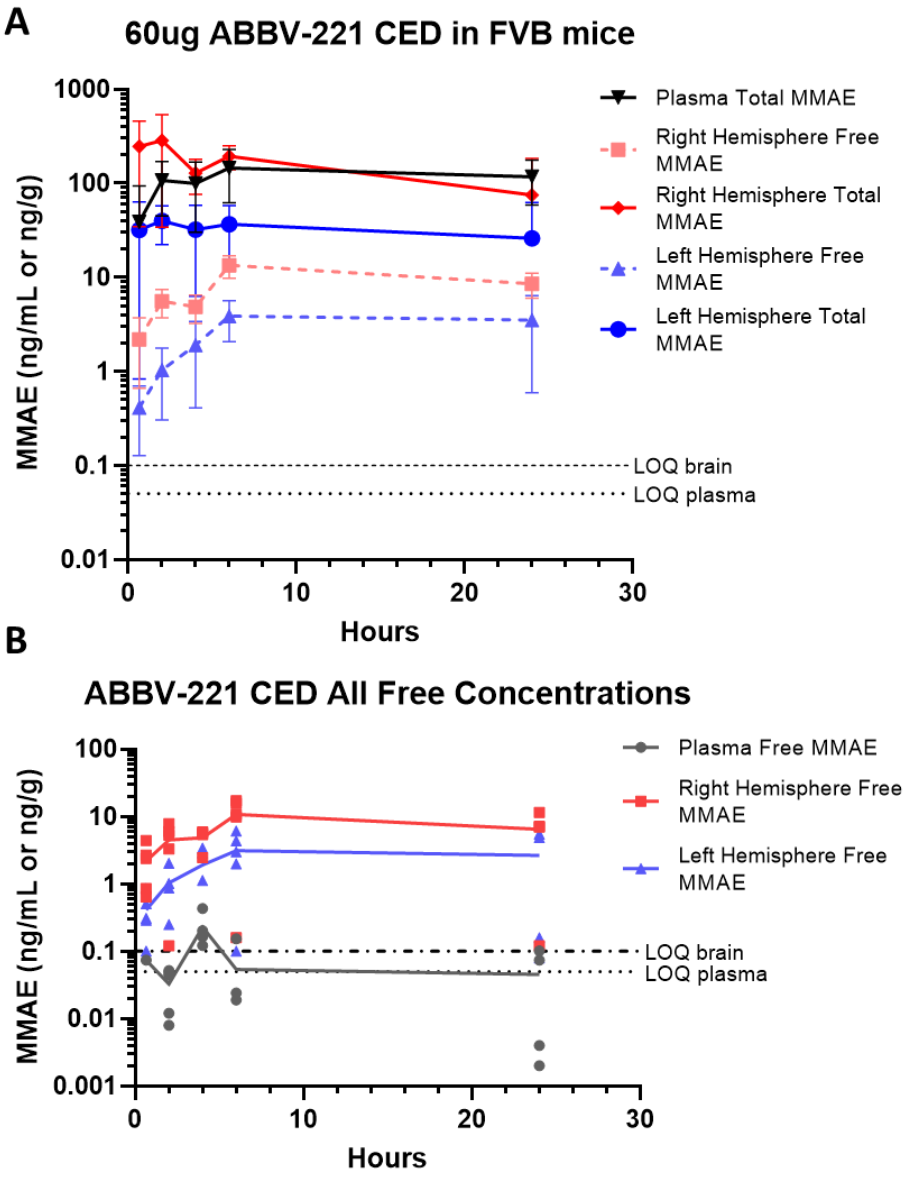

Table 6.4 Free and Total MMAE Tissue Exposures Following CED Administration of ABBV-221

AUC_{last} for free and total MMAE in plasma and brain following administration of 60µg ABBV-221 via CED. Mean concentrations to determine AUCs did not include concentrations below LOQ, and therefore AUC_{last} was not calculated (NC) for free MMAE in plasma.

Data are presented as mean ± SD.

Tissue	AUC_{last} (h*ng/mL or h*ng/g)
Plasma Free MMAE	NC
Plasma Total MMAE	2924 ± 449
Right Hemisphere Free MMAE	311 ± 131
Right Hemisphere Total MMAE	3073 ± 635
Left Hemisphere Free MMAE	102 ± 44
Left Hemisphere Total MMAE	625 ± 177

Table 6.5 Matrix of P-values Following AUC_{last} Comparisons for ABBV-221 CED Pharmacokinetic Study

Variance around AUC_{last} for all concentration time profiles was calculated using NCA in Phoenix WinNonlin. AUCs were then compared using an unpaired t-test. Because a mean concentration-time profile could not be constructed for free MMAE in plasma, no comparisons were made against these data.

$p<0.05$ was considered significant.

Tissue	Plasma Free MMAE	Plasma Total MMAE	Right Hemisphere Free MMAE	Right Hemisphere Total MMAE	Left Hemisphere Free MMAE
Plasma Free MMAE	---	NC	NC	NC	NC
Plasma Total MMAE	NC	---	---	---	---
Right Hemisphere Free MMAE	NC	<0.001	---	---	---
Right Hemisphere Total MMAE	NC	0.864	<0.001	---	---
Left Hemisphere Free MMAE	NC	<0.001	0.153	<0.001	---
Left Hemisphere Total MMAE	NC	<0.001	0.162	0.002	0.008

6.4 DISCUSSION

Antibody-drug conjugates have significantly improved the treatment and prognosis for patients diagnosed with a number of cancers. However, their translation to the treatment of tumors in the CNS has heretofore been unsuccessful. Due to their high molecular weight and the difficulty of delivering drugs across the BBB, one potential strategy proposed for the use of large molecules like ADCs to treat CNS tumors is to deliver them directly to the brain parenchyma via CED. Despite decades of research into the optimization, modeling, and characterization of CED (Morrison *et al.*, 1994, 1999), relatively sparse information has been published on the CNS and systemic pharmacokinetics of antibody-based drugs following CED. The therapeutic index of macromolecular drugs to treat brain tumors is likely to be significantly enhanced if they are delivered directly to tumors. In the case of ADCs, the distribution of highly toxic payloads after their cleavage from the antibody plays a central role in the dose-limiting side effects that have hindered their development (Norsworthy *et al.*, 2018). The current study characterizes and compares the brain distribution and pharmacokinetics of a common payload, MMAE, following systemic and CED administration of both free (unconjugated) MMAE and ABBV-221, a novel EGFR-targeted ADC in development for the potential use in GBM.

The two studies described herein assess the brain penetration and plasma pharmacokinetics of MMAE following IV administration of 0.5 mg/kg of the free drug. The disposition in wild-type mice agrees with previous reports (EMA, 2012; Chang *et al.*, 2021). The concentration-time profile of MMAE in the plasma of wild-type mice shows a rapid distributional phase followed by more prolonged elimination with a half-life of 5.5 hours (**Table 6.1**). This half-life can be accounted for by the extensive distribution of MMAE into peripheral tissues and its binding to intracellular tubulin, which results in a large volume of distribution of nearly 20 L/kg in mice. While it has also been previously

shown that MMAE has limited distribution into the brain (Chang *et al.*, 2021), the TKO mouse studies conclusively show, for the first time, that efflux transport plays a central role in the CNS exclusion of MMAE *in vivo*, with 12-fold higher brain exposures measured in mice lacking P-gp and BCRP (see **Table 6.1**). Previous work has implicated P-gp but not BCRP in MMAE efflux regarding drug resistance to ADCs *in vitro* (Liu-Kreyche *et al.*, 2019). Future studies should determine whether BCRP plays a significant role in the efflux of MMAE at the BBB. There are no studies on BCRP and MMAE in the literature, and previous studies from our group have shown that P-gp and BCRP may work in cooperation to efflux some drugs from the brain (Chen *et al.*, 2009; Agarwal and Elmquist, 2012; Laramy *et al.*, 2018).

Following IP administration of ABBV-221 at doses comparable to those used in preclinical studies of EGFR-directed ADCs for GBM (Marin *et al.*, 2021), there was rapid uptake of the ADC from the peritoneum. Over the 24-hour time course, limited amounts of MMAE were liberated from the antibody, resulting in low free (unconjugated) concentrations in the plasma. It might be expected that over multiple days, more free MMAE might be released, as the vc linker in ABBV-221 is known to be liable to the high amounts of carboxylesterase in mouse plasma, but the vc linker has not been shown to be labile in human plasma (Anami *et al.*, 2018). The IP administration of ABBV-221 results in limited brain penetration of free MMAE (**Figure 6.3A**). Indeed, the majority of mice showed undetectable concentrations of free MMAE in the brain (**Figure 6.3B**). Importantly, when the total brain concentrations of MMAE, as measured by LC-MS/MS analysis, were corrected for residual blood using the total concentrations of MMAE in the plasma, the calculated concentrations were less than 0. Therefore, a concentration-time profile could not be constructed for total MMAE in the brain. This indicates the total MMAE concentrations measured in the brain homogenate via LC-MS/MS analysis were due to ABBV-221 in the residual blood, and that the ADC remains largely confined to the

microvasculature despite high plasma concentrations of the drug. This underscores previous studies showing that a systemic administration of ADCs is unlikely to result in effective treatment of brain tumors with a relatively intact BBB (Marin *et al.*, 2021).

The present study examines the administration of MMAE by CED and is the first to our knowledge to characterize both the spatial distribution of a small molecule drug between brain hemispheres and also the impact of CED on systemic pharmacokinetics. The dose of free MMAE administered via CED was chosen to reflect the total amount of payload administered in 60µg of ABBV-221. It has been a consensus in the literature that the systemic exposure of many drugs following CED is low (Hunt Bobo *et al.*, 1994; Noble *et al.*, 2006; Tosi *et al.*, 2020). The present studies agree with this assessment, as the plasma exposure is 100-fold lower than the right hemisphere (**see Table 6.3**). The exposure in the left hemisphere, contralateral to the site of infusion, was also 10-fold lower than the right. Given the low concentrations in the plasma, and the P-gp mediated exclusion of MMAE at the BBB, it is concluded that the drug in the left hemisphere originated from the CED infusion into the right hemisphere, indicating the extent of distribution of drugs following CED. Additionally, it is clear from the sustained concentrations in both hemispheres following CED that MMAE rapidly distributes into cells, likely binding to intracellular tubulin. Despite the clear role that efflux plays in the exclusion of MMAE from the brain following systemic delivery, it is probable that the slow release of MMAE from intracellular binding sites, not P-gp efflux, is the rate-limiting process in free MMAE clearance from the brain following CED. This behavior may be widely disparate among small molecules with varying distribution into intracellular compartments in the brain, and should be investigated in comparison to their systemic disposition.

The administration of ABBV-221 via CED showed similar patterns in parenchymal distribution of drug to the free MMAE studies. However, total exposures of

MMAE in the left hemisphere were approximately 5-fold lower than the right side, as opposed to a 10-fold difference following the CED of free MMAE (**Table 6.4**). Given the rapid distribution of MMAE into cells (Chang *et al.*, 2021), it is possible that the ADC may have more broad distribution. This observation may result from differences in parenchymal distribution parameters between the free MMAE and the antibody-conjugated MMAE. Resistance to spatial distribution (the “sink” effect) includes both efflux clearance and possible transport of IgG within the perivascular spaces of the brain (Pizzo *et al.*, 2018). Despite this, the exposures of brain to free MMAE following CED of the ADC were lower than those observed following CED of the unconjugated drug in all cases. Interestingly, the CED administration of ABBV-221 showed higher plasma concentrations of total MMAE than the administration of the free MMAE alone (**Figure 6.4, Table 6.4**). Early reports of antibody disposition following intraparenchymal administration described rapid efflux of IgG from rodent brain. The mechanism for this clearance from the brain is unclear. Some proposed mechanisms are FcR-mediated transcytosis (Zhang and Pardridge, 2001; Cooper *et al.*, 2013), though this is highly debated (Garg and Balthasar, 2009; Abuqayyas and Balthasar, 2013). Other possibilities could be nonspecific clearance into the CSF or some other glycan-specific efflux (Cserr *et al.*, 1992; Finke *et al.*, 2017). Regardless of the mechanism of efflux of IgG from brain, it is probable that the presence of a target antigen within the CNS, namely EGFRviii-expressing tumors, likely alters the disposition of ABBV-221. This could result in higher retention through binding of the ADC to tumor cells as opposed to normal brain (publication in press). Given this possibility, these studies provide a non-tumor bearing baseline for investigations into the disposition of ADCs in tumor-bearing animals following CED.

Taken as a whole, the wide distribution of total MMAE in brain and plasma following the central administration of ABBV-221 shows the importance of the protective aspects of ADCs and the need for stable and selective linker chemistry. Peripheral neuropathy is commonly associated with microtubule-targeting agents like taxanes (Velasco and Bruna, 2015) and vinca alkaloids. Peripheral neuropathy is also the second most common dose-limiting toxicity in the use of MMAE-containing ADCs for peripheral cancers (EMA, 2012; Masters *et al.*, 2018; Velasco *et al.*, 2021). Central neurotoxicity is generally avoided with systemic administration, as many of these drugs are substrates for efflux (Waghray and Zhang, 2018). The retention of MMAE in the brain following CED of free MMAE counters the hypothesis that the CED of ABBV-221 would significantly enhance the brain exposure of MMAE by avoiding P-gp efflux. However, it should be noted that CED administration of free MMAE is unlikely to be tolerated, given the well-documented risks of neuronal toxicity with microtubule-stabilizing agents (Lidar *et al.*, 2004). In contrast, low exposures of free MMAE are observed in all tissues following both IP and CED administration of ABBV-221. In the case where EGFR-expressing brain tumors are present, the therapeutic index of MMAE is likely to be further improved. Although, given the potent toxicity of the payload, a conservative approach should be taken in the future development of the administration of ADCs via CED.

CHAPTER 7

RECAPITULATION

The central nervous system (CNS) barriers are a central consideration in drug development, in that they can modulate both the CNS efficacy of a drug and determine whether there are off-target CNS effects. The blood-brain barrier (BBB) in particular plays an important role in protecting the brain and maintaining a delicate and critical homeostasis, preserving an environment optimal for neuronal functioning. On the other hand, the BBB has been implicated as one of the greatest obstacles in the development of drugs to treat CNS disease, often preventing efficacious delivery. In **Chapter 1**, the factors influencing both sides of this paradigm are discussed. These factors include the total delivery of drugs across the BBB, the robust efflux transport of drugs from the CNS by ATP-binding cassette proteins like P-glycoprotein (P-gp, ABCB1, MDR1) and breast cancer resistance protein (BCRP, ABCG2), and the nonspecific binding of small molecules to brain and plasma components. **Chapter 1** also introduces how both aspects of the BBB—protection and limited drug delivery—can play a role in two very different applications: pain management and the treatment of brain tumors.

In **Chapter 2**, opioid agonists and their delivery to the CNS are discussed. Opioid agonists are the focus of the first part of this dissertation. This Chapter discusses the long history of the use of derivatives of the opium poppy, which spans millennia, as well as the isolation of opioid-derived alkaloids and their broad use in the early pharmacopoeia. The physiology of opioid receptors, including the ubiquitous nature of their expression in both peripheral and CNS tissues provides insight into the dangerous side effects that opioids can elicit, including addiction and respiratory depression. There is diverse signaling among the three main classes of opioid receptors, and there are many possible receptor subtypes. All of these receptors may have biased signaling dependent on specific opioid agonists. This signaling diversity provides many opportunities for novel drug development for the treatment of pain and the reduction of off target effects. This Chapter also provides the rationale for the experiments described

in **Chapters 3** and **4**, as the CNS distribution and pharmacokinetics of these drugs can play a significant role in producing off target effects.

Previous work has described synergistic antihyperalgesic and analgesic effects from combinations of opioid agonists, including the combination of loperamide and oxymorphindole (OMI). There is evidence that there may be unique signaling when these two drugs are administered in combination. The role that the distribution and pharmacokinetics of these drugs might play in their interaction has not been determined. **Chapter 3** describes the efficacy of OMI and loperamide following oral administration for the first time, in which the potency of loperamide was significantly enhanced when co-administered with OMI. It also describes the systemic pharmacokinetics and CNS distribution of loperamide and OMI alone and in combination following both oral and IV administration in ICR mice. These data show that loperamide reduces the clearance of OMI by approximately half, but that OMI has no effect on the systemic disposition of loperamide. In addition, these data show that OMI does not change the CNS penetration of loperamide, which is of interest in the safety of these two drugs in combination. The oral administration of these two drugs shows that the bioavailability of OMI is significantly reduced in the presence of loperamide. However, given that the oral ED_{50} was 100-fold lower than the dose administered in these studies, this change in bioavailability does not appear likely to hinder the efficacy of the combination.

Chapter 4 deals with the potential of these drugs to interact at CNS barriers. Loperamide has long been known to be a P-gp substrate, which limits its absorption and CNS penetration following oral administration, and has made it a useful drug in the treatment of diarrhea. Given this characterization, it was imperative to determine whether OMI was a substrate for efflux at the CNS barriers, and whether this might cause some significant interaction that contributes to the synergy between these two drugs. Following IV administration of both drugs, alone and in combination, to 4

genotypes of FVB mice with and without P-gp and BCRP, it was determined that OMI is a P-gp substrate, which could not have been determined based on its overall brain penetration in the studies in **Chapter 3**. However, it was also discovered that, despite the status of both drugs as substrates for efflux, P-gp does not appear to be saturated at the doses administered. Therefore there does not appear to be a significant interaction between the two drugs at the CNS barriers that alters either the safety or efficacy of the combination. These studies provide evidence for the protective capacity of P-gp efflux transport at the BBB, and the importance of assessing all factors that impact CNS drug delivery. Future work on these molecules might include the development of dual-agonists (bispecific for mu and delta-opioid receptors) for pain management.

The second portion of this dissertation deals with the treatment of brain tumors. The prognosis for many brain tumors, both primary and metastatic, is poor when compared to many other cancers. **Chapter 5** provides a thorough review of the current state of the treatment of CNS tumors and how the heterogeneity of BBB breakdown in and around brain tumors has hindered the development of novel treatments. This Chapter also discusses the various strategies that have been investigated to overcome this problem. These strategies may be invasive, through the use of direct-to-brain drug delivery methods like convection-enhanced delivery (CED), or non-invasive, including the use of blood-brain barrier disruption and a wide variety of novel therapeutic modalities to facilitate transport of drugs into the CNS.

The use of CED to improve drug delivery to brain tumors has become an area of interest in light of the benefits that large molecule therapies have provided in the treatment of peripheral cancers. **Chapter 6** assesses how CED impacts the delivery and retention of antibody-drug conjugate (ADC) payloads in the CNS. This Chapter focuses on distribution and systemic pharmacokinetics of MMAE, a common payload molecule, and ABBV-221, a novel EGFR-targeted ADC, in mice. These studies show that MMAE is

a substrate for efflux at the BBB. Despite this efflux status, free MMAE has significant retention within cells in the brain, which poses a risk for neurotoxicity. In contrast, the administration of ABBV-221 showed a more rapid efflux of the ADC from the CNS. When administered systemically, the ADC had negligible brain penetration, exemplifying how the systemic administration of ADCs is unlikely to result in efficacious drug delivery to brain tumors with a relatively intact BBB. However, the administration of MMAE conjugated to the ADC protected both the brain and the systemic circulation from high exposures of the free drug, underscoring the protective aspects of ADCs in general. Future work on these molecules will include similar experiments in tumor-bearing mice. These future studies will codify whether the retention of ADC in the brain is changed in the presence of tumor, and whether the therapeutic index of ADCs delivered via CED is altered when a tumor cell target that actively releases payload is present near the site of administration.

As a whole, the studies in this dissertation show how variable the CNS disposition of drugs can be, even within the same class of molecules. These studies show that CNS delivery of molecules is dependent on a matrix of factors, and that attempting to predict the CNS distribution of a drug based on lipophilicity, size, observed CNS effects, or total brain penetration alone can be misleading. A complete assessment of CNS disposition of novel therapies is necessary to make full conclusions on the safety or barriers to efficacy of these drugs. This assessment reflects a growing consensus in the field of CNS drug delivery and pharmacokinetics: with complete information, the best decisions can be made. Put another way, “To measure is to know.”

BIBLIOGRAPHY

Aasen SN, Espedal H, Holte CF, Keunen O, Karlsen TV, Tenstad O, Maherally Z, Miletic H, Hoang T, Eikeland AV, Baghirov H, Olberg DE, Pilkington GJ, Sarkar G, Jenkins RB, Sundstrøm T, Bjerkvig R, and Thorsen F (2019) Improved drug delivery to brain metastases by peptide-mediated permeabilization of the blood–brain barrier. *Mol Cancer Ther*, doi: 10.1158/1535-7163.MCT-19-0160.

Abbott NJ (2013) Blood-brain barrier structure and function and the challenges for CNS drug delivery.

Abbott NJ, Patabendige AAK, Dolman DEM, Yusof SR, and Begley DJ (2010) Structure and function of the blood–brain barrier. *Neurobiol Dis* **37**:13–25, Academic Press.

Aboody KS, Najbauer J, and Danks MK (2008) Stem and progenitor cell-mediated tumor selective gene therapy.

Abuqayyas L, and Balthasar JP (2013) Investigation of the role of FcγR and FcRn in mAb distribution to the brain. *Mol Pharm*, doi: 10.1021/mp300214k.

Adkins CE, Mohammad AS, Terrell-Hall TB, Dolan EL, Shah N, Sechrest E, Griffith J, and Lockman PR (2016) Characterization of passive permeability at the blood-tumor barrier in five preclinical models of brain metastases of breast cancer. *Clin Exp Metastasis* **33**:373–83, NIH Public Access.

Agarwal S, and Elmquist WF (2012) Insight into the Cooperation of P-glycoprotein (ABCB1) and Breast Cancer Resistance Protein (ABCG2) at the Blood–Brain Barrier: A Case Study Examining Sorafenib Efflux Clearance. *Mol Pharm* **9**:678–684, American Chemical Society.

Agarwal S, Mittapalli RK, Zellmer DM, Gallardo JL, Donelson R, Seiler C, Decker SA, SantaCruz KS, Pokorny JL, Sarkaria JN, Elmquist WF, and Ohlfest JR (2012) Active efflux of dasatinib from the brain limits efficacy against murine glioblastoma: Broad implications for the clinical use of molecularly targeted agents. *Mol Cancer Ther*, doi: 10.1158/1535-7163.MCT-12-0552.

Agarwal S, Sane R, Oberoi R, Ohlfest JR, and Elmquist WF (2011) Delivery of molecularly targeted therapy to malignant glioma, a disease of the whole brain. *Expert Rev Mol Med* **13**:e17.

AMMAYA AK (1963) SUBCUTANEOUS RESERVOIR AND PUMP FOR STERILE ACCESS TO VENTRICULAR CEREBROSPINAL FLUID. *Lancet* **186**:983–984.

Anami Y, Yamazaki CM, Xiong W, Gui X, Zhang N, An Z, and Tsuchikama K (2018) Glutamic acid-valine-citrulline linkers ensure stability and efficacy of antibody-drug conjugates in mice. *Nat Commun*, doi: 10.1038/s41467-018-04982-3.

Argaw AT, Gurfein BT, Zhang Y, Zameer A, and John GR (2009) VEGF-mediated disruption of endothelial CLN-5 promotes blood-brain barrier breakdown. *Proc Natl Acad Sci U S A*, doi: 10.1073/pnas.0808698106.

Arvanitis CD, Askoxylakis V, Guo Y, Datta M, Kloepper J, Ferraro GB, Bernabeu MO, Fukumura D, McDannold N, and Jain RK (2018) Mechanisms of enhanced drug delivery in brain metastases with focused ultrasound-induced blood–tumor barrier disruption. *Proc Natl Acad Sci U S A*, doi: 10.1073/pnas.1807105115.

Arvanitis CD, Ferraro GB, and Jain RK (2020) The blood–brain barrier and blood–tumour barrier in brain tumours and metastases.

Arvold ND, Lee EQ, Mehta MP, Margolin K, Alexander BM, Lin NU, Anders CK, Soffietti R, Camidge DR, Vogelbaum MA, Dunn IF, and Wen PY (2016) Updates in the management of brain metastases.

Askoxylakis V, Ferraro GB, Kodack DP, Badeaux M, Shankaraiah RC, Seano G, Kloepper J, Vardam T, Martin JD, Naxerova K, Bezwada D, Qi X, Selig MK, Brachtel E, Duda DG, Huang P, Fukumura D, Engelman JA, and Jain RK (2016) Preclinical Efficacy of Ado-trastuzumab Emtansine in the Brain Microenvironment. *J Natl Cancer Inst*, doi: 10.1093/jnci/djv313.

Assi HI, Mahmoud T, Saadeh FS, and El Darsa H (2018) Management of

leptomeningeal metastasis in breast cancer, Elsevier B.V.

Azcona P, Zysler R, and Lassalle V (2016) Simple and novel strategies to achieve shape and size control of magnetite nanoparticles intended for biomedical applications. *Colloids Surfaces A Physicochem Eng Asp*, doi: 10.1016/j.colsurfa.2016.05.064.

Bailer AJ (1988) Testing for the equality of area under the curves when using destructive measurement techniques. *J Pharmacokinet Biopharm*, doi: 10.1007/BF01062139.

Ballard P, Yates JWT, Yang Z, Kim DW, Yang JCH, Cantarini M, Pickup K, Jordan A, Hickey M, Grist M, Box M, Johnström P, Varnäs K, Malmquist J, Thress KS, Jänne PA, and Cross D (2016) Preclinical comparison of osimertinib with other EGFR-TKIs in EGFR-mutant NSCLC brain metastases models, and early evidence of clinical brain metastases activity. *Clin Cancer Res*, doi: 10.1158/1078-0432.CCR-16-0399.

Batrakova E V., Gendelman HE, and Kabanov A V. (2011) Cell-mediated drug delivery.

Beckett AH, and Casy AF (1954) SYNTHETIC ANALGESICS: STEREOCHEMICAL CONSIDERATIONS. *J Pharm Pharmacol*, doi: 10.1111/j.2042-7158.1954.tb11033.x.

Beffinger M, Schellhammer L, Pantelyushin S, and Vom Berg J (2019) Delivery of antibodies into the murine brain via convection-enhanced delivery. *J Vis Exp*, doi: 10.3791/59675.

Bellavance MA, Blanchette M, and Fortin D (2008) Recent advances in blood-brain barrier disruption as a CNS delivery strategy. *AAPS J* **10**:166–177.

Bergman I, Burckart G, … CP-… of P and, and 1998 undefined (n.d.) Pharmacokinetics of IgG and IgM anti-ganglioside antibodies in rats and monkeys after intrathecal administration. *ASPET*.

Bird GH, Madani N, Perry AF, Princiotto AM, Supko JG, He X, Gavathiotis E, Sodroski JG, and Walensky LD (2010) Hydrocarbon double-stapling remedies the proteolytic

instability of a lengthy peptide therapeutic. *Proc Natl Acad Sci U S A* **107**:14093–8.

Boado RJ, Hui EKW, Lu JZ, and Pardridge WM (2016) Very high plasma concentrations of a monoclonal antibody against the human insulin receptor are produced by subcutaneous injection in the rhesus monkey. *Mol Pharm*, doi: 10.1021/acs.molpharmaceut.6b00456.

Bobo RH, Laske DW, Akbasak A, Morrison PF, Dedrick RL, and Oldfield EH (1994) Convection-enhanced delivery of macromolecules in the brain. *Proc Natl Acad Sci U S A* **91**:2076–2080, National Academy of Sciences.

Boström E, Hammarlund-Udenaes M, and Simonsson USH (2008) Blood-brain barrier transport helps to explain discrepancies in in vivo potency between oxycodone and morphine. *Anesthesiology*, doi: 10.1097/ALN.0b013e318164cf9e.

Boström E, Simonsson USH, and Hammarlund-Udenaes M (2006) In vivo blood-brain barrier transport of oxycodone in the rat: Indications for active influx and implications for pharmacokinetics/pharmacodynamics. *Drug Metab Dispos*, doi: 10.1124/dmd.106.009746.

Brandsma D, Dieras V, Altintas S, Anders C, Arnedos M, Gelderblom H, Soetekouw P, Jager A, van Linde M, and Aftimos P (2014) P08.03 * 2B3-101, GLUTATHIONE PEGYLATED LIPOSOMAL DOXORUBICIN, IN PATIENTS WITH RECURRENT HIGH GRADE GLIOMAS AND BREAST CANCER BRAIN METASTASES. *Neuro Oncol*, doi: 10.1093/neuonc/nou174.191.

Breckwoldt MO, Bode J, Sahm F, Krüwel T, Solecki G, Hahn A, Wirthschaft P, Berghoff AS, Haas M, Venkataramani V, Von Deimling A, Wick W, Herold-Mende C, Heiland S, Platten M, Bendszus M, Kurz FT, Winkler F, and Tews B (2019) Correlated MRI and ultramicroscopy (MR-UM) of brain tumors reveals vast heterogeneity of tumor infiltration and neoangiogenesis in preclinical models and human disease. *Front Neurosci*, doi: 10.3389/fnins.2018.01004.

Broom DC, Nitsche JF, Pintar JE, Rice KC, Woods JH, and Traynor JR (2002) Comparison of receptor mechanisms and efficacy requirements for δ-agonist-induced convulsive activity and antinociception in mice. *J Pharmacol Exp Ther* **303**:723–729.

Brown TJ, Brennan MC, Li M, Church EW, Brandmeir NJ, Rakszawski KL, Patel AS, Rizk EB, Suki D, Sawaya R, and Glantz M (2016) Association of the Extent of Resection With Survival in Glioblastoma. *JAMA Oncol*, doi: 10.1001/jamaoncol.2016.1373.

Bruce DJ, Peterson CD, Kitto KF, Akgün E, Lazzaroni S, Portoghese PS, Fairbanks CA, and Wilcox GL (2019) Combination of a δ-opioid Receptor Agonist and Loperamide Produces Peripherally-mediated Analgesic Synergy in Mice. *Anesthesiology*, doi: 10.1097/ALN.0000000000002840.

Burgess A, and Hynynen K (2013) Noninvasive and targeted drug delivery to the brain using focused ultrasound. *ACS Chem Neurosci* **4**:519–526.

Burgess A, Shah K, Hough O, and Hynynen K (2016) Endothelial cell metabolism in normal and diseased vasculature. *Circ Res* **116**:1231–1244.

Caffery B, Lee JS, and Alexander-Bryant AA (2019) Vectors for glioblastoma gene therapy: Viral & non-viral delivery strategies.

Carpentier A, Canney M, Vignot A, Reina V, Beccaria K, Horodyckid C, Karachi C, Leclercq D, Lafon C, Chapelon JY, Capelle L, Cornu P, Sanson M, Hoang-Xuan K, Delattre JY, and Idbaih A (2016) Clinical trial of blood-brain barrier disruption by pulsed ultrasound. *Sci Transl Med* **8**.

Cavaco M, Gaspar D, Castanho MARB, and Neves V (2020) Antibodies for the treatment of brain metastases, a dream or a reality?

Chang HP, Cheung YK, and Shah DK (2021) Whole-body pharmacokinetics and physiologically based pharmacokinetic model for monomethyl auristatin e (Mmae).

J Clin Med, doi: 10.3390/jcm10061332.

Chen Y, Agarwal S, Shaik NM, Chen C, Yang Z, and Elmquist WF (2009) P-glycoprotein and Breast Cancer Resistance Protein Influence Brain Distribution of Dasatinib. *J Pharmacol Exp Ther* **330**:956–963.

Chen YM, Chen MC, Tsai CM, and Perng RP (2003) Intrathecal gemcitabine chemotherapy for non-small cell lung cancer patients with meningeal carcinomatosis - A case report. *Lung Cancer* **40**:99–101, Elsevier Ireland Ltd.

Choi JJ, Pernot M, Small SA, and Konofagou EE (2007) Noninvasive, transcranial and localized opening of the blood-brain barrier using focused ultrasound in mice. *Ultrasound Med Biol* **33**:95–104.

Chotsampancharoen T, Sripornsawan P, and Wongchanchailert M (2016) Two Fatal Cases of Accidental Intrathecal Vincristine Administration: Learning from Death Events. *Chemotherapy* **61**:108–110, S. Karger AG.

Collins JM (1983) Pharmacokinetics of intraventricular administration. *J Neurooncol* **1**:283–291, Kluwer Academic Publishers.

Cooper PR, Ciambrone GJ, Kliwinski CM, Maze E, Johnson L, Li Q, Feng Y, and Hornby PJ (2013) Efflux of monoclonal antibodies from rat brain by neonatal Fc receptor, FcRn. *Brain Res*, doi: 10.1016/j.brainres.2013.08.035.

Costa R, and Kumthekar P (2018) Management of central nervous system metastases in breast cancer, in *The Breast: Comprehensive Management of Benign and Malignant Diseases* pp 942-960.e7, Elsevier Inc.

Cserr HF, DePasquale M, Harling-Berg CJ, Park JT, and Knopf PM (1992) Afferent and efferent arms of the humoral immune response to CSF-administered albumins in a rat model with normal blood-brain barrier permeability. *J Neuroimmunol*, doi: 10.1016/0165-5728(92)90070-2.

D'Amico RS, Aghi MK, Vogelbaum MA, and Bruce JN (2021) Convection-enhanced drug

delivery for glioblastoma: a review.

Dagenais C, Graff CL, and Pollack GM (2004) Variable modulation of opioid brain uptake by P-glycoprotein in mice. *Biochem Pharmacol*, doi: 10.1016/j.bcp.2003.08.027.

Dahlhamer J, Lucas J, Zelaya, C, Nahin R, Mackey S, DeBar L, Kerns R, Von Korff M, Porter L, and Helmick C (2018) Prevalence of Chronic Pain and High-Impact Chronic Pain Among Adults — United States, 2016. *MMWR Morb Mortal Wkly Rep*, doi: 10.15585/mmwr.mm6736a2.

Daniels DJ, Lenard NR, Etienne CL, Law PY, Roerig SC, and Portoghese PS (2005) Opioid-induced tolerance and dependence in mice is modulated by the distance between pharmacophores in a bivalent ligand series. *Proc Natl Acad Sci U S A*, doi: 10.1073/pnas.0506627102.

de Gooijer MC, Kemper EM, Buil LCM, Çitirikkaya CH, Buckle T, Beijnen JH, and van Tellingen O (2021) ATP-binding cassette transporters restrict drug delivery and efficacy against brain tumors even when blood-brain barrier integrity is lost. *Cell Reports Med*, doi: 10.1016/j.xcrm.2020.100184.

Demeule M, Regina A, Ché C, Poirier J, Nguyen T, Gabathuler R, Castaigne JP, and Béliveau R (2008) Identification and design of peptides as a new drug delivery system for the brain. *J Pharmacol Exp Ther*, doi: 10.1124/jpet.107.131318.

Derouiche L, Pierre F, Doridot S, Ory S, and Massotte D (2020) Heteromerization of endogenous mu and delta opioid receptors induces ligand-selective co-targeting to lysosomes. *Molecules*, doi: 10.3390/molecules25194493.

Ding H, Kiguchi N, Yasuda D, Daga PR, Polgar WE, Lu JJ, Czoty PW, Kishioka S, Zaveri NT, and Ko MC (2018) A bifunctional nociceptin and mu opioid receptor agonist is analgesic without opioid side effects in nonhuman primates. *Sci Transl Med*, doi: 10.1126/scitranslmed.aar3483.

Dixit S, Novak T, Miller K, Zhu Y, Kenney ME, and Broome AM (2015) Transferrin receptor-targeted theranostic gold nanoparticles for photosensitizer delivery in brain tumors. *Nanoscale*, doi: 10.1039/c4nr04853a.

Dong X (2018) Current strategies for brain drug delivery.

Doolittle ND, Miner ME, Hall WA, Siegal T, Hanson EJ, Osztie E, McAllister LD, Bubalo JS, Kraemer DF, Fortin D, Nixon R, Muldoon LL, and Neuwelt EA (2000) Safety and efficacy of a multicenter study using intraarterial chemotherapy in conjunction with osmotic opening of the blood-brain barrier for the treatment of patients with malignant brain tumors. *Cancer* **88**:637–647.

Dowell D, Haegerich TM, and Chou R (2016) CDC guideline for prescribing opioids for chronic pain-United States, 2016. *JAMA - J Am Med Assoc*, doi: 10.1001/jama.2016.1464.

Durmus S, Hendrikx JJMA, and Schinkel AH (2015) Apical ABC Transporters and Cancer Chemotherapeutic Drug Disposition. *Adv Cancer Res* **125**:1–41, Academic Press.

Eaton JS, Miller PE, Mannis MJ, and Murphy CJ (2015) Ocular Adverse Events Associated with Antibody-Drug Conjugates in Human Clinical Trials.

Ekblom M, Gårdmark M, and Hammarlund-Udenaes M (1992) Estimation of unbound concentrations of morphine from microdialysate concentrations by use of nonlinear regression analysis in vivo and in vitro during steady state conditions. *Life Sci*, doi: 10.1016/0024-3205(92)90413-J.

EMA (2012) Assessment report: Adcetris. *CHMP Assess Rep* **44**.

Ferguson RK, and Woodbury DM (1969) Penetration of 14C-inulin and 14C-sucrose into brain, cerebrospinal fluid, and skeletal muscle of developing rats. *Exp Brain Res* **7**:181–194, Springer-Verlag.

Figura NB, Long W, Yu M, Robinson TJ, Mokhtari S, Etame AB, Tran ND, Diaz R,

Soliman H, Han HS, Sahebjam S, Forsyth PA, and Ahmed KA (2018) Intrathecal trastuzumab in the management of HER2+ breast leptomeningeal disease: a single institution experience. *Breast Cancer Res Treat* **169**:391–396, Springer New York LLC.

Fink JR, Muzi M, Peck M, and Krohn KA (2015) Multimodality brain tumor imaging: MR imaging, PET, and PET/MR imaging. *J Nucl Med*, doi: 10.2967/jnumed.113.131516.

Finke JM, Ayres KR, Brisbin RP, Hill HA, Wing EE, and Banks WA (2017) Antibody blood-brain barrier efflux is modulated by glycan modification. *Biochim Biophys Acta - Gen Subj*, doi: 10.1016/j.bbagen.2017.06.008.

Fowler MJ, Cotter JD, Knight BE, Sevick-Muraca EM, Sandberg DI, and Sirianni RW (2020) Intrathecal drug delivery in the era of nanomedicine. *Adv Drug Deliv Rev*, doi: 10.1016/j.addr.2020.02.006, Elsevier B.V.

Fridén M, Ljungqvist H, Middleton B, Bredberg U, and Hammarlund-Udenaes M (2010) Improved measurement of drug exposure in the brain using drug-specific correction for residual blood. *J Cereb Blood Flow Metab*, doi: 10.1038/jcbfm.2009.200.

Fu Z, Li S, Han S, Shi C, and Zhang Y (2022) Antibody drug conjugate: the “biological missile” for targeted cancer therapy.

G. S, G. C, and R. J (2013) Crossing the blood-brain barrier: Brain delivery of unmodified cancer therapeutics via intravenous route mediated by a peptide transporter. *Neuro Oncol*, doi: 10.1093/neuonc/not176 LK - http://vu.on.worldcat.org/atoztitles/link?sid=EMBASE&issn=15228517&id=doi:10.1093%2Fneuonc%2Fnot176&atitle=Crossing+the+blood-brain+barrier%3A+Brain+delivery+of+unmodified+cancer+therapeutics+via+intravenous+route+mediated+by+a+peptide+transporter&stitle=Neuro-Oncology&title=Neuro-Oncology&volume=15&issue=&spage=iii56&epage=iii57&aulast=Sarkar&aufirst=G

obinda&auinit=G.&aufull=Sarkar+G.&coden=&isbn=&pages=iii56-iii57&date=2013&auinit1=G&auinitm=.

Gaillard PJ, Appeldoorn CCM, Dorland R, Van Kregten J, Manca F, Vugts DJ, Windhorst B, Van Dongen GAMS, De Vries HE, Maussang D, and Van Tellingen O (2014) Pharmacokinetics, brain delivery, and efficacy in brain tumor-bearing mice of glutathione pegylated liposomal doxorubicin (2B3-101). *PLoS One*, doi: 10.1371/journal.pone.0082331.

Gampa G, Kenchappa RS, Mohammad AS, Parrish KE, Kim M, Crish JF, Luu A, West R, Hinojosa AQ, Sarkaria JN, Rosenfeld SS, and Elmquist WF (2020) Enhancing Brain Retention of a KIF11 Inhibitor Significantly Improves its Efficacy in a Mouse Model of Glioblastoma. *Sci Rep*, doi: 10.1038/s41598-020-63494-7.

Gampa G, Kim M, Mohammad AS, Parrish KE, Mladek AC, Sarkaria JN, and Elmquist WF (2019) Brain Distribution and Active Efflux of Three panRAF Inhibitors: Considerations in the Treatment of Melanoma Brain Metastases. *J Pharmacol Exp Ther*, doi: 10.1124/jpet.118.253708.

Gan HK, van den Bent M, Lassman AB, Reardon DA, and Scott AM (2017) Antibody–drug conjugates in glioblastoma therapy: the right drugs to the right cells. *Nat Rev Clin Oncol* **14**:695–707.

García FJV, Carrión NP, and de la Cruz-Merino L (2020) Long-term complete response to intrathecal trastuzumab in a patient with leptomeningeal carcinomatosis due to her2- overexpressing breast cancer. *Medicine (Baltimore)* **99**:e18298, Lippincott Williams and Wilkins.

Garg A, and Balthasar JP (2009) Investigation of the influence of FcRn on the distribution of IgG to the brain. *AAPS J*, doi: 10.1208/s12248-009-9129-9.

Gomes I, Gupta A, Filipovska J, Szeto HH, Pintar JE, and Devi LA (2004) A role for heterodimerization of μ and δ opiate receptors in enhancing morphine analgesia.

Proc Natl Acad Sci U S A, doi: 10.1073/pnas.0307601101.

Gomes I, Jordan BA, Gupta A, Trapaidze N, Nagy V, and Devi LA (2000) Heterodimerization of mu and delta opioid receptors: A role in opiate synergy. *J Neurosci*, doi: 10.1523/jneurosci.20-22-j0007.2000.

Goutal S, Gerstenmayer M, Auvity S, Caillé F, Mériaux S, Buvat I, Larrat B, and Tournier N (2018) Physical blood-brain barrier disruption induced by focused ultrasound does not overcome the transporter-mediated efflux of erlotinib. *J Control Release*, doi: 10.1016/j.jconrel.2018.11.009.

Grahn AY, Bankiewicz KS, Dugich-Djordjevic M, Bringas JR, Hadaczek P, Johnson GA, Eastman S, and Luz M (2009) Non-PEGylated liposomes for convection-enhanced delivery of topotecan and gadodiamide in malignant glioma: Initial experience. *J Neurooncol* **95**:185–197.

Griffith JI, Kim M, Bruce DJ, Peterson CD, Kitto KF, Mohammad AS, Rathi S, Fairbanks CA, Wilcox GL, and Elmquist WF (2022) Central Nervous System Distribution of an Opioid Agonist Combination with Synergistic Activity. *J Pharmacol Exp Ther*, doi: 10.1124/JPET.121.000821.

Griffith JI, Rathi S, Zhang Wenqiu, Zhang Wenjuan, Drewes LR, Sarkaria JN, and Elmquist WF (2020) Addressing BBB heterogeneity: A new paradigm for drug delivery to brain tumors.

Griffith JI, Sarkaria JN, and Elmquist WF (2021) Efflux Limits Tumor Drug Delivery Despite Disrupted BBB.

Gril B, Wei D, Zimmer AS, Robinson C, Khan I, Difilippantonio S, Overstreet MG, and Steeg PS (2020) HER2 antibody-drug conjugate controls growth of breast cancer brain metastases in hematogenous xenograft models, with heterogeneous blood–tumor barrier penetration unlinked to a passive marker. *Neuro Oncol*, doi: 10.1093/neuonc/noaa118.

Guhasarkar D, Su Q, Gao G, and Sena-Esteves M (2016) Systemic AAV9-IFNβ gene delivery treats highly invasive glioblastoma. *Neuro Oncol*, doi: 10.1093/neuonc/now097.

Gulia S, Gupta S, and Singh A (2016) Intrathecal trastuzumab for leptomeningeal carcinomatosis in patients with human epidermal growth factor receptor 2 positive breast cancer. *Indian J Med Paediatr Oncol* **37**:196–198, Medknow Publications.

Ha D, Yang N, and Nadithe V (2016) Exosomes as therapeutic drug carriers and delivery vehicles across biological membranes: current perspectives and future challenges.

Hammarlund-Udenaes M, Fridén M, Syvänen S, and Gupta A (2008) On the rate and extent of drug delivery to the brain.

Haqqani AS, Thom G, Burrell M, Delaney CE, Brunette E, Baumann E, Sodja C, Jezierski A, Webster C, and Stanimirovic DB (2018) Intracellular sorting and transcytosis of the rat transferrin receptor antibody OX26 across the blood–brain barrier in vitro is dependent on its binding affinity. *J Neurochem*, doi: 10.1111/jnc.14482.

Hargreaves K, Dubner R, Brown F, Flores C, and Joris J (1988) A new and sensitive method for measuring thermal nociception in cutaneous hyperalgesia. *Pain*, doi: 10.1016/0304-3959(88)90026-7.

Hedegaard H, Chen LH, and Warner M (2015) Drug-poisoning deaths involving heroin: United States, 2000-2013. *NCHS Data Brief*.

Hedegaard H, Warner M, and Miniño AM (2017) Drug Overdose Deaths in the United States, 1999–2016. NCHS Data Brief, no 294. *NCHS Data Brief*.

Himuro S (2007) Physicochemical characteristics of microbubbles. *Kagaku Koguku* **71**:165–169.

Hoyos-Ceballos GP, Ruozi B, Ottonelli I, Da Ros F, Vandelli MA, Forni F, Daini E, Vilella

A, Zoli M, Tosi G, Duskey JT, and López-Osorio BL (2020) PLGA-PEG-Ang–2 nanoparticles for blood–brain barrier crossing: Proof-of-concept study. *Pharmaceutics*, doi: 10.3390/pharmaceutics12010072.

Huang TT, Hlavaty J, Ostertag D, Espinoza FL, Martin B, Petznek H, Rodriguez-Aguirre M, Ibañez CE, Kasahara N, Gunzburg W, Gruber HE, Pertschuk D, Jolly DJ, and Robbins JM (2013) Toca 511 gene transfer and 5-fluorocytosine in combination with temozolomide demonstrates synergistic therapeutic efficacy in a temozolomide-sensitive glioblastoma model. *Cancer Gene Ther*, doi: 10.1038/cgt.2013.51.

Hunt Bobo R, Laske DW, Akbasak A, Morrison PF, Dedrick RL, and Oldfield EH (1994) Convection-enhanced delivery of macromolecules in the brain. *Proc Natl Acad Sci U S A*, doi: 10.1073/pnas.91.6.2076.

Hynynen K, and Jolesz FA (1998) Demonstration of potential noninvasive ultrasound brain therapy through an intact skull. *Ultrasound Med Biol* **24**:275–283.

Idbaih A, Canney M, Belin L, Desseaux C, Vignot A, Bouchoux G, Asquier N, Law-Ye B, Leclercq D, Bissery A, De Rycke Y, Trosch C, Capelle L, Sanson M, Hoang-Xuan K, Dehais C, Houillier C, Laigle-Donadey F, Mathon B, André A, Lafon C, Chapelon JY, Delattre JY, and Carpentier A (2019) Safety and feasibility of repeated and transient blood-brain barrier disruption by pulsed ultrasound in patients with recurrent glioblastoma. *Clin Cancer Res* **25**:3793–3801.

Jabbour E, O'Brien S, Kantarjian H, Garcia-Manero G, Ferrajoli A, Ravandi F, Cabanillas M, and Thomas DA (2007) Neurologic complications associated with intrathecal liposomal cytarabine given prophylactically in combination with high-dose methotrexate and cytarabine to patients with acute lymphocytic leukemia. *Blood* **109**:3214–3218, American Society of Hematology.

Jahangiri A, Chin AT, Flanigan PM, Chen R, Bankiewicz K, and Aghi MK (2017)

Convection-enhanced delivery in glioblastoma: A review of preclinical and clinical studies, American Association of Neurological Surgeons.

Jallouli Y, Paillard A, Chang J, Sevin E, and Betbeder D (2007) Influence of surface charge and inner composition of porous nanoparticles to cross blood-brain barrier in vitro. *Int J Pharm*, doi: 10.1016/j.ijpharm.2007.06.023.

Johnsen KB, Burkhart A, Melander F, Kempen PJ, Vejlebo JB, Siupka P, Nielsen MS, Andresen TL, and Moos T (2017) Targeting transferrin receptors at the blood-brain barrier improves the uptake of immunoliposomes and subsequent cargo transport into the brain parenchyma. *Sci Rep*, doi: 10.1038/s41598-017-11220-1.

Jordan BA, and Devi LA (1999) G-protein-coupled receptor heterodimerization modulates receptor function. *Nature*, doi: 10.1038/21441.

Kalvass JC, and Maurer TS (2002) Influence of nonspecific brain and plasma binding on CNS exposure: Implications for rational drug discovery. *Biopharm Drug Dispos*, doi: 10.1002/bdd.325.

Kalvass JC, Olson ER, Cassidy MP, Selley DE, and Pollack GM (2007) Pharmacokinetics and pharmacodynamics of seven opioids in P-glycoprotein-competent mice: Asssessment of unbound brain EC50,u and correlation of in vitro, preclinical, and clinical data. *J Pharmacol Exp Ther*, doi: 10.1124/jpet.107.119560.

Karaoglu Hanzatian D, Schwartz A, Gizatullin F, Erickson J, Deng K, Villanueva R, Stedman C, Harris C, Ghayur T, and Goodearl A (2018) Brain uptake of multivalent and multi-specific DVD-Ig proteins after systemic administration. *MAbs*, doi: 10.1080/19420862.2018.1465159.

Kariolis MS, Wells RC, Getz JA, Kwan W, Mahon CS, Tong R, Kim DJ, Srivastava A, Bedard C, Henne KR, Giese T, Assimon VA, Chen X, Zhang Y, Solanoy H, Jenkins K, Sanchez PE, Kane L, Miyamoto T, Chew KS, Pizzo ME, Liang N, Calvert MEK, DeVos SL, Baskaran S, Hall S, Sweeney ZK, Thorne RG, Watts RJ, Dennis MS,

Silverman AP, and Zuchero YJY (2020) Brain delivery of therapeutic proteins using an Fc fragment blood-brain barrier transport vehicle in mice and monkeys. *Sci Transl Med*, doi: 10.1126/scitranslmed.aay1359.

Kelly PJ, Daumas-Duport C, Kispert DB, Kall BA, Scheithauer BW, and Illig JJ (1987) Imaging-based stereotaxic serial biopsies in untreated intracranial glial neoplasms. *J Neurosurg*, doi: 10.3171/jns.1987.66.6.0865.

Kemper EM, Boogerd W, Thuis I, Beijnen JH, and van Tellingen O (2004) Modulation of the blood-brain barrier in oncology: Therapeutic opportunities for the treatment of brain tumours? *Cancer Treat Rev* **30**:415–423.

Kim G, Kim M, Lee Y, Byun JW, Hwang DW, and Lee M (2020) Systemic delivery of microRNA-21 antisense oligonucleotides to the brain using T7-peptide decorated exosomes. *J Control Release*, doi: 10.1016/j.jconrel.2019.11.009.

Kim M, Laramy JK, Mohammad AS, Talele S, Fisher J, Sarkaria JN, and Elmquist WF (2019) Brain distribution of a panel of epidermal growth factor receptor inhibitors using cassette dosing in wild-type and ABCB1/ABCG2-deficient mice. *Drug Metab Dispos*, doi: 10.1124/dmd.118.084210.

Kim M, Ma DJ, Calligaris D, Zhang S, Feathers RW, Vaubel RA, Meaux I, Mladek AC, Parrish KE, Jin F, Barriere C, Debussche L, Watters J, Tian S, Decker PA, Eckel-Passow JE, Kitange GJ, Johnson AJ, Parney IF, Anastasiadis PZ, Agar NYR, Elmquist WF, and Sarkaria JN (2018) Efficacy of the MDM2 Inhibitor SAR405838 in Glioblastoma Is Limited by Poor Distribution Across the Blood–Brain Barrier. *Mol Cancer Ther* **17**:1893–1901.

Kim SS, Harford JB, Moghe M, Slaughter T, Doherty C, and Chang EH (2019) A tumor-targeting nanomedicine carrying the p53 gene crosses the blood–brain barrier and enhances anti-PD-1 immunotherapy in mouse models of glioblastoma. *Int J Cancer*, doi: 10.1002/ijc.32531.

Kobus T, Zervantonakis IK, Zhang Y, and McDannold NJ (2016) Growth inhibition in a brain metastasis model by antibody delivery using focused ultrasound-mediated blood-brain barrier disruption. *J Control Release* **238**:281–288, Elsevier B.V.

Kreuter J (2013) Mechanism of polymeric nanoparticle-based drug transport across the blood-brain barrier (BBB). *J Microencapsul*, doi: 10.3109/02652048.2012.692491.

Krikorian AD (1975) Were the opium poppy and opium known in the ancient near east? *J Hist Biol* **8**:95–114.

Kroll RA, and Neuwelt EA (1998) Outwitting the blood-brain barrier for therapeutic purposes: Osmotic opening and other means. *Neurosurgery* **42**:1083–1100.

Kuang Y, An S, Guo Y, Huang S, Shao K, Liu Y, Li J, Ma H, and Jiang C (2013) T7 peptide-functionalized nanoparticles utilizing RNA interference for glioma dual targeting. *Int J Pharm*, doi: 10.1016/j.ijpharm.2013.07.019.

Kumar NN, Pizzo ME, Nehra G, Wilken-Resman B, Boroumand S, and Thorne RG (2018) Passive Immunotherapies for Central Nervous System Disorders: Current Delivery Challenges and New Approaches. *Bioconjug Chem*, doi: 10.1021/acs.bioconjchem.8b00548.

Kumar V (2022) *Handbook on Opium: History and Basis of Opioids in Therapeutics*, Academic Press Inc., London, UK.

Kumthekar P, Tang SC, Brenner AJ, Kesari S, Piccioni DE, Anders C, Carrillo J, Chalasani P, Kabos P, Puhalla S, Tkaczuk K, Garcia AA, Ahluwalia MS, Wefel JS, Lakhani N, and Ibrahim N (2020) ANG1005, a Brain-Penetrating Peptide–Drug Conjugate, Shows Activity in Patients with Breast Cancer with Leptomeningeal Carcinomatosis and Recurrent Brain Metastases. *Clin Cancer Res*, doi: 10.1158/1078-0432.CCR-19-3258.

Lakoma A, Barbieri E, Agarwal S, Jackson J, Chen Z, Kim Y, McVay M, Shohet JM, and Kim ES (2015) The MDM2 small-molecule inhibitor RG7388 leads to potent tumor

inhibition in p53 wild-type neuroblastoma. *Cell Death Discov* **1**:15026.

Lang FF, Bruner JM, Fuller GN, Aldape K, Prados MD, Chang S, Berger MS, McDermoff MW, Kunwar SM, Junck LR, Chandler W, Zwiebel JA, Kaplan RS, and Yung WKA (2003) Phase I trial of adenovirus-mediated p53 gene therapy for recurrent glioma: Biological and clinical results. *J Clin Oncol*, doi: 10.1200/JCO.2003.21.13.2508.

Laramy JK, Kim M, Parrish KE, Sarkaria JN, and Elmquist WF (2018) Pharmacokinetic Assessment of Cooperative Efflux of the Multitargeted Kinase Inhibitor Ponatinib Across the Blood-Brain Barrier. *J Pharmacol Exp Ther* **365**:249–261.

Laurence Lalanne, Gulebru Ayranci, Brigitte LK, and Lutz PE (2014) The kappa opioid receptor: From addiction to depression, and back.

Law PY, Reggio PH, and Loh HH (2013) Opioid receptors: Toward separation of analgesic from undesirable effects.

Lei W, Vekariya RH, Ananthan S, and Streicher JM (2020) A Novel Mu-Delta Opioid Agonist Demonstrates Enhanced Efficacy With Reduced Tolerance and Dependence in Mouse Neuropathic Pain Models. *J Pain*, doi: 10.1016/j.jpain.2019.05.017.

Lenard NR, Daniels DJ, Portoghese PS, and Roerig SC (2007) Absence of conditioned place preference or reinstatement with bivalent ligands containing mu-opioid receptor agonist and delta-opioid receptor antagonist pharmacophores. *Eur J Pharmacol*, doi: 10.1016/j.ejphar.2007.02.040.

Letrent SP, Pollack GM, Brouwer KR, and Brouwer KLR (1999) Effects of a potent and specific P-glycoprotein inhibitor on the blood- brain barrier distribution and antinoclceptive effect of morphine in the rat. *Drug Metab Dispos*.

Levin AB, Duff TA, and Javid MJ (1979) Treatment of increased intracranial pressure: A comparison of different hyperosmotic agents and the use of thiopental.

Li F, Emmerton KK, Jonas M, Zhang X, Miyamoto JB, Setter JR, Nicholas ND, Okeley

NM, Lyon RP, Benjamin DR, and Law CL (2016) Intracellular released payload influences potency and bystander-killing effects of antibody-drug conjugates in preclinical models. *Cancer Res*, doi: 10.1158/0008-5472.CAN-15-1795.

Li J, Zhou L, Ye D, Huang S, Shao K, Huang R, Han L, Liu Y, Liu S, Ye L, Lou J, and Jiang C (2011) Choline-derivate-modified nanoparticles for brain-targeting gene delivery. *Adv Mater*, doi: 10.1002/adma.201101899.

Li Y, Gu C, Gruenhagen J, Yehl P, Chetwyn NP, and Medley CD (2016) An enzymatic deconjugation method for the analysis of small molecule active drugs on antibody-drug conjugates. *MAbs*, doi: 10.1080/19420862.2016.1151590.

Liao W, Du Y, Zhang C, Pan F, Yao Y, Zhang T, and Peng Q (2019) Exosomes: The next generation of endogenous nanomaterials for advanced drug delivery and therapy.

Lidar Z, Mardor Y, Jonas T, Pfeffer R, Faibel M, Nass D, Hadani M, and Ram Z (2004) Convection-enhanced delivery of paclitaxel for the treatment of recurrent malignant glioma: A Phase I/II clinical study. *J Neurosurg*, doi: 10.3171/jns.2004.100.3.0472.

Lin CY, Li RJ, Huang CY, Wei KC, and Chen PY (2018) Controlled release of liposome-encapsulated temozolomide for brain tumour treatment by convection-enhanced delivery. *J Drug Target* **26**:325–332, Taylor and Francis Ltd.

Lipsman N, Meng Y, Bethune AJ, Huang Y, Lam B, Masellis M, Herrmann N, Heyn C, Aubert I, Boutet A, Smith GS, Hynynen K, and Black SE (2018) Blood–brain barrier opening in Alzheimer's disease using MR-guided focused ultrasound. *Nat Commun* **9**:1–8.

Liu-Kreyche P, Shen H, Marino AM, Iyer RA, Humphreys WG, and Lai Y (2019) Lysosomal P-gp-MDR1 Confers Drug Resistance of Brentuximab Vedotin and Its Cytotoxic Payload Monomethyl Auristatin E in Tumor Cells. *Front Pharmacol*, doi: 10.3389/fphar.2019.00749.

Liu A, Kozhich A, Passmore D, Gu H, Wong R, Zambito F, Rangan VS, Myler H, Aubry AF, Arnold ME, and Wang J (2015) Quantitative bioanalysis of antibody-conjugated payload in monkey plasma using a hybrid immuno-capture LC-MS/MS approach: Assay development, validation, and a case study. *J Chromatogr B Anal Technol Biomed Life Sci*, doi: 10.1016/j.jchromb.2015.08.007.

Liu H, Chen L, Liu J, Meng H, Zhang R, Ma L, Wu L, Yu S, Shi F, Li Y, Zhang L, Wang L, Feng S, Zhang Q, Peng Y, Wu Q, Liu C, Chang X, Yang L, Uemura Y, Yu X, and Liu T (2017) Co-delivery of tumor-derived exosomes with alpha-galactosylceramide on dendritic cell-based immunotherapy for glioblastoma. *Cancer Lett*, doi: 10.1016/j.canlet.2017.09.022.

Lockman PR, Mittapalli RK, Taskar KS, Rudraraju V, Gril B, Bohn KA, Adkins CE, Roberts A, Thorsheim HR, Gaasch JA, Huang S, Palmieri D, Steeg PS, and Smith QR (2010) Heterogeneous Blood-Tumor Barrier Permeability Determines Drug Efficacy in Experimental Brain Metastases of Breast Cancer. *Clin Cancer Res* **16**:5664–5678.

Lockman PR, Mumper RJ, Khan MA, and Allen DD (2002) Nanoparticle technology for drug delivery across the blood-brain barrier.

Lu NT, Raizer J, Gabor EP, Liu NM, Vu JQ, Slamon DJ, and Barstis JL (2015) Intrathecal trastuzumab: Immunotherapy improves the prognosis of leptomeningeal metastases in HER-2+ breast cancer patient. *J Immunother Cancer* **3**:41, BioMed Central Ltd.

Luo Z, Jin K, Pang Q, Shen S, Yan Z, Jiang T, Zhu X, Yu L, Pang Z, and Jiang X (2017) On-Demand Drug Release from Dual-Targeting Small Nanoparticles Triggered by High-Intensity Focused Ultrasound Enhanced Glioblastoma-Targeting Therapy. *ACS Appl Mater Interfaces*, doi: 10.1021/acsami.7b10866.

Luther DC, Huang R, Jeon T, Zhang X, Lee YW, Nagaraj H, and Rotello VM (2020)

Delivery of drugs, proteins, and nucleic acids using inorganic nanoparticles.

Lyle LT, Lockman PR, Adkins CE, Mohammad AS, Sechrest E, Hua E, Palmieri D, Liewehr DJ, Steinberg SM, Kloc W, Izycka-Swieszewska E, Duchnowska R, Nayyar N, Brastianos PK, Steeg PS, and Gril B (2016) Alterations in Pericyte Subpopulations Are Associated with Elevated Blood-Tumor Barrier Permeability in Experimental Brain Metastasis of Breast Cancer. *Clin Cancer Res* **22**:5287–5299, NIH Public Access.

Macht DI (1915) The history of opium and some of its preparations and alkaloids. *J Am Med Assoc*, doi: 10.1001/jama.1915.02570320001001.

Mainprize T, Lipsman N, Huang Y, Meng Y, Bethune A, Ironside S, Heyn C, Alkins R, Trudeau M, Sahgal A, Perry J, and Hynynen K (2019) Blood-Brain Barrier Opening in Primary Brain Tumors with Non-invasive MR-Guided Focused Ultrasound: A Clinical Safety and Feasibility Study. *Sci Rep* **9**:1–7, Springer US.

Malani R, Fleisher M, Priya Kumthekar ·, Lin · Xuling, Omuro A, Groves MD, Lin NU, Melisko M, Andrew ·, Lassman B, Jeyapalan S, Seidman A, Skakodub A, Boire A, Deangelis LM, Rosenblum M, Raizer J, and Pentsova · Elena (2020) Cerebrospinal fluid circulating tumor cells as a quantifiable measurement of leptomeningeal metastases in patients with HER2 positive cancer. *J Neurooncol* **148**:599–606.

Marin BM, Porath KA, Jain S, Kim M, Conage-Pough JE, Oh JH, Miller CL, Talele S, Kitange GJ, Tian S, Burgenske DM, Mladek AC, Gupta SK, Decker PA, McMinn MH, Stopka SA, Regan MS, He L, Carlson BL, Bakken K, Burns TC, Parney IF, Giannini C, Agar NYR, Eckel-Passow JE, Cochran JR, Elmquist WF, Vaubel RA, White FM, and Sarkaria JN (2021) Heterogeneous delivery across the blood-brain barrier limits the efficacy of an EGFR-targeting antibody drug conjugate in glioblastoma. *Neuro Oncol*, doi: 10.1093/neuonc/noab133.

Marks RM, and Sachar EJ (1973) Undertreatment of medical inpatients with narcotic

analgesics. *Ann Intern Med*, doi: 10.7326/0003-4819-78-2-173.

Masters JC, Nickens DJ, Xuan D, Shazer RL, and Amantea M (2018) Clinical toxicity of antibody drug conjugates: a meta-analysis of payloads.

Matthes HWD, Maldonado R, Simonin F, Valverde O, Slowe S, Kitchen I, Befort K, Dierich A, Le Meur M, Dolie P, Tzavara E, Hanoune J, Roques BP, and Kieffer BL (1996) Loss of morphine-induced analgesia, reward effect and withdrawal symptoms in mice lacking the μ-opioid-receptor gene. *Nature*, doi: 10.1038/383819a0.

Mehta AM, Sonabend AM, and Bruce JN (2017) Convection-Enhanced Delivery, Springer New York LLC.

Mendes M, Sousa JJ, Pais A, and Vitorino C (2018) Targeted theranostic nanoparticles for brain tumor treatment.

Milano MT, Okunieff P, Donatello RS, Mohile NA, Sul J, Walter KA, and Korones DN (2010) Patterns and timing of recurrence after temozolomide-based chemoradiation for glioblastoma. *Int J Radiat Oncol Biol Phys* **78**:1147–55.

Miller DB, and O'Callaghan JP (2017) New horizons for focused ultrasound (FUS) – therapeutic applications in neurodegenerative diseases. *Metabolism* **69**:S3–S7, Elsevier Inc.

Mittapalli RK, Chung AH, Parrish KE, Crabtree D, Halvorson KG, Hu G, Elmquist WF, and Becher OJ (2016) ABCG2 and ABCB1 Limit the Efficacy of Dasatinib in a PDGF-B-Driven Brainstem Glioma Model. *Mol Cancer Ther* **15**:819–829.

Miyazaki H, Nambu K, Matsunaga Y, and Hashimoto M (1979) Disposition and metabolism of [14C]loperamide in rats. *Eur J Drug Metab Pharmacokinet*, doi: 10.1007/BF03189427.

Morrison PF, Chen MY, Chadwick RS, Lonser RR, and Oldfield EH (1999) Focal delivery during direct infusion to brain: Role of flow rate, catheter diameter, and tissue

mechanics. *Am J Physiol - Regul Integr Comp Physiol*, doi: 10.1152/ajpregu.1999.277.4.r1218.

Morrison PF, Laske DW, Bobo H, Oldfield EH, and Dedrick RL (1994) High-flow microinfusion: Tissue penetration and pharmacodynamics.

Mrugala MM, Kim B, Sharma A, Johnson N, Graham C, Kurland BF, and Gralow J (2019) Phase II Study of Systemic High-dose Methotrexate and Intrathecal Liposomal Cytarabine for Treatment of Leptomeningeal Carcinomatosis From Breast Cancer. *Clin Breast Cancer* **19**:311–316, Elsevier Inc.

Múzquiz-Ramos EM, Guerrero-Chávez V, Macías-Martínez BI, López-Badillo CM, and García-Cerda LA (2015) Synthesis and characterization of maghemite nanoparticles for hyperthermia applications. *Ceram Int*, doi: 10.1016/j.ceramint.2014.08.083.

Nair A (2016) Implications of Intrathecal Chemotherapy for Anaesthesiologists: A Brief Review, Hindawi Limited.

Nayak L, Lee EQ, and Wen PY (2012) Epidemiology of brain metastases. *Curr Oncol Rep*, doi: 10.1007/s11912-011-0203-y.

Neuwelt EA (1980) Reversible osmotic blood-brain barrier disruption in humans: implications for the chemotherapy of malignant brain tumors.

Newbould BB (1963) CHEMOTHERAPY OF ARTHRITIS INDUCED IN RATS BY MYCOBACTERIAL ADJUVANT. *Br J Pharmacol Chemother*, doi: 10.1111/j.1476-5381.1963.tb01508.x.

Niwińska A, Rudnicka H, and Murawska M (2015) Breast cancer leptomeningeal metastasis: The results of combined treatment and the comparison of methotrexate and liposomal cytarabine as intra-cerebrospinal fluid chemotherapy. *Clin Breast Cancer* **15**:66–72, Elsevier Inc.

Noble CO, Krauze MT, Drummond DC, Yamashita Y, Saito R, Berger MS, Kirpotin DB,

Bankiewicz KS, and Park JW (2006) Novel nanoliposomal CPT-11 infused by convection-enhanced delivery in intracranial tumors: Pharmacology and efficacy. *Cancer Res* **66**:2801–2806.

Nordling-David MM, Yaffe R, Guez D, Meirow H, Last D, Grad E, Salomon S, Sharabi S, Levi-Kalisman Y, Golomb G, and Mardor Y (2017) Liposomal temozolomide drug delivery using convection enhanced delivery. *J Control Release* **261**:138–146, Elsevier B.V.

Norsworthy KJ, Ko C-W, Lee JE, Liu J, John CS, Przepiorka D, Farrell AT, and Pazdur R (2018) FDA Approval Summary: Mylotarg for Treatment of Patients with Relapsed or Refractory CD33-Positive Acute Myeloid Leukemia. *Oncologist*, doi: 10.1634/theoncologist.2017-0604.

O'Donnell JK, Gladden RM, and Seth P (2017) Trends in Deaths Involving Heroin and Synthetic Opioids Excluding Methadone, and Law Enforcement Drug Product Reports, by Census Region — United States, 2006–2015. *MMWR Morb Mortal Wkly Rep*, doi: 10.15585/mmwr.mm6634a2.

Oller-Salvia B, Sánchez-Navarro M, Giralt E, and Teixidó M (2016a) Blood-brain barrier shuttle peptides: An emerging paradigm for brain delivery.

Oller-Salvia B, Sánchez-Navarro M, Giralt E, and Teixidó M (2016b) Blood-brain barrier shuttle peptides: An emerging paradigm for brain delivery.

On NH, Mitchell R, Savant SD, Bachmeier CJ, Hatch GM, and Miller DW (2013) Examination of blood-brain barrier (BBB) integrity in a mouse brain tumor model. *J Neurooncol*, doi: 10.1007/s11060-012-1006-1.

Osswald M, Blaes J, Liao Y, Solecki G, Gömmel M, Berghoff AS, Salphati L, Wallin JJ, Phillips HS, Wick W, and Winkler F (2016) Impact of blood-brain barrier integrity on tumor growth and therapy response in brain metastases. *Clin Cancer Res*, doi: 10.1158/1078-0432.CCR-16-1327.

Ostrom QT, Cioffi G, Gittleman H, Patil N, Waite K, Kruchko C, and Barnholtz-Sloan JS (2019) CBTRUS Statistical Report: Primary Brain and Other Central Nervous System Tumors Diagnosed in the United States in 2012-2016.

Ozerov S, Thomale UW, Schulz M, Schaumann A, Samarin A, and Kumirova E (2018) The use of a smartphone-assisted ventricle catheter guide for Ommaya reservoir placement—experience of a retrospective bi-center study. *Child's Nerv Syst* **34**:853–859, Springer Verlag.

P. Kumthekar, S. T, A.J. B, S. K, C.K. A, J.A. C, P. C, P. Kabos, M.S. A, and N.K. I (2016) A phase II study of ANG1005, a novel BBB/BCB penetratant taxane in patients with recurrent brain metastases and leptomeningeal carcinomatosis from breast cancer. *Neuro Oncol*.

Pan Y, Wang C, Wang H, Tao Q, Xiong S, and Zhai Z (2016) Transverse myelopathy occurring with intrathecal administration of methotrexate and cytarabine chemotherapy: A case report. *Oncol Lett* **11**:4066–4068, Spandidos Publications.

Pan Z, Yang G, He H, Zhao G, Yuan T, Li Yu, Shi W, Gao P, Dong L, and Li Yunqian (2016) Concurrent radiotherapy and intrathecal methotrexate for treating leptomeningeal metastasis from solid tumors with adverse prognostic factors: A prospective and single-arm study. *Int J Cancer* **139**:1864–1872, Wiley-Liss Inc.

Pandit R, Chen L, and Götz J (2019) The blood-brain barrier: Physiology and strategies for drug delivery. *Adv Drug Deliv Rev*, doi: 10.1016/j.addr.2019.11.009.

Pang HH, Chen PY, Wei KC, Huang CW, Shiue YL, Huang CY, and Yang HW (2019) Convection-enhanced delivery of a virus-like nanotherapeutic agent with dual-modal imaging for besiegement and eradication of brain tumors. *Theranostics* **9**:1752–1763, Ivyspring International Publisher.

Pardridge WM (2020) Blood-Brain Barrier and Delivery of Protein and Gene Therapeutics to Brain.

Pardridge WM (2016) CSF, blood-brain barrier, and brain drug delivery. *Expert Opin Drug Deliv* **13**:963–975.

Pardridge WM (2005) The blood-brain barrier: Bottleneck in brain drug development. *NeuroRx*, doi: 10.1602/neurorx.2.1.3.

Park EJ, Zhang YZ, Vykhodtseva N, and McDannold N (2012) Ultrasound-mediated blood-brain/blood-tumor barrier disruption improves outcomes with trastuzumab in a breast cancer brain metastasis model. *J Control Release* **163**:277–284, Elsevier B.V.

Parodi A, Rudzińska M, Deviatkin AA, Soond SM, Baldin A V., and Zamyatnin AA (2019) Established and emerging strategies for drug delivery across the blood-brain barrier in brain cancer.

Parrish KE, Pokorny J, Mittapalli RK, Bakken K, Sarkaria JN, and Elmquist WF (2015) Efflux Transporters at the Blood-Brain Barrier Limit Delivery and Efficacy of Cyclin-Dependent Kinase 4/6 Inhibitor Palbociclib (PD-0332991) in an Orthotopic Brain Tumor Model. *J Pharmacol Exp Ther* **355**:264–271.

Partap S, Murphy PA, Vogel H, Barnes PD, Edwards MSB, and Fisher PG (2011) Liposomal cytarabine for central nervous system embryonal tumors in children and young adults. *J Neurooncol* **103**:561–566, Springer.

Pattinson KTS (2008) Opioids and the control of respiration.

Peng J, Sarkar S, and Chang SL (2012) Opioid receptor expression in human brain and peripheral tissues using absolute quantitative real-time RT-PCR. *Drug Alcohol Depend*, doi: 10.1016/j.drugalcdep.2012.01.013.

Pert CB, and Snyder SH (1973) Opiate receptor: demonstration in nervous tissue. *Science (80-)*, doi: 10.1126/science.179.4077.1011.

Pessina F, Navarria P, Cozzi L, Ascolese AM, Simonelli M, Santoro A, Clerici E, Rossi M, Scorsetti M, and Bello L (2017) Maximize surgical resection beyond contrast-

enhancing boundaries in newly diagnosed glioblastoma multiforme: is it useful and safe? A single institution retrospective experience. *J Neurooncol*, doi: 10.1007/s11060-017-2559-9.

Phillips AC, Boghaert ER, Vaidya KS, Falls HD, Mitten MJ, DeVries PJ, Benatuil L, Hsieh CM, Meulbroek JA, Panchal SC, Buchanan FG, Durbin KR, Voorbach MJ, Reuter DR, Mudd SR, Loberg LI, Ralston SL, Cao D, Gan HK, Scott AM, and Reilly EB (2018) Characterization of ABBV-221, a tumor-selective EGFR-targeting antibody drug conjugate. *Mol Cancer Ther*, doi: 10.1158/1535-7163.MCT-17-0710.

Phillips AC, Boghaert ER, Vaidya KS, Mitten MJ, Norvell S, Falls HD, Devries PJ, Cheng D, Meulbroek JA, Buchanan FG, McKay LM, Goodwin NC, and Reilly EB (2016) ABT-414, an antibody-drug conjugate targeting a tumor-selective EGFR epitope. *Mol Cancer Ther*, doi: 10.1158/1535-7163.MCT-15-0901.

Pitcher MH, Von Korff M, Bushnell MC, and Porter L (2019) Prevalence and Profile of High-Impact Chronic Pain in the United States. *J Pain*, doi: 10.1016/j.jpain.2018.07.006.

Pitz MW, Desai A, Grossman SA, and Blakeley JO (2011) Tissue concentration of systemically administered antineoplastic agents in human brain tumors.

Pizzo ME, Wolak DJ, Kumar NN, Brunette E, Brunnquell CL, Hannocks MJ, Abbott NJ, Meyerand ME, Sorokin L, Stanimirovic DB, and Thorne RG (2018) Intrathecal antibody distribution in the rat brain: surface diffusion, perivascular transport and osmotic enhancement of delivery. *J Physiol*, doi: 10.1113/JP275105.

Pluchart H, Jacquet E, Charlety D, Allenet B, Bedouch P, and Mousseau M (2016) Long-Term Survivor with Intrathecal and Intravenous Trastuzumab Treatment in Metastatic Breast Cancer. *Target Oncol* **11**:687–691, Springer-Verlag France.

Pokorny JL, Calligaris D, Gupta SK, Iyekegbe DO, Mueller D, Bakken KK, Carlson BL, Schroeder MA, Evans DL, Lou Z, Decker PA, Eckel-Passow JE, Pucci V, Ma B,

Shumway SD, Elmquist WF, Agar NYR, and Sarkaria JN (2015) The efficacy of the wee1 inhibitor MK-1775 combined with temozolomide is limited by heterogeneous distribution across the blood-brain barrier in glioblastoma. *Clin Cancer Res*, doi: 10.1158/1078-0432.CCR-14-2588.

Portenoy RK, and Foley KM (1986) Chronic use of opioid analgesics in non-malignant pain: Report of 38 cases. *Pain*, doi: 10.1016/0304-3959(86)90091-6.

Portoghese PS (1965) A New Concept on the Mode of Interaction of Narcotic Analgesics with Receptors. *J Med Chem*, doi: 10.1021/jm00329a013.

Portoghese PS, Sultana M, Nagase H, and Takemori AE (1988) Application of the message-address concept in the design of highly potent and selective non-peptide .delta. opioid receptor antagonists. *J Med Chem*, doi: 10.1021/jm00397a001.

Prades R, Guerrero S, Araya E, Molina C, Salas E, Zurita E, Selva J, Egea G, López-Iglesias C, Teixidó M, Kogan MJ, and Giralt E (2012) Delivery of gold nanoparticles to the brain by conjugation with a peptide that recognizes the transferrin receptor. *Biomaterials*, doi: 10.1016/j.biomaterials.2012.06.063.

Pradhan AAA, Becker JAJ, Scherrer G, Tryoen-Toth P, Filliol D, Matifas A, Massotte D, Gavériaux-Ruff C, and Kieffer BL (2009) In vivo delta opioid receptor internalization controls behavioral effects of agonists. *PLoS One*, doi: 10.1371/journal.pone.0005425.

Presley CC, and Lindsley CW (2018a) DARK Classics in Chemical Neuroscience: Opium, a Historical Perspective. *ACS Chem Neurosci*, doi: 10.1021/acschemneuro.8b00459.

Presley CC, and Lindsley CW (2018b) DARK Classics in Chemical Neuroscience: Opium, a Historical Perspective. *ACS Chem Neurosci* **9**.

Rapoport SI (2000) Osmotic opening of the blood-brain barrier: Principles, mechanism, and therapeutic applications. *Cell Mol Neurobiol* **20**:217–230.

Rapoport SI, Fredericks WR, Ohno K, and Pettigrew KD (1980) Quantitative aspects of reversible osmotic opening of the blood-brain barrier. *Am J Physiol - Regul Integr Comp Physiol* **7**:421–431.

Rapoport SI, Hori M, and Klatzo I (1972) Testing of a hypothesis for osmotic opening of the blood-brain barrier. *Am J Physiol* **223**:323–331.

Rechberger JS, Power EA, Lu VM, Zhang L, Sarkaria JN, and Daniels DJ (2020) Evaluating infusate parameters for direct drug delivery to the brainstem: A comparative study of convection-enhanced delivery versus osmotic pump delivery. *Neurosurg Focus* **48**, American Association of Neurological Surgeons.

Recht L, Torres CO, Smith TW, Raso V, and Griffin TW (1990) Transferrin receptor in normal and neoplastic brain tissue: Implications for brain-tumor immunotherapy. *J Neurosurg*, doi: 10.3171/jns.1990.72.6.0941.

Regina A, Demeule M, Tripathy S, Lord-Dufour S, Currie JC, Iddir M, Annabi B, Castaigne JP, and Lachowicz JE (2015) ANG4043, a novel brain-penetrant peptide-mAb conjugate, is efficacious against HER2-positive intracranial tumors in mice. *Mol Cancer Ther*, doi: 10.1158/1535-7163.MCT-14-0399.

Reilly EB, Phillips AC, Buchanan FG, Kingsbury G, Zhang Y, Meulbroek JA, Cole TB, Devries PJ, Falls HD, Beam C, Gu J, Digiammarino EL, Palma JP, Donawho CK, Goodwin NC, and Scott AM (2015) Characterization of ABT-806, a humanized tumor-specific anti-EGFR monoclonal antibody. *Mol Cancer Ther*, doi: 10.1158/1535-7163.MCT-14-0820.

Reungwetwattana T, Nakagawa K, Cho BC, Cobo M, Cho EK, Bertolini A, Bohnet S, Zhou C, Lee KH, Nogami N, Okamoto I, Leighl N, Hodge R, McKeown A, Brown AP, Rukazenkov Y, Ramalingam SS, and Vansteenkiste J (2018) CNS response to osimertinib versus standard epidermal growth factor receptor tyrosine kinase inhibitors in patients with untreated EGFR-mutated advanced non-small-cell lung

cancer, in *Journal of Clinical Oncology* p.

Richardson DR, and Morgan EH (2004) The transferrin homologue, melanotransferrin (p97), is rapidly catabolized by the liver of the rat and does not effectively donate iron to the brain. *Biochim Biophys Acta - Mol Basis Dis*, doi: 10.1016/j.bbadis.2004.06.002.

Rip J, Chen L, Hartman R, Van Den Heuvel A, Reijerkerk A, Van Kregten J, Van Der Boom B, Appeldoorn C, De Boer M, Maussang D, De Lange ECM, and Gaillard PJ (2014) Glutathione PEGylated liposomes: Pharmacokinetics and delivery of cargo across the blood-brain barrier in rats. *J Drug Target*, doi: 10.3109/1061186X.2014.888070.

Roberts JC, Grocholski BM, Kitto KF, and Fairbanks CA (2005) Pharmacodynamic and pharmacokinetic studies of agmatine after spinal administration in the mouse. *J Pharmacol Exp Ther*, doi: 10.1124/jpet.105.086173.

Rudd RA, Paulozzi LJ, Bauer MJ, Burleson RW, Carlson RE, Dao D, Davis JW, Dudek J, Eichler BA, Fernandes JC, Fondario A, Gabella B, Hume B, Huntamer T, Kariisa M, Largo TW, Miles J, Newmyer A, Nitcheva D, Perez BE, Proescholdbell SK, Sabel JC, Skiba J, Slavova S, Stone K, Tharp JM, Wendling T, Wright D, Zehner AM, and Centers for Disease Control and Prevention (CDC) (2014) Increases in heroin overdose deaths - 28 States, 2010 to 2012. *MMWR Morb Mortal Wkly Rep*.

S. Hersh D, S. Wadajkar A, B. Roberts N, G. Perez J, P. Connolly N, Frenkel V, A. Winkles J, F. Woodworth G, and J. Kim A (2016) Evolving Drug Delivery Strategies to Overcome the Blood Brain Barrier. *Curr Pharm Des*, doi: 10.2174/1381612822666151221150733.

Sadeque AJM, Wandel C, He H, Shah S, and Wood AJJ (2000) Increased drug delivery to the brain by P-glycoprotein inhibition. *Clin Pharmacol Ther*, doi: 10.1067/mcp.2000.109156.

Saka R, Sathe P, and Khan W (2019) Brain local delivery strategy, in *Brain Targeted Drug Delivery System* pp 241–286, Elsevier.

Salphati L, Heffron TP, Alicke B, Nishimura M, Barck K, Carano RA, Cheong J, Edgar KA, Greve J, Kharbanda S, Koeppen H, Lau S, Lee LB, Pang J, Plise EG, Pokorny JL, Reslan HB, Sarkaria JN, Wallin JJ, Zhang X, Gould SE, Olivero AG, and Phillips HS (2012) Targeting the PI3K pathway in the brain - Efficacy of a PI3K inhibitor optimized to cross the blood-brain barrier. *Clin Cancer Res*, doi: 10.1158/1078-0432.CCR-12-0720.

Sanai N, and Berger MS (2008) Glioma extent of resection and its impact on patient outcome.

Sanai N, Li J, Boerner J, Stark K, Wu J, Kim S, Derogatis A, Mehta S, Dhruv HD, Heilbrun LK, Berens ME, and LoRusso PM (2018) Phase 0 trial of azd1775 in first-recurrence glioblastoma patients. *Clin Cancer Res*, doi: 10.1158/1078-0432.CCR-17-3348.

Sarkar G, Curran GL, Sarkaria JN, Lowe VJ, and Jenkins RB (2014) Peptide carrier-mediated non-covalent delivery of unmodified cisplatin, methotrexate and other agents via intravenous route to the brain. *PLoS One*, doi: 10.1371/journal.pone.0097655.

Sarkaria JN, Hu LS, Parney IF, Pafundi DH, Brinkmann DH, Laack NN, Giannini C, Burns TC, Kizilbash SH, Laramy JK, Swanson KR, Kaufmann TJ, Brown PD, Agar NYR, Galanis E, Buckner JC, and Elmquist WF (2018a) Is the blood-brain barrier really disrupted in all glioblastomas? A critical assessment of existing clinical data. *Neuro Oncol*, doi: 10.1093/neuonc/nox175.

Sarkaria JN, Hu LS, Parney IF, Pafundi DH, Brinkmann DH, Laack NN, Giannini C, Burns TC, Kizilbash SH, Laramy JK, Swanson KR, Kaufmann TJ, Brown PD, Agar NYR, Galanis E, Buckner JC, and Elmquist WF (2018b) Is the blood-brain barrier

really disrupted in all glioblastomas? A critical assessment of existing clinical data. *Neuro Oncol*, doi: 10.1093/neuonc/nox175.

Sawicki K, Czajka M, Matysiak-Kucharek M, Fal B, Drop B, Męczyńska-Wielgosz S, Sikorska K, Kruszewski M, and Kapka-Skrzypczak L (2019) Toxicity of metallic nanoparticles in the central nervous system. *Nanotechnol Rev*, doi: 10.1515/ntrev-2019-0017.

Schinkel AH, Wagenaar E, Mol CAAM, and Van Deemter L (1996) P-glycoprotein in the blood-brain barrier of mice influences the brain penetration and pharmacological activity of many drugs. *J Clin Invest*, doi: 10.1172/JCI118699.

Schlachetzki F, Zhu C, and Pardridge WM (2002) Expression of the neonatal Fc receptor (FcRn) at the blood-brain barrier. *J Neurochem*, doi: 10.1046/j.1471-4159.2002.00840.x.

Schmitz R (1985) Friedrich Wilhelm Sertürner and the discovery of morphine. *Pharm Hist*.

Schuster DJ, Metcalf MD, Kitto KF, Messing RO, Fairbanks CA, and Wilcox GL (2015) Ligand requirements for involvement of PKCε in synergistic analgesic interactions between spinal μ and δ opioid receptors. *Br J Pharmacol*, doi: 10.1111/bph.12774.

Scott BJ, Oberheim-Bush NA, and Kesari S (2016) Leptomeningeal metastasis in breast cancer - a systematic review. *Oncotarget* **7**:3740–3747, Impact Journals LLC.

Scott BJ, van Vugt VA, Rush T, Brown T, Chen CC, Carter BS, Schwab R, Fanta P, Helsten T, Bazhenova L, Parker B, Pingle S, Saria MG, Brown BD, Piccioni DE, and Kesari S (2014) Concurrent intrathecal methotrexate and liposomal cytarabine for leptomeningeal metastasis from solid tumors: a retrospective cohort study. *J Neurooncol* **119**:361–368.

Senzer N, Nemunaitis J, Nemunaitis D, Bedell C, Edelman G, Barve M, Nunan R, Pirollo KF, Rait A, and Chang EH (2013) Phase i study of a systemically delivered p53

nanoparticle in advanced solid tumors, in *Molecular Therapy* p.

Sheets KT, Bagó JR, and Hingtgen SD (2018) Delivery of cytotoxic mesenchymal stem cells with biodegradable scaffolds for treatment of postoperative brain cancer, in *Methods in Molecular Biology* p.

Sheikov N, McDannold N, Sharma S, and Hynynen K (2008) Effect of Focused Ultrasound Applied With an Ultrasound Contrast Agent on the Tight Junctional Integrity of the Brain Microvascular Endothelium. *Ultrasound Med Biol* **34**:1093–1104.

Shi Y, Jiang Y, Cao J, Yang W, Zhang J, Meng F, and Zhong Z (2018) Boosting RNAi therapy for orthotopic glioblastoma with nontoxic brain-targeting chimaeric polymersomes. *J Control Release*, doi: 10.1016/j.jconrel.2018.10.034.

Siegal T, Rubinstein R, Bokstein F, Schwartz A, Lossos A, Shalom E, Chisin R, and Gomori JM (2000) In vivo assessment of the window of barrier opening after osmotic blood- brain barrier disruption in humans. *J Neurosurg* **92**:599–605.

Simon EJ, Hiller JM, and Edelman I (1973) Stereospecific binding of the potent narcotic analgesic [3H] etorphine to rat brain homogenate (opiate receptor/morphine/antagonist). *Proc Natl Acad Sci U S A*, doi: 10.1073/pnas.70.7.1947.

Singh AP, and Shah DK (2017) Measurement and mathematical characterization of cell-level pharmacokinetics of antibody-drug conjugates: A case study with trastuzumab-vc-MMAE. *Drug Metab Dispos*, doi: 10.1124/dmd.117.076414.

Singleton WGB, Bieneman AS, Woolley M, Johnson D, Lewis O, Wyatt MJ, Damment SJP, Boulter LJ, Killick-Cole CL, Asby DJ, and Gill SS (2018) The distribution, clearance, and brainstem toxicity of panobinostat administered by convection-enhanced delivery, in *Journal of Neurosurgery: Pediatrics* pp 288–296, American Association of Neurological Surgeons.

Smith MT, Wyse BD, Edwards SR, El-Tamimy M, Gaetano G, and Gavin P (2015) Topical Application of a Novel Oxycodone Gel Formulation (Tocopheryl Phosphate Mixture) in a Rat Model of Peripheral Inflammatory Pain Produces Localized Pain Relief Without Significant Systemic Exposure. *J Pharm Sci*, doi: 10.1002/jps.24502.

St-Amour I, Paré I, Alata W, Coulombe K, Ringuette-Goulet C, Drouin-Ouellet J, Vandal M, Soulet D, Bazin R, and Calon F (2013) Brain bioavailability of human intravenous immunoglobulin and its transport through the murine blood-brain barrier. *J Cereb Blood Flow Metab*, doi: 10.1038/jcbfm.2013.160.

Stanimirovic D, Kemmerich K, Haqqani AS, and Farrington GK (2014) Engineering and pharmacology of blood-brain barrier-permeable bispecific antibodies, in *Advances in Pharmacology* p.

Stein C (2016) Opioid receptors. *Annu Rev Med*, doi: 10.1146/annurev-med-062613-093100.

Stein C, and Machelska H (2011) Modulation of peripheral sensory neurons by the immune system: Implications for pain therapy. *Pharmacol Rev*, doi: 10.1124/pr.110.003145.

Sweeney MD, Zhao Z, Montagne A, Nelson AR, and Zlokovic B V. (2019) Blood-brain barrier: From physiology to disease and back.

Taillibert S, and Chamberlain MC (2018) Leptomeningeal metastasis, in *Handbook of Clinical Neurology* pp 169–204, Elsevier B.V.

Takemori AE, Sultana M, Nagase H, and Portoghese PS (1992) Agonist and antagonist activities of ligands derived from naltrexone and oxymorphone. *Life Sci* **50**.

Talele S, Zhang W, Burgenske DM, Kim M, Mohammad AS, Dragojevic S, Gupta SK, Bindra RS, Sarkaria JN, and Elmquist WF (2021) Brain Distribution of Berzosertib: An Ataxia Telangiectasia and Rad3-Related Protein Inhibitor for the Treatment of Glioblastoma. *J Pharmacol Exp Ther*, doi: 10.1124/jpet.121.000845.

Talele S, Zhang W, Oh J-H, Burgenske DM, Mladek AC, Dragojevic S, Sarkaria JN, and Elmquist WF (2022) CNS delivery of the DNA-PK cs inhibitor peposertib as radiosensitizer for brain metastases . *J Pharmacol Exp Ther* JPET-AR-2021-001069.

Tallarida RJ, and Murray RB (1987) Graded dose—response, in *Manual of Pharmacologic Calculations* p.

Tang F, Li L, and Chen D (2012) Mesoporous silica nanoparticles: Synthesis, biocompatibility and drug delivery. *Adv Mater*, doi: 10.1002/adma.201104763.

Taskar KS, Rudraraju V, Mittapalli RK, Samala R, Thorsheim HR, Lockman J, Gril B, Hua E, Palmieri D, Polli JW, Castellino S, Rubin SD, Lockman PR, Steeg PS, and Smith QR (2012) Lapatinib Distribution in HER2 Overexpressing Experimental Brain Metastases of Breast Cancer. *Pharm Res* **29**:770–781.

Terasaki T, and Ohtsuki S (2005) Brain-to-blood transporters for endogenous substrates and xenobiotics at the blood-brain barrier: An overview of biology and methodology. *Neurotherapeutics*, doi: 10.1007/bf03206643.

Terrell-Hall TB, Nounou MI, El-Amrawy F, Griffith JIG, and Lockman PR (2017) Trastuzumab distribution in an in-vivo and in-vitro model of brain metastases of breast cancer. *Oncotarget* **8**:83734–83744, Impact Journals, LLC.

Thakkar JP, Dolecek TA, Horbinski C, Ostrom QT, Lightner DD, Barnholtz-Sloan JS, and Villano JL (2014) Epidemiologic and molecular prognostic review of glioblastoma.

Thomas FC, Taskar K, Rudraraju V, Goda S, Thorsheim HR, Gaasch JA, Mittapalli RK, Palmieri D, Steeg PS, Lockman PR, and Smith QR (2009) Uptake of ANG1005, a novel paclitaxel derivative, through the blood-brain barrier into brain and experimental brain metastases of breast cancer. *Pharm Res*, doi: 10.1007/s11095-009-9964-5.

Tian X, Nyberg S, Sharp PS, Madsen J, Daneshpour N, Armes SP, Berwick J, Azzouz

M, Shaw P, Abbott NJ, and Battaglia G (2015) LRP-1-mediated intracellular antibody delivery to the Central Nervous System. *Sci Rep*, doi: 10.1038/srep11990.

Timbie KF, Mead BP, and Price RJ (2015) Drug and gene delivery across the blood-brain barrier with focused ultrasound. *J Control Release* **219**:61–75, Elsevier B.V.

Tong JTW, Harris PWR, Brimble MA, and Kavianinia I (2021) An insight into fda approved antibody-drug conjugates for cancer therapy.

Tosi U, Kommidi H, Adeuyan O, Guo H, Maachani UB, Chen N, Su T, Zhang G, Pisapia DJ, Dahmane N, Ting R, and Souweidane MM (2020) *PET, image-guided HDAC inhibition of pediatric diffuse midline glioma improves survival in murine models*.

Treat LH, McDannold N, Vykhodtseva N, Zhang Y, Tam K, and Hynynen K (2007) Targeted delivery of doxorubicin to the rat brain at therapeutic levels using MRI-guided focused ultrasound. *Int J Cancer* **121**:901–907.

Tsai HC, Tsai CH, Chen WS, Inserra C, Wei KC, and Liu HL (2018) Safety evaluation of frequent application of microbubble-enhanced focused ultrasound blood-brain-barrier opening. *Sci Rep* **8**:1–13, Springer US.

Tung Y-S, Vlachos F, Feshitan JA, Borden MA, and Konofagou EE (2011) The mechanism of interaction between focused ultrasound and microbubbles in blood-brain barrier opening in mice. *J Acoust Soc Am* **130**:3059–3067.

Tzeng SY, and Green JJ (2013) Therapeutic nanomedicine for brain cancer, NIH Public Access.

Uhelski ML, Bruce D, Speltz R, Wilcox GL, and Simone DA (2020) Topical Application of Loperamide/Oxymorphindole, Mu and Delta Opioid Receptor Agonists, Reduces Sensitization of C-fiber Nociceptors that Possess NaV1.8. *Neuroscience*, doi: 10.1016/j.neuroscience.2020.08.022.

Ullman JC, Arguello A, Getz JA, Bhalla A, Mahon CS, Wang J, Giese T, Bedard C, Kim DJ, Blumenfeld JR, Liang N, Ravi R, Nugent AA, Davis SS, Ha C, Duque J, Tran

HL, Wells RC, Lianoglou S, Daryani VM, Kwan W, Solanoy H, Nguyen H, Earr T, Dugas JC, Tuck MD, Harvey JL, Reyzer ML, Caprioli RM, Hall S, Poda S, Sanchez PE, Dennis MS, Gunasekaran K, Srivastava A, Sandmann T, Henne KR, Thorne RG, Di Paolo G, Astarita G, Diaz D, Silverman AP, Watts RJ, Sweeney ZK, Kariolis MS, and Henry AG (2020) Brain delivery and activity of a lysosomal enzyme using a blood-brain barrier transport vehicle in mice. *Sci Transl Med*, doi: 10.1126/scitranslmed.aay1163.

van den Bent M, Eoli M, Sepulveda JM, Smits M, Walenkamp A, Frenel J-S, Franceschi E, Clement PM, Chinot O, de Vos F, Whenham N, Sanghera P, Weller M, Dubbink HJ, French P, Looman J, Dey J, Krause S, Ansell P, Nuyens S, Spruyt M, Brilhante J, Coens C, Gorlia T, and Golfinopoulos V (2019) INTELLANCE 2/EORTC 1410 randomized phase II study of Depatux-M alone and with temozolomide vs temozolomide or lomustine in recurrent EGFRamplified glioblastoma. *Neuro Oncol*, doi: 10.1093/neuonc/noz222.

Vandenbossche J, Huisman M, Xu Y, Sanderson-Bongiovanni D, and Soons P (2010) Loperamide and P-glycoprotein inhibition: assessment of the clinical relevance. *J Pharm Pharmacol*, doi: 10.1211/jpp.62.04.0001.

Velasco R, and Bruna J (2015) Taxane-induced peripheral neurotoxicity.

Velasco R, Domingo-Domenech E, and Sureda A (2021) Brentuximab-induced peripheral neurotoxicity: A multidisciplinary approach to manage an emerging challenge in hodgkin lymphoma therapy.

Verdino P, Atwell S, and Demarest SJ (2018) Emerging trends in bispecific antibody and scaffold protein therapeutics.

Waghray D, and Zhang Q (2018) Inhibit or Evade Multidrug Resistance P-Glycoprotein in Cancer Treatment.

Wang D, Sun X, Bohn LM, and Sadée W (2005) Opioid receptor homo- and

heterodimerization in living cells by quantitative bioluminescence resonance energy transfer. *Mol Pharmacol*, doi: 10.1124/mol.104.010272.

Wang X, Xiong Z, Liu Z, Huang X, and Jiang X (2018) Angiopep-2/IP10-EGFRvIIIscFv modified nanoparticles and CTL synergistically inhibit malignant glioblastoma. *Sci Rep*, doi: 10.1038/s41598-018-30072-x.

Watanabe M, Tanaka R, and Takeda N (1992) Magnetic resonance imaging and histopathology of cerebral gliomas. *Neuroradiology*, doi: 10.1007/BF00598951.

Watkins S, Robel S, Kimbrough IF, Robert SM, Ellis-Davies G, and Sontheimer H (2014) Disruption of astrocyte-vascular coupling and the blood-brain barrier by invading glioma cells. *Nat Commun*, doi: 10.1038/ncomms5196.

Wessendorf MW, and Dooyema J (2001) Coexistence of kappa- and delta-opioid receptors in rat spinal cord axons. *Neurosci Lett*, doi: 10.1016/S0304-3940(00)01700-6.

Witorsch P, Williams TW, Ommaya AK, and Utz JP (1965) Intraventricular Administration of Amphotericin B: Use of Subcutaneous Reservoir in Four Patients With Mycotic Meningitis. *JAMA J Am Med Assoc* **194**:699–702.

Xie R, and Hammarlund-Udenaes M (1998) Blood-brain barrier equilibration of codeine in rats studied with microdialysis. *Pharm Res*, doi: 10.1023/A:1011929910782.

Xu L, Huang CC, Huang W, Tang WH, Rait A, Yin YZ, Cruz I, Xiang LM, Pirollo KF, and Chang EH (2002) Systemic tumor-targeted gene delivery by anti-transferrin receptor scFv-immunoliposomes. *Mol Cancer Ther*.

Xue J, Zhao Z, Zhang L, Xue L, Shen S, Wen Y, Wei Z, Wang L, Kong L, Sun H, Ping Q, Mo R, and Zhang C (2017) Neutrophil-mediated anticancer drug delivery for suppression of postoperative malignant glioma recurrence. *Nat Nanotechnol*, doi: 10.1038/nnano.2017.54.

Yang T, Martin P, Fogarty B, Brown A, Schurman K, Phipps R, Yin VP, Lockman P, and

Bai S (2015) Exosome delivered anticancer drugs across the blood-brain barrier for brain cancer therapy in Danio Rerio. *Pharm Res*, doi: 10.1007/s11095-014-1593-y.

Yokosawa M, Sonoda Y, Sugiyama S ichiro, Saito R, Yamashita Y, Nishihara M, Satoh T, Kumabe T, Yokoyama M, and Tominaga T (2010) Convection-enhanced delivery of a synthetic retinoid Am80, loaded into polymeric micelles, prolongs the survival of rats bearing intracranial glioblastoma xenografts. *Tohoku J Exp Med* **221**:257–264.

Yu YJ, Zhang Y, Kenrick M, Hoyte K, Luk W, Lu Y, Atwal J, Elliott JM, Prabhu S, Watts RJ, and Dennis MS (2011) Boosting brain uptake of a therapeutic antibody by reducing its affinity for a transcytosis target. *Sci Transl Med*, doi: 10.1126/scitranslmed.3002230.

Yuan H, Shengjia C, Yinyi W, Leiming L, Yuelin G, and Dhaval L (2022) Effect of the Size of Protein Therapeutics on Brain Pharmacokinetics Following Systematic Administration. *AAPS J*, doi: 10.1208/s12248-022-00701-5, Springer International Publishing.

Yuan J (1993) Estimation of variance for AUC in animal studies. *J Pharm Sci*, doi: 10.1002/jps.2600820718.

Zagouri F, Zoumpourlis P, Le Rhun E, Bartsch R, Zografos E, Apostolidou K, Dimopoulos MA, and Preusser M (2020) Intrathecal administration of anti-HER2 treatment for the treatment of meningeal carcinomatosis in breast cancer: A metanalysis with meta-regression, W.B. Saunders Ltd.

Zhan W, Arifin DY, Lee TK, and Wang CH (2017) Mathematical Modelling of Convection Enhanced Delivery of Carmustine and Paclitaxel for Brain Tumour Therapy. *Pharm Res* **34**:860–873, Springer New York LLC.

Zhan W, and Wang CH (2018) Convection enhanced delivery of liposome encapsulated doxorubicin for brain tumour therapy. *J Control Release* **285**:212–229, Elsevier B.V.

Zhang C, Nance EA, Mastorakos P, Chisholm J, Berry S, Eberhart C, Tyler B, Brem H,

Suk JS, and Hanes J (2017) Convection enhanced delivery of cisplatin-loaded brain penetrating nanoparticles cures malignant glioma in rats. *J Control Release* **263**:112–119, Elsevier B.V.

Zhang R, Saito R, Mano Y, Sumiyoshi A, Kanamori M, Sonoda Y, Kawashima R, and Tominaga T (2016) Convection-enhanced delivery of SN-38-loaded polymeric micelles (NK012) enables consistent distribution of SN-38 and is effective against rodent intracranial brain tumor models. *Drug Deliv* **23**:2780–2786, Taylor and Francis Ltd.

Zhang RD, Price JE, Fujimaki T, Bucana CD, and Fidler IJ (1992) Differential permeability of the blood-brain barrier in experimental brain metastases produced by human neoplasms implanted into nude mice. *Am J Pathol*.

Zhang X, He T, Chai Z, Samulski RJ, and Li C (2018) Blood-brain barrier shuttle peptides enhance AAV transduction in the brain after systemic administration. *Biomaterials*, doi: 10.1016/j.biomaterials.2018.05.041.

Zhang Y, and Pardridge WM (2001) Mediated efflux of IgG molecules from brain to blood across the blood-brain barrier. *J Neuroimmunol*, doi: 10.1016/S0165-5728(01)00242-9.

Zhang Y, Zhu C, and Pardridge WM (2002) Antisense gene therapy of brain cancer with an artificial virus gene delivery system. *Mol Ther*, doi: 10.1006/mthe.2002.0633.

Zhu Y, Jiang Y, Meng F, Deng C, Cheng R, Zhang J, Feijen J, and Zhong Z (2018) Highly efficacious and specific anti-glioma chemotherapy by tandem nanomicelles co-functionalized with brain tumor-targeting and cell-penetrating peptides. *J Control Release*, doi: 10.1016/j.jconrel.2018.03.025.

Zhu Y, King MA, Schuller AGP, Nitsche JF, Reidl M, Elde RP, Unterwald E, Pasternak GW, and Pintar JE (1999) Retention of supraspinal delta-like analgesia and loss of morphine tolerance in δ opioid receptor knockout mice. *Neuron*, doi:

10.1016/S0896-6273(00)80836-3.

Zong J, and Pollack GM (2000) Morphine antinociception is enhanced in mdr1a gene-deficient mice. *Pharm Res*, doi: 10.1023/A:1007546719287.